

# Lawrence Berkeley National Laboratory

## Recent Work

**Title**

DECAY SCHEMES OF ODD-ODD EINSTEINIUM ISOTOPES.

**Permalink**

<https://escholarship.org/uc/item/2dt0m2z1>

**Author**

McHarris, William Charles

**Publication Date**

1965-07-01

**University of California**  
**Ernest O. Lawrence**  
**Radiation Laboratory**

DECAY SCHEMES OF ODD-ODD EINSTEINIUM ISOTOPES

**TWO-WEEK LOAN COPY**

*This is a Library Circulating Copy  
which may be borrowed for two weeks.  
For a personal retention copy, call  
Tech. Info. Division, Ext. 5545*

**Berkeley, California**

## **DISCLAIMER**

This document was prepared as an account of work sponsored by the United States Government. While this document is believed to contain correct information, neither the United States Government nor any agency thereof, nor the Regents of the University of California, nor any of their employees, makes any warranty, express or implied, or assumes any legal responsibility for the accuracy, completeness, or usefulness of any information, apparatus, product, or process disclosed, or represents that its use would not infringe privately owned rights. Reference herein to any specific commercial product, process, or service by its trade name, trademark, manufacturer, or otherwise, does not necessarily constitute or imply its endorsement, recommendation, or favoring by the United States Government or any agency thereof, or the Regents of the University of California. The views and opinions of authors expressed herein do not necessarily state or reflect those of the United States Government or any agency thereof or the Regents of the University of California.

UNIVERSITY OF CALIFORNIA  
Lawrence Radiation Laboratory  
Berkeley, California

AEC Contract No. W-7405-eng-48

DECAY SCHEMES OF ODD-ODD EINSTEINIUM ISOTOPES

William Charles McHarris  
(Ph.D. Thesis)

July 1965

DECAY SCHEMES OF ODD-ODD EINSTEINIUM ISOTOPES

Contents

Abstract	v
I. Introduction	1
II. Es <sup>254</sup>	
A. Relation between Es <sup>254</sup> and Es <sup>254m</sup>	3
B. Experimental Procedure	
1. Source Preparation	8
2. Alpha Spectroscopy	10
3. Electron Spectroscopy	21
4. Gamma-Ray Spectroscopy	28
5. Delays and Time-to-Height	
Coincidences	
a. 63-keV Gamma-Ray	42
b. Alpha vs. L-X-Ray	
Coincidences	42
c. L-X-Ray vs. L-X-Ray	
Coincidences	50
d. 63-keV Gamma-Ray vs. L-X-Ray	
Coincidences	52
e. The Cascade Shown	
Graphically	52
C. Discussion	
1. Decay Scheme	59
2. Spin and Nilsson-Level Assignments	65
3. Alpha Transition Probabilities	78
4. Gamma-Ray Transition Probabilities	86
5. Higher-Energy States	91
6. Rotational Spacings	101
7. Conclusion	103

III. Es <sup>252</sup>	
A. Experimental Procedure	
1. Source Preparation	107
2. Alpha Spectroscopy	109
3. Electron Spectroscopy	112
4. Gamma-Ray Spectroscopy	112
B. Discussion	
1. Decay Scheme	119
2. Nilsson-Level Assignments	128
3. Relation between Bk <sup>248</sup> and Bk <sup>248m</sup>	139
4. Alpha Transition Probabilities	140
5. Rotational Spacings	143
6. Conclusion	146
IV. The Nuclear Coriolis Interaction	
A. Background and Development	148
B. Application to Es <sup>254</sup> Decay (Bk <sup>250</sup> )	160
C. Application to Es <sup>252</sup> Decay (Bk <sup>248</sup> )	174
V. Conclusion	175
Acknowledgments	176
References and Notes	177
List of Figures	184
List of Tables	186

DECAY SCHEMES OF ODD-ODD EINSTEINIUM ISOTOPES

William Charles McHarris

Lawrence Radiation Laboratory  
University of California  
Berkeley, California

July 1965

ABSTRACT

The radiations from the heavy odd-odd, alpha-emitting isotopes,  ${}_{99}^{\text{Es}}{}_{155}^{254}$  and  ${}_{99}^{\text{Es}}{}_{153}^{252}$ , were studied and interpreted in light of the Bohr-Mottelson unified theory of deformed nuclei and the accompanying Nilsson wave functions. The study was based on their alpha-particle spectra, which were obtained both with Si alpha detectors and with a high-resolution, double-focussing magnetic spectrograph. Complementing these were gamma-ray spectra obtained with NaI scintillators and Ge gamma detectors, conversion-electron spectra obtained with Si electron detectors and precision permanent-magnet spectrographs, and various time-to-height and delayed-coincidence spectra.

Levels in the daughter nuclei were grouped into rotational bands, and the experimental properties of these were compared with predictions based on couplings of the odd-nucleon states found in neighboring odd-mass nuclei. Agreement was found to be excellent, indicating that the odd proton and odd neutron in these odd-odd states move with considerable independence of each other.

The decay scheme of  ${}_{99}^{\text{Es}}{}_{155}^{254}$  was worked out in detail, indicating that the 6.437-MeV, favored alpha group populates a  $K\pi I = 7+7$  level at 85.5 keV above the ground state of  ${}_{97}^{\text{Bk}}{}_{150}^{250}$ . A cascade of three electromagnetic transitions is required to de-excite this level to the 2-2 ground state: (1) a 7-keV E2, with a half-life of 213  $\mu\text{sec}$ , that leads to a 4+5 level at 78.1 keV above ground, (2) a fast 42.6-keV M1-E2 rotational transition to the 4+4 level at 35.5 keV, and (3) branching transitions, mostly a 35.5-keV M2, that give the 4+4 level a 29  $\mu\text{sec}$  half-life and connect it with the ground state. Many subsidiary bands and levels were also studied and assigned.

$\text{Es}^{252}$  decays across the 152-neutron subshell. Consequently, its favored alpha decay populates a level at 625 keV above the  $\text{Bk}^{248}$  ground state, while the lower-lying levels in  $\text{Bk}^{248}$  involve neutron states from below the subshell. The ground state band is a  $K\pi = 8^-$  one that is highly distorted. In fact, there appears to be extreme mixing and distortion of most of the bands in  $\text{Bk}^{248}$ , and, as a result, all the alpha-decay hindrance factors are abnormally small.

To explain the distortions found for many of the bands in  $\text{Bk}^{250}$  and  $\text{Bk}^{248}$ , the nuclear Coriolis interaction was invoked. This was developed from the model of a particle coupled to a rigid rotor, and semi-quantitative calculations were made that explained the experimental data quite adequately.



## I. INTRODUCTION

The study of energy levels in odd-odd nuclei is of particular interest both from the viewpoint of systematics and that of theory. Much less information is available concerning their structure than is available for even-even or odd-mass nuclei; thus, it becomes of interest to fill in some of the gaps in the tabulated systematics. Also, odd-odd nuclei should give direct information about the residual nucleon-nucleon interaction outside the nuclear core, perhaps the least well understood aspect of nuclear theory at the present time. The dearth of information comes primarily from the difficulty of preparing radioactive isotopes that will populate these odd-odd levels, especially in the heavy-element region. In this region even-even nuclei with a neutron excess are extremely difficult to prepare, while the somewhat more readily prepared neutron-deficient ones customarily decay by alpha emission, thus populating even-even rather than odd-odd levels. Furthermore, the beta decay of an even-even nucleus is highly selective and usually will not reveal many of the low-lying states, particularly if these have high spin values. However, now and then a heavy odd-odd nucleus lies close enough to the line of beta stability or has a high enough spin to make beta decay unfavorable; it consequently decays by alpha emission. With the wealth of information about low-lying, odd-odd levels that results from studying these complex alpha-decay schemes, these nuclei become powerful tools both for evaluating predictions of the collective nuclear model and for studying the residual interaction between the last odd proton and odd neutron.

The two einsteinium isotopes,  ${}_{99}^{254}\text{Es}_{155}$  and  ${}_{99}^{252}\text{Es}_{153}$ , are nuclei of this type. They have the additional advantage of lying above the accidental subshell at 152 neutrons,<sup>1</sup> another region for which little information is available. Indeed, the alpha decay of  $\text{Es}^{252}$  crosses this subshell, elucidates properties of neutron states on both sides of it, and furnishes the first quantitative information about the energy separation of the neutron states caused by the subshell.<sup>2</sup>

The research described in this thesis has obtained decay schemes for these nuclei within the framework of the Bohr-Mottelson unified model for deformed nuclei,<sup>3</sup> together with the accompanying Nilsson wave functions.<sup>4</sup> The foundation of this work consists of the alpha spectra of these einsteinium isotopes taken with a high-resolution magnetic spectrograph and with solid-state detectors. Supplementing and complementing these have been various gamma, electron, coincidence, and delayed-coincidence spectra. Since the experimental procedures for forcing these nuclei to yield information did not follow predicatably set patterns and differed for the two cases, the thesis has been organized into separate sections for Es<sup>254</sup> and Es<sup>252</sup>. The general experimental procedures are discussed under the Es<sup>254</sup> section, while the Es<sup>252</sup> section makes references back to these and discusses more fully the procedures unique to it. Some of the more specialized experiments were conceived as a result of partial information that had already been incorporated into a decay scheme; therefore, a few of these are introduced in the discussion sections, where they have more point than they would if one first met them in the general experimental sections.

The most extreme, perhaps one should say blatant, cases of Coriolis interaction and distortion that have yet been encountered occur in the states of Bk<sup>250</sup> and Bk<sup>248</sup> populated by these einsteinium nuclei. Thus, a rather lengthy development and analysis of this interaction is included. Although the basic ideas are not at all new, some of the finer points and applications are either new or unique to these cases, so perhaps we may be forgiven for spending so much time on this subject.

Finally, the logic behind many of the conclusions in the decay schemes is not at all straightforward, and many cross-references and seemingly redundant experiments have been necessary. This has all been duly recorded with the result that the writing may at times seem verbose. However, it should not leave the reader wondering about a missing step or declaring that a particular result was reached in sleight-of-hand fashion.

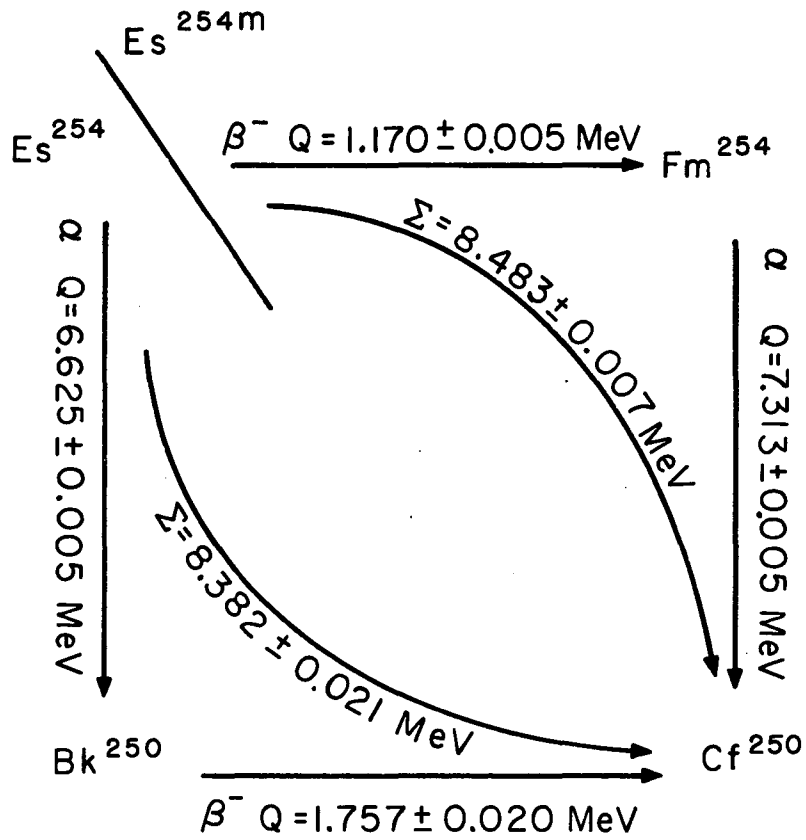
## II. Es<sup>254</sup>

### A. Relation between Es<sup>254</sup> and Es<sup>254m</sup>

Einsteinium-254 exists in two isomeric forms, a beta emitter with a half-life of  $38.5 \pm 1.0$  hours<sup>5,6,7</sup> and an alpha emitter with half-life of approximately 280 days.<sup>8,9</sup> Until the present work there has been no information concerning the relationship of these isomers to each other. This work on the alpha-active isomer, a continuation of work started previously,<sup>10,11</sup> has established that it is the ground-state isomer, the beta-active one thus being Es<sup>254m</sup>. Figure 1 shows the closed cycle by which this was determined. By comparing the sum of the Q's for Es<sup>254m</sup> beta decay ( $1.170 \pm 0.005$  MeV)<sup>7</sup> and Fm<sup>254</sup> alpha decay ( $7.313 \pm 0.005$  MeV)<sup>12</sup> with the sum for Es<sup>254</sup> alpha decay ( $6.625 \pm 0.005$  MeV, this work) and Bk<sup>250</sup> beta decay ( $1.757 \pm 0.020$  MeV),<sup>13</sup> one obtains  $8.483 \pm 0.007$  MeV vs.  $8.382 \pm 0.021$  MeV, respectively. From this one would expect the beta-active Es<sup>254m</sup> to lie  $101 \pm 22$  keV above the ground-state alpha emitter. [N. B. All alpha energies obtained from or quoted in this work have been corrected to the Rytz calibration.]<sup>14</sup>

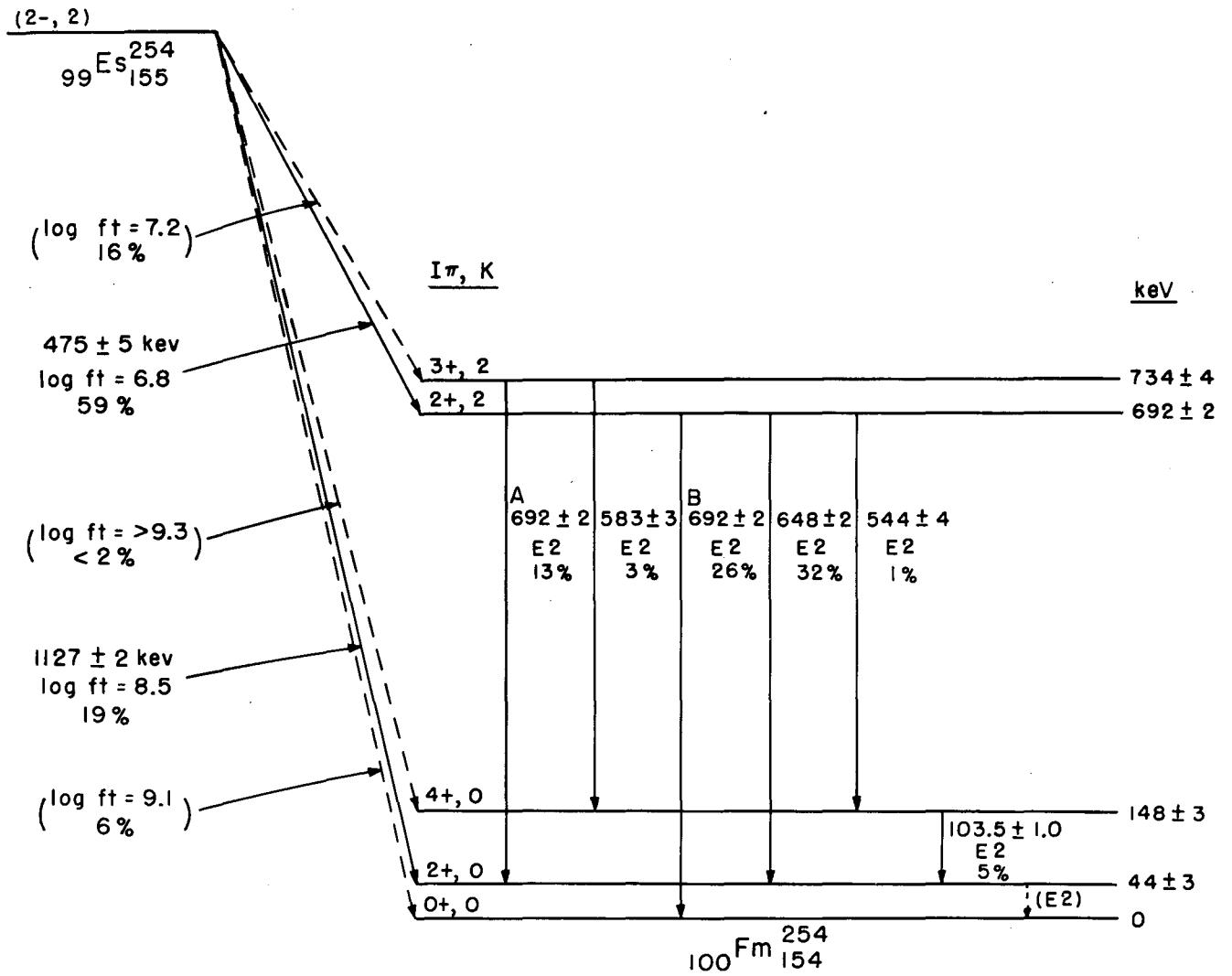
The question arises concerning the possibility of observing the isomeric transition between Es<sup>254m</sup> and Es<sup>254</sup>. Rather complete decay-scheme studies have been made on the beta-active Es<sup>254m</sup>.<sup>7,15,16</sup> Asaro and Perlman<sup>15</sup> and Unik, Day, and Vandenbosch<sup>7</sup> have assigned it a spin of 2, most likely with odd parity. This is based on findings that 59% of its beta decay populates the  $K\pi I = 2+2$  member of the gamma-vibrational band in Fm<sup>254</sup>, 16% populates the 2+3 member, and only 19% populates the 0+2 member of the ground-state rotational band. The respective log ft values are 6.8, 7.2, and 8.5; these and the branching ratios are more consistent with first-forbidden transitions than with second-forbidden (or allowed, for that matter) transitions, which would be necessary if the parity of the Es<sup>254m</sup> ground state were even. These and other aspects of this decay scheme can be seen in Fig. 2.

On the other hand, from the present alpha-spectroscopic studies on Es<sup>254</sup> decay, it has been found to have a high spin, namely  $K\pi I = 7+7$ ,



MU-35133

Fig. 1. The closed cycle by which it was determined that the alpha-emitting species of  $Es^{254}$  is the ground state and the beta-emitting species is the isomeric state.



MUB-1557

Fig. 2. The decay scheme of  $^{254}_{99}\text{Es}$  as determined by Asaro and Perlman<sup>15</sup> and Unik, Day, and Vandenbosch.<sup>7</sup>

resulting from a triplet coupling of the  $\Omega\pi$  [ $N n_Z \Lambda\Sigma$ ] =  $7/2+$  [633  $\uparrow$ ] Nilsson proton state with the  $7/2 +$  [613 $\uparrow$ ] neutron state. Thus, an isomeric transition to the ground state would have to be of E5 multipolarity. Using the Weisskopf estimate,<sup>17</sup> one finds a single-particle half-life of approximately 32y (including conversion) for a 100-keV E5 transition.

In the study of  $\text{Am}^{242m}$  decay<sup>18</sup> and, as will be shown later, in the study of  $\text{Es}^{254}$  and  $\text{Es}^{252}$  decays, there has been great success in predicting the composition of low-lying odd-odd states in terms of the most probable single-particle states available as found in the neighboring odd-mass nuclei. If one explains the  $\text{Es}^{254m}$  assignment of 2- in these terms, we have available a triplet coupling of the  $3/2 -$  [521 $\uparrow$ ] proton state and the  $1/2 +$  [620 $\uparrow$ ] neutron state. This means that this configuration has neither the proton nor the neutron state in common with  $\text{Es}^{254}$ ; the isomerism between  $\text{Es}^{254}$  and  $\text{Es}^{254m}$  is of a different nature from that observed in other odd-odd nuclei such as  $\text{Am}^{242}$ ,  $\text{Am}^{244}$ , and  $\text{Np}^{238}$ , where the isomeric states are the singlet and triplet couplings of the same proton and neutron states.<sup>19</sup> Thus both the proton and the neutron quasi-particle states would have to change in the isomeric transition, making it a so-called double-particle transition. This could easily hinder the transition by two or more orders of magnitude. The maximum branching of  $\text{Es}^{254m}$  decay through this isomeric transition would then be  $1.3 \times 10^{-4}$  (for a 32y  $t_{1/2}$ ) and could be much lower; therefore, it is not at all unreasonable that such a transition would be difficult to observe.

These assignments and the observed decay properties imply that the 0+0 state resulting from singlet coupling of the  $7/2 +$  [633 $\uparrow$ ] proton and the  $7/2 +$  [613 $\uparrow$ ] neutron must lie above the 2-2 state. In a few other odd-odd nuclei the singlet-triplet spacing has been as low as 50 keV; in this case it must be  $>100$  keV.

Investigations were also made on the possibilities of beta branching from  $\text{Es}^{254}$  and alpha branching from  $\text{Es}^{254m}$ . To detect any beta branching from  $\text{Es}^{254}$ , one needs only to look for the 7.200-MeV alpha particles<sup>12</sup> from its daughter,  $\text{Fm}^{254}$ . Since  $\text{Fm}^{254}$  has a 3.24-hr half-life,<sup>20</sup> all of

it resulting from the decay of  $\text{Es}^{254m}$  originally present in the source would have long since decayed (the source was two years old when this investigation was made). We looked for these high-energy alpha particles with a solid-state detector (see Sec. II.B.2. and Fig. 4) and found an upper limit of  $2 \times 10^{-4}$  % at the expected energy, which corresponds to a beta half-life of  $>4 \times 10^5$  years.  $\text{Es}^{254}$  has only 1.07 MeV available for beta decay, and, since high-K states in even-even nuclei result only from breaking pairs of particles, it is unlikely that there are any high-K states below this energy in  $\text{Fm}^{254}$ . One of the lowest known, the  $K = 6$  state in  $\text{Cm}^{244}$  (a singlet coupling of a  $5/2 + [622\uparrow]$  and a  $7/2 + [624\downarrow]$  neutron),<sup>21</sup> lies at 1.042 MeV, and this is below the neutron subshell at 152 neutrons. The neutron energy gap should be raised, if anything, when the abundance of neutron states just above the subshell contributes to the pairing correlation,<sup>22</sup> and the proton energy gap is expected to be greater than the neutron energy gap.

Beta decay to the  $6+$  member of the ground-state ( $K = 0$ ) band or to a comparable member of the gamma-vibrational ( $K = 2$ ) band would be slower than the observed upper limit, hence consistent with it.

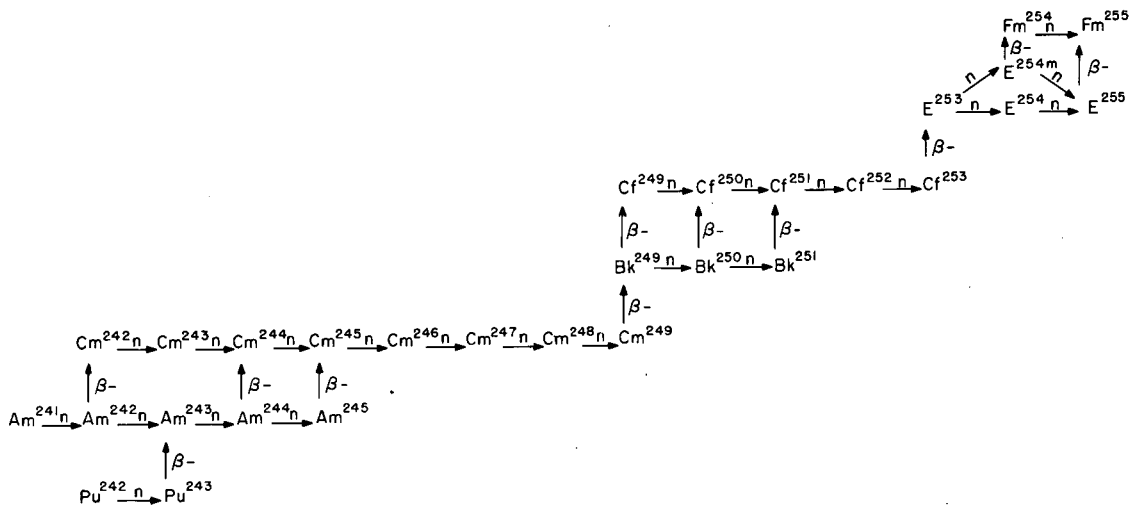
There remains the question of alpha branching from  $\text{Es}^{254m}$ . Since the ground state of  $\text{Bk}^{250}$  most likely has the same intrinsic configuration as  $\text{Es}^{254m}$  (see Sec. II.C.2.), the favored alpha decay should be to this state. These alpha particles could be expected to have an energy of  $6.62 \pm 0.02$  MeV. For a hindrance factor the same as in  $\text{Es}^{254}$  favored decay, the alpha branching should be approximately three per cent of the total  $\text{Es}^{254m}$  decay. We made a cursory search for these alpha particles with the magnetic spectrograph but did not see them. Unfortunately, with available neutron fluxes ( $3 \times 10^{14}$  neutrons/cm<sup>2</sup>-sec) the maximum  $\text{Es}^{254m}$  activity (total activity) that one can prepare is one to two per cent of the activity of the  $\text{Es}^{253}$  used as a target. This isotope has a principal alpha energy of 6.640 MeV and quite effectively conceals any  $\text{Es}^{254m}$  alphas that might be present. It would be worthwhile to prepare  $\text{Es}^{254m}$  by a method that would minimize the  $\text{Es}^{253}$  and perhaps use an isotope separator to purify it further, because, if it does produce alpha groups, they should populate levels in  $\text{Bk}^{250}$  with somewhat lower spins than are populated by  $\text{Es}^{254}$  alpha groups.

## B. Experimental Procedure

### 1. Source Preparation

The sources of  $\text{Es}^{254}$  used in this work were prepared as part of the Lawrence Radiation Laboratory heavy-element program; in this case mixed targets of  $\text{Pu}^{242}$  and  $\text{Am}^{241}$  were irradiated for as long as two years at an average flux of  $4 \times 10^{14}$  thermal neutrons/cm<sup>2</sup>-sec in the Materials Testing Reactor, Idaho Falls, Idaho. Figure 3 shows the path of build-up for the einsteinium and other heavy-actinide activities. Because of the intense radiation levels involved, the initial chemical separations and purifications were performed by remote control in water-shielded "caves."<sup>23</sup> A fraction consisting of the californium and higher actinides was first separated from the lower actinides and fission products (except for the heavy lanthanides) by a procedure described elsewhere.<sup>24</sup> The einsteinium was then separated from the californium by means of cation exchange, using  $\alpha$ -hydroxy isobutyric acid as eluant.<sup>25</sup> Extraneous mass (i.e., any foreign ions) was removed by means of an HCl anion-exchange "clean-up" column.<sup>26</sup> The einsteinium fraction thus consisted initially of  $\text{Es}^{253}$ ,  $\text{Es}^{254}$ ,  $\text{Es}^{254m}$ , and  $\text{Es}^{255}$ , with small amounts of californium remaining in the sample; fermium and californium activities also grew in rather quickly from the einsteinium decays. The  $\text{Es}^{254}$  was obtained in reasonably pure isotopic form simply by allowing the sample to age until the other einsteinium activities had decayed out, approximately a year from the time it was removed from the reactor. It was then necessary to separate out the considerable  $\text{Cf}^{249}$  (daughter of  $\text{Es}^{253}$ ) and  $\text{Cf}^{250}$  (granddaughter of  $\text{Es}^{254}$  and  $\text{Es}^{254m}$ ) that had grown in, as well as the small amount of  $\text{Cf}^{252}$  and fermium remaining in the sample; this was done with another  $\alpha$ -hydroxy-isobutyric-acid cation-exchange column, followed by several "clean-up" columns. This left  $\text{Bk}^{250}$ , a 193-min<sup>13</sup> beta emitter essentially in secular equilibrium with its  $\text{Es}^{254}$  parent, and a lanthanide activity, thought to be primarily  $\text{Tb}^{160}$ , as the only appreciable contaminants. For the alpha spectroscopy the sources were prepared from the  $\text{Es}^{254}$  in this form, although for later quantitative





MU-35134

Fig. 3. The path of build-up for producing einsteinium by successive neutron captures on lower actinides.

gamma measurements the lanthanide activity was removed by means of an alcoholic-HCl cation-exchange column.<sup>27</sup>

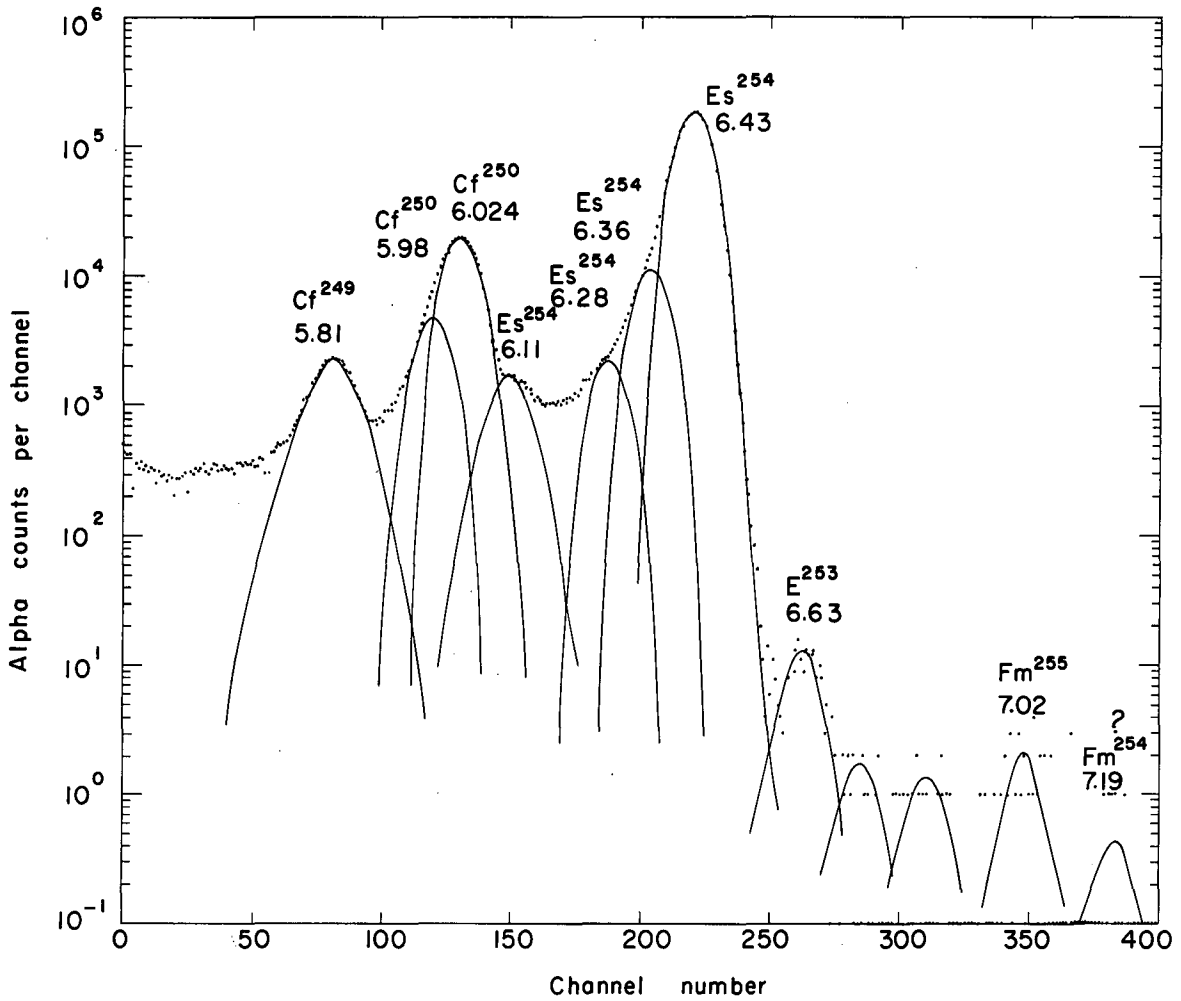
The sources used for alpha spectroscopy were vaporized in vacuo from a white-hot tungsten filament-through onto a cold platinum plate. The activity was deposited in a narrow line, 0.02-inch  $\times$  0.75-inch. For the permanent-magnet electron spectrograph the Es<sup>254</sup> was similarly vaporized onto one side of a 0.02-inch diameter platinum wire, the activity again being deposited for a length of 0.75 inch. For the L-x-ray coincidence studies a special source was prepared by vaporizing the activity onto a 0.001-inch thick nickel backing. And for L-x-ray intensity measurements, coincidences, and M-electron studies using a windowless proportional counter, sources were prepared by drying small amounts of Es<sup>254</sup> (chloride) in water solution on 0.001-inch thick aluminized Mylar films.

The sources used ranged in activity from fewer than 1000 dis/min for some time-to-height coincidence measurements involving long ramp sweeps to  $6 \times 10^5$  dis/min for the permanent-magnet electron-spectrograph measurements.

## 2. Alpha Spectroscopy

Two separate methods were used to obtain alpha spectra of Es<sup>254</sup>. The first of these, for high efficiency, was the use of solid-state alpha detectors consisting of gold-doped silicon crystals. They had efficiencies of up to 30%, depending upon the size of the detector and the geometry of the counting arrangement. Signals from these detectors were fed through biased amplifiers and displayed on 400-channel pulse-height analyzers. The best resolution we were able to obtain with our Es<sup>254</sup> source was 30 keV (full width of peak at half maximum).

Figure 4 shows an alpha spectrum obtained with a gold-doped, lithium-drifted, 0.5-cm square, 0.5-mm thick, silicon detector, using 30-V bias. It covers the energy range 5.6-7.2 MeV and is a 72-hr run. In addition to showing the detailed composition of the sample, this spectrum was taken to look for the presence of Fm<sup>254</sup> as discussed in Sec. II.A. The species present and their relative intensities are listed in Table I. The energy calibration for this spectrum, as for all the



MUB-5129

Fig. 4. Es<sup>254</sup> alpha-particle spectrum taken with a solid-state alpha detector. This spectrum covers the energy range 5.6-7.2 MeV and shows the detailed composition of the sources used in the higher-resolution spectra. Zero events are plotted at one-tenth. Energies of alpha groups are given in MeV.

solid-state alpha spectra, was obtained by normalizing a pulser-generated energy-vs-channel-number straight line to at least three peaks from known alpha standards such as Am<sup>241</sup>, Cm<sup>243</sup>, Cf<sup>250</sup>, or Es<sup>253</sup>.

As a corollary to this "wide-range" alpha spectrum and the search for Fm<sup>254</sup>, we were able to obtain a new value for the half-life of Es<sup>255</sup>. It can be seen from Fig. 4 and Table I. that Fm<sup>255</sup> was present to the extent of 0.001%. Since the source at this time was two years old and Fm<sup>255</sup> itself has a half-life of 21.5 hr,<sup>28</sup> its presence in the sample could be due only to its longer-lived parent, Es<sup>255</sup>. Although the peak assigned to Fm<sup>255</sup> in Fig. 4 appears at the correct energy and has the spread toward higher energies that is characteristic of Fm<sup>255</sup> (due to pile-up from the many conversion electrons from its decay),<sup>12</sup> the fermium was separated chemically from the einsteinium fraction by means of an  $\alpha$ -hydroxy-isobutyric-acid cation-exchange column, and its decay was followed for a week in a Frisch grid chamber to make sure it decayed with the Fm<sup>255</sup> half-life. Agreement was good, and, from knowing the composition of the original source immediately after it left the reactor, we were able to calculate a half-life of  $38 \pm 3$  days for Es<sup>255</sup>. This is somewhat longer than the previously reported half-lives of 30 days,<sup>29,30</sup> and  $24 \pm 2$  days.<sup>28</sup>

The spectrum shown in Fig. 5. was obtained with a silicon alpha detector similar to the one used to obtain the spectrum in Fig. 4. This was a 40-hr run, using a source with approximately  $2 \times 10^4$  alpha dis/min. In it the Es<sup>254</sup> alpha groups are shown on a much more expanded scale than in Fig. 4. It can be seen, of course, that practically every group is complex, but, since this spectrum furnishes very good statistics, the intensities of these complex groups, given in Table II., are a good corroboration of the summed intensities of their component peaks as obtained with the magnetic alpha spectrograph.

After the source had gone through a number of chemical processes to remove the californium, fermium, and lanthanide impurities, and after all the gamma-ray and magnetic-spectrograph alpha spectroscopy had been completed, further alpha spectra were taken with solid-state detectors. They are not shown, since they look very much like Figs. 4 or 5, but they

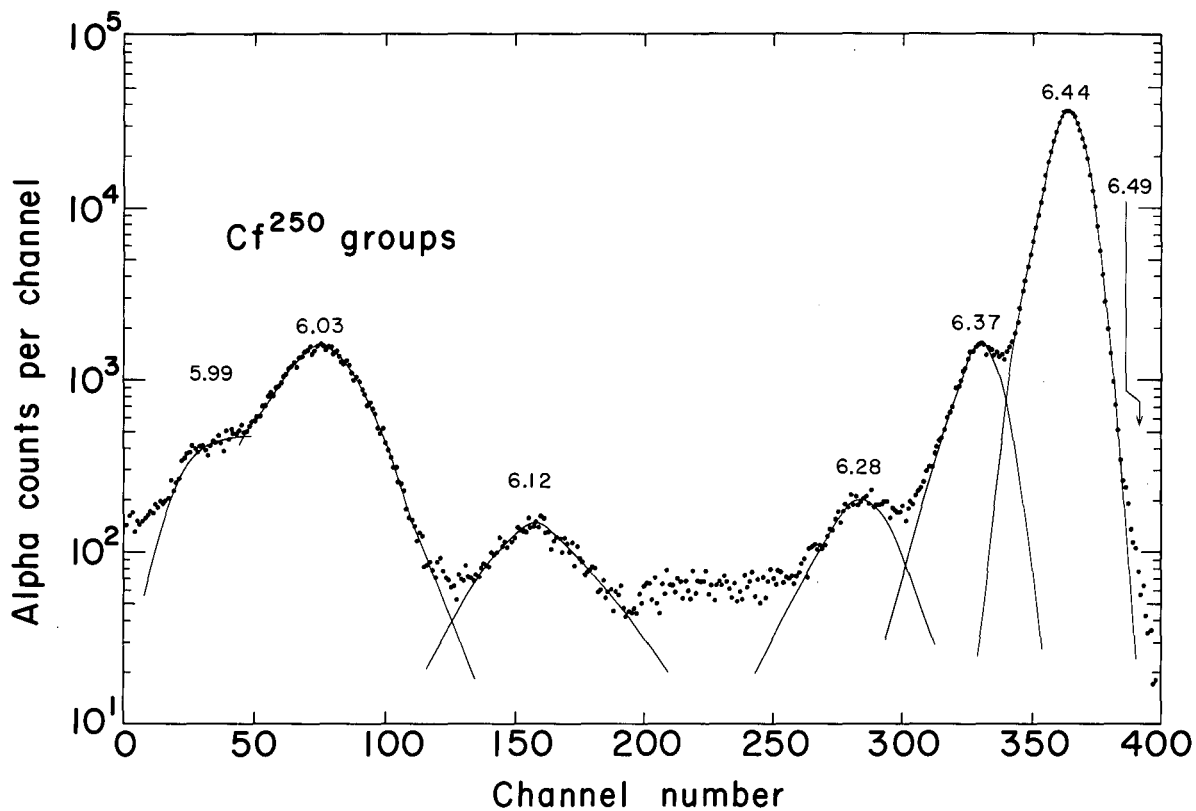
Table I. Activities present in the  $\text{Es}^{254}$  source used for alpha spectroscopy; obtained from Fig. 4.

Alpha energy (MeV)	Nuclide	Half-life	Amount present (%)
5.81, etc. (Ref. 31)	$\text{Cf}^{249}$	360 y (Ref. 32)	1.27
5.99 6.03 (Ref. 33)	$\text{Cf}^{250}$	10.9 y	10.7 <sup>a</sup>
6.11 6.29 6.37 6.44, etc.	$\text{Es}^{254}$	280 d (Ref. 8,9)	87.2
6.64 (Ref. 34)	$\text{Es}^{253}$	20.03 d (Ref. 28)	0.006
7.03 (Ref. 12)	$\text{Fm}^{255}$	"35 d" <sup>b</sup>	0.001
7.20 ? (Ref. 12)	$\text{Fm}^{254}$	"280 d" <sup>c</sup>	$\leq 0.0002$

<sup>a</sup> $\text{Cf}^{250}$  is growing in continuously as the granddaughter of  $\text{Es}^{254}$ ; therefore, its relative intensity will be always increasing.

<sup>b</sup> $\text{Fm}^{255}$  is essentially in secular equilibrium with its parent,  $\text{Es}^{255}$ , and thus exhibits the half-life of the latter.

<sup>c</sup>Similarly,  $\text{Fm}^{254}$ , if present, would exhibit the half-life of  $\text{Es}^{254}$ .



MU-36134

Fig. 5. Es<sup>254</sup> alpha-particle spectrum taken with a solid-state alpha detector. This spectrum covers the energy range 5.9-6.5 MeV and shows the composite Es<sup>254</sup> peaks spread out as much as was possible with a high-geometry silicon detector. The "resolved" curves do not separate the peaks into their components or follow any standard peak shape; they merely indicate the areas integrated to obtain the intensities of Table II.

Table II. Relative intensities of the various (complex) alpha groups from  $\text{Es}^{254}$ ; obtained from Fig. 5.

Alpha energy of principal component (MeV)	Relative intensity (%)
6.44	95.4
6.37	3.6
6.28	0.4
6.12	0.6
Cf <sup>250</sup> groups (6.03, 5.99)	12.2 <sup>a</sup>

<sup>a</sup>Relative to all  $\text{Es}^{254}$  groups = 100%.

furnished proof that the relative intensities of what had been assigned as  $\text{Es}^{254}$  peaks did not change either when the californium was removed or as a function of time. In particular, it should be noted that, although the group at 6.12 MeV is very close to the  $\text{Cf}^{252}$  ground-state alpha group,<sup>33</sup> its relative intensity did not change when the californium was removed. The source was also counted for its spontaneous fission content immediately after the magnetic-spectrograph runs. It was found that the  $\text{Cf}^{250}$  in the source, having an  $\alpha/\text{SF}$  ratio of  $1330 \pm 45$ ,<sup>35</sup> accounted very satisfactorily for all the fission events we found, another fact against the 6.12-MeV group being all or part  $\text{Cf}^{252}$ . (The  $\text{Es}^{254}$   $\alpha/\text{SF}$  ratio is discussed at the end of this section.)

The second tool for obtaining alpha spectra, for high-resolution, was a  $180^\circ$  double-focussing magnetic spectrograph, which has been discussed in many other places.<sup>36-38</sup> Suffice it to say that this instrument has an optical radius of 35 cm and has an inhomogeneous field in such a manner as to produce vertical as well as horizontal focussing. Thus, one gets an approximate picture of the source at the detector or place, and the widest or worst part of the source no longer is the limiting factor in resolution. The transmission is also increased, in this instrument being approximately  $5 \times 10^{-4}$  of  $4\pi$ . Individual tracks left by the alpha particles on a nuclear-emulsion photographic plate were counted with the aid of a microscope. The resolutions we obtained were around 10 keV, with the limiting factor generally being the source itself. In order to minimize low-energy tailing due to self-absorption in the source, the source must be made essentially "massless." This is the reason for going to chemical extremes to purify the activity and for vaporizing the activity onto the backing plate rather than depositing it in some more efficient fashion. We had so little  $\text{Es}^{254}$  that it was not feasible to make repeated vaporizations until an optimum source was obtained. Because of the relatively weak sources it was also necessary to make long exposures, on the order of ten days; during this period the current in the electromagnet had to be kept quite constant, and some broadening of the peaks may have been due to small, momentary current



drifts. Since best resolution was obtainable only near the middle of each plate, two spectra are shown. In Fig. 6 the alpha groups from favored decay are centered for best resolution, while in Fig. 7 the groups populating higher-lying states in  $\text{Bk}^{250}$  are centered. The energy scale for these spectra is roughly linear; the actual energies of the groups were explicitly calculated to a calibration determined by Asaro and Pilger.<sup>37</sup> The best energies and intensities obtained from these two spectra are listed in Table III. Both the 6.437-MeV group<sup>39</sup> from  $\text{Es}^{254}$  and the 6.031-MeV group<sup>33</sup> from  $\text{Cf}^{250}$  were used as standards, the energies of the other groups being calculated relative to the nearer of these two. A separate spectrum was taken having the  $\text{Cf}^{250}$  group centered so as to obtain a standard peak shape (known not to be complex) that aided in resolving small peaks from large ones, such as the 6.424-MeV from the 6.437-MeV one.

Related to and perhaps best discussed under the alpha-spectroscopy section was a determination of the spontaneous-fission half-life of  $\text{Es}^{254}$ . This was prompted by the announcement of the discovery of isomer(s) of  $\text{Am}^{242}$  with extremely short (msec) spontaneous-fission half-lives.<sup>40</sup> There has been no satisfactory explanation for such extremely short spontaneous-fission half-lives, but it was wondered if perhaps the isomer(s) involved had a very large spin that produced a centrifugal aid to fission. Since  $\text{Es}^{254}$  was known to have a large spin, we made a careful determination of its spontaneous-fission half-life to determine whether or not its spin has any noticeable effect on shortening its half-life over what would be predicted by systematics. A source containing 754 alpha c/min was very carefully freed from californium contamination by  $\alpha$ -hydroxy-isobutyric-acid cation exchange. It was then counted for 171.5 hr in the same proportional counter used to count alphas but now with a plateau voltage to count only fissions. During this time we obtained 111 pulses, of which 8 could be attributed to  $\text{Cf}^{250}$  growing in. Thus, the  $\alpha/\text{SF}$  ratio for  $\text{Es}^{254}$  was found to be  $88,700 \pm 1200$ , yielding a half-life for spontaneous fission of approximately  $6.8 \times 10^5$  yr. This is a little longer than the value of  $1.5 \times 10^5$  yr. reported by Ghiorso<sup>41</sup> in 1955, and it seems as if

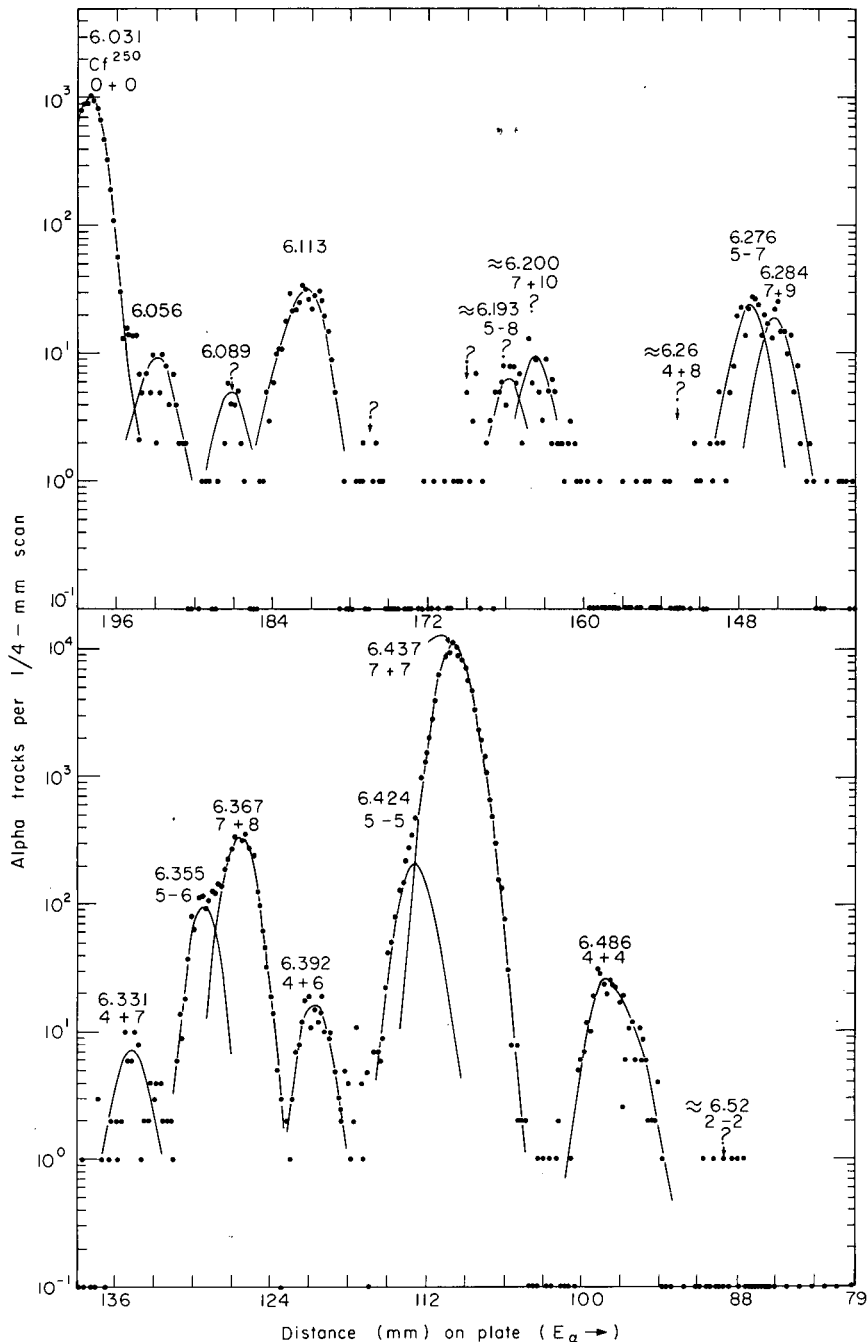
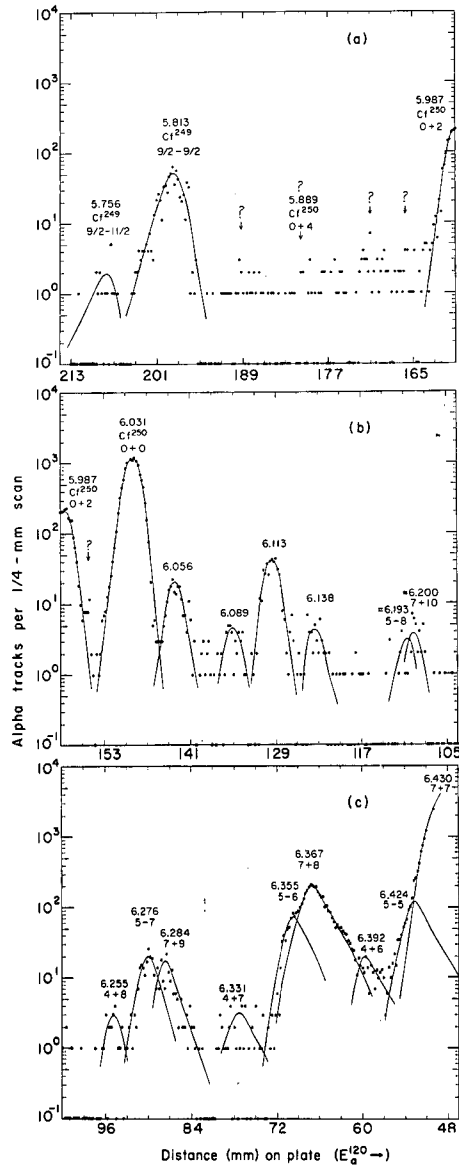


Fig. 6.  $Es^{254}$  alpha-particle spectrum taken with a double-focussing magnetic spectrograph. In this spectrum the alpha groups resulting from favored decay are centered for best resolution. Zero events are plotted at one-tenth. Energies of alpha groups are given in MeV.



MU-36133

Fig. 7.  $Es^{254}$  alpha-particle spectrum taken with a double-focussing magnetic spectrograph. In this spectrum the alpha groups populating higher-lying levels in  $Bk^{250}$  are centered for best resolution. Zero events are plotted at one-tenth. Energies of alpha groups are given in MeV.

Table III. Es<sup>254</sup> alpha groups and their intensities; obtained from the high-resolution magnetic-spectrograph runs shown in Figs. 6 and 7.

Alpha-particle energy (MeV)	Intensity (%)	Excited-state energy <sup>a</sup> (keV)
6.524 ± 0.010	0.005	0 (e <sup>-</sup> )
6.486 ± 0.005	0.27	35.5 (e <sup>-</sup> )
6.437 ± 0.005	93.0	85.5
6.424 ± 0.005	1.71	99 (γ,α)
6.392 ± 0.005	0.13	131
6.367 ± 0.005	2.91	155.9 (e <sup>-</sup> )
6.355 ± 0.005	0.74	169 (γ,e <sup>-</sup> )
6.331 ± 0.005	0.05	193
6.284 ± 0.005	0.16	241 (e <sup>-</sup> ,α)
6.276 ± 0.005	0.22	249 (γ,α,e <sup>-</sup> )
6.255 ± 0.010	0.01	270
6.200 ± 0.010	0.05	327 (α,syst.)
6.193 ± 0.010	0.08	334 (α,syst.)
6.18 ± 0.01 ?	≈ 0.02	≈ 345
6.14 ± 0.01	≈ 0.05	≈ 390
6.113 ± 0.005	0.33	416 (γ,α)
6.089 ± 0.005	0.08	434 (γ)
6.068 ± 0.005	0.16	473 (γ,α)
6.00 ± 0.02 <sup>b</sup>	0.03 <sup>b</sup>	≈ 538 (γ)

<sup>a</sup>Although the alpha-particle spectra were the basis for determining these energies, in most cases the precision was improved by considering other measurements. The symbols in parentheses indicate the measurements considered in each level-energy determination: (e<sup>-</sup>), permanent-magnet electron spectra; (γ), solid-state gamma spectra; (γ,α), solid-state gamma spectra aided by magnetic-spectrograph alpha; (α,syst.), rotational-band systematics used to aid in resolving alpha spectrum; etc.

<sup>b</sup>This group was masked by Cf<sup>250</sup>; it was obtained from the coincidence experiment discussed in Sec. II.B.4.

the spin has little or no effect on spontaneous fission of Es<sup>254</sup>.

### 3. Electron Spectroscopy

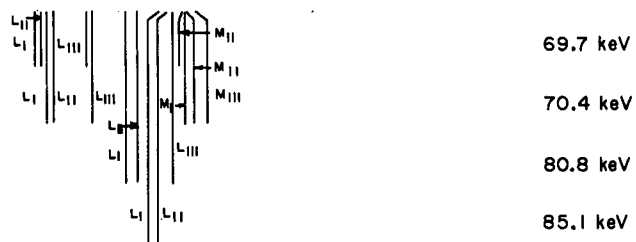
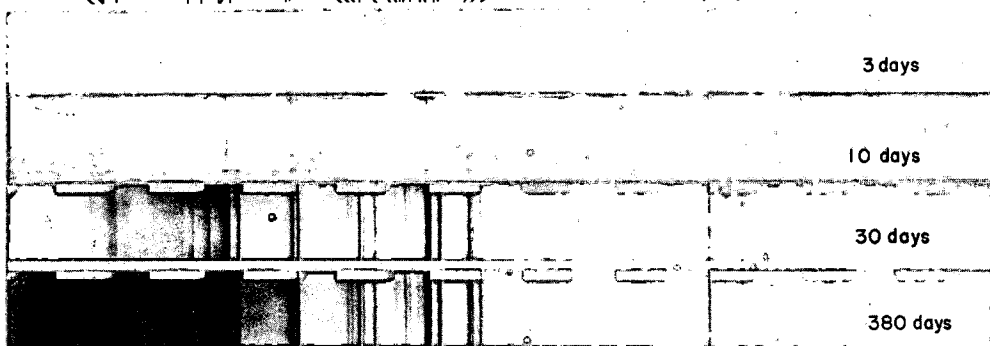
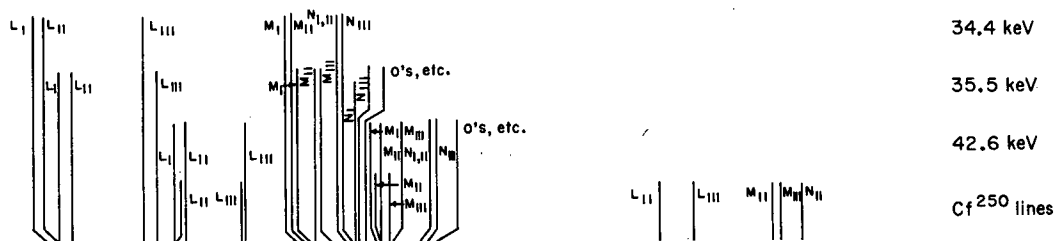
The conversion-electron spectra were measured primarily with a 180° permanent-magnet spectrograph having a uniform 100-gauss field.<sup>42</sup> A 0.020-inch-diameter platinum wire having the Es<sup>254</sup> vaporized on one side served as the source. Since the instrument had no vertical focussing, the transmission changed as a function of energy, becoming smaller at higher energies where the longer paths taken by the electrons from source to plate represent smaller solid angles; for the energies with which we were concerned, the transmission varied in the range of  $10^{-5}$  -  $10^{-4}$  of  $4\pi$ . Exposures of 3, 10, 30, and 380 days were made with our source, which contained  $6 \times 10^4$  alpha dis/min initially. Photographs of the plates from these exposures are shown in Fig. 8, where the lines assigned to seven transitions (and the Cf<sup>250</sup> lines from Bk<sup>250</sup> decay) are indicated; the width of a typical line was 0.1 keV. The position of a line was read from its high-energy side to eliminate low-energy tailing, and these positions were converted into Bp by means of a quadratic virial equation,

$$(Bp)^2 = a + b\Delta x + c(\Delta x)^2,$$

where  $\Delta x$  is the distance of the line from a standard reference point on the plate; the constants in this equation were evaluated with lines from Es<sup>253</sup> and Am<sup>241</sup> sources prepared in an identical manner.<sup>34, 43, 44</sup> The Bp were converted into energies with the tables of Breivogel and Holtz.<sup>45</sup> These energies are expected to be precise to  $\approx 0.2\%$ .

In Table IV. the electron lines are listed with their assignments and approximate relative intensities. The precise electron binding energies determined by Hollander, et al.,<sup>46</sup> for berkelium were used to obtain the energies of the transitions themselves. The seven transitions listed are rather clear due to the number of lines observed for each of them. Other much-less-certain transitions possibly can be identified using some of the unassigned lines, and, of course, some of the low-energy unassigned lines belong to Auger electrons.

Fig. 8. The conversion-electron lines for  $\text{Es}^{254}$  decay obtained with a uniform-field, permanent-magnet spectrograph. Increasing energy is toward the right on each plate. The energies listed are the gamma-transition energies of the transitions to which these conversion lines have been assigned. Each line is identified as to subshell just opposite the level where the transition energy is listed.



ZN-4908

Multipolarity assignments can be made reasonably unambiguously merely from a knowledge of the subshell conversion ratios, i.e., without knowing much about the absolute conversion coefficients. This comes about because each multipolarity in this energy region converts among the various subshells in a rather individual pattern. For example, E1 transitions convert in all three L subshells in approximately equal amounts; M1 transitions convert primarily in the  $L_I$  subshell; E2 transitions convert in the  $L_{II}$  and  $L_{III}$  subshells in approximately equal amounts, much less in the  $L_I$  subshell; and M2 transitions convert in the  $L_I$  and  $L_{III}$  subshells in approximately equal amounts, much less in the  $L_{II}$  subshell. The ratios among the  $M_I$ ,  $M_{II}$ , and  $M_{III}$  subshells are analogous to those among the corresponding L subshells, etc.<sup>47</sup> Such multipolarity assignments have been made and are listed in Table IV. It is perhaps worth pointing out that the M2 assignment for the 35.5-keV transition is quite strongly indicated by the unusual ratios involved. A combined M1-E2 transition would, of course, convert approximately equally in all three subshells as would an E1, but E1 transitions are easily ruled out for the M1-E2 assignments in Table IV. E1 transitions would have low ( $\approx 0.3-0.6$ ) overall conversion coefficients, so one would have to see a large portion of photons for these transitions if they were E1. In fact, we saw no photons for any other than the 42.6-keV one (see Sec. II. B.5.b.), and its intensity (0.3%) was quite consistent with an M1-E2 assignment.

It will be seen in Sec. II.B.4. that  $Es^{254}$  has a number of higher-energy (200-400 keV), low-intensity gamma-rays. Looking for their conversion electrons with the permanent-magnet spectrograph was out of the question because of its low transmission. We observed them with a TMC lithium-drifted silicon electron detector, 2-cm diameter  $\times$  2-mm thick, with a 0.5-micron window (estimated energy-loss for electrons in the energy range of interest was 4 keV). Since the beta decay of  $Bk^{250}$  in the source created a high background, a fast-slow coincidence circuit (described in Sec. II.B.4.) was used; alpha pulses from a silicon alpha detector were used as gates. The source was 800 c/min  $Es^{254}$  dried on a



Table IV. Electron lines from Es<sup>254</sup>.

Electron energy (keV)	Subshell	Binding energy <sup>a</sup> (keV)	Gamma-ray energy (keV)	Relative electron intensity <sup>b</sup> (%)	Transition intensity (%)
9.18	L <sub>I</sub>	25.28	34.46	VW	
10.04	L <sub>II</sub>	24.39	34.43	M	
14.93	L <sub>III</sub>	19.45	34.38	W	
27.81	M <sub>I</sub>	6.56	34.37	W	
28.22	M <sub>II</sub>	6.15	34.37	W	
masked	M <sub>III</sub>	-----	-----	-----	
32.74	N <sub>I</sub> <sup>c</sup>				
	N <sub>II</sub> <sup>c</sup>	1.57 <sup>d</sup>	34.31	VVW	
33.20	N <sub>III</sub>	1.26 <sup>d</sup>	34.46	VVWV	
		Best Value	34.4 M1-E2		≈30
10.24	L <sub>I</sub>	25.28	35.52	M	
≈10.87	L <sub>II</sub>	24.39	≈35.3	VVW	
16.05	L <sub>III</sub>	19.45	35.50	MS	
28.95	M <sub>I</sub>	6.56	35.51	MS	
29.42	M <sub>II</sub>	6.15	35.57	MW	
30.54	M <sub>III</sub>	4.98	35.52	M	
33.80	N <sub>I</sub>	1.76	35.56	W	
34.32	N <sub>III</sub>	1.26 <sup>d</sup>	35.58	VW	
35.15	O's, etc.	≈0.39 <sup>d</sup>	≈35.54	VVW	
		Best Value	35.5 M2		≈70
17.36	L <sub>I</sub>	25.28	42.64	VS	
18.19	L <sub>II</sub>	24.39	42.58	MS-S	
23.18	L <sub>III</sub>	19.45	42.63	MS	
36.17	M <sub>I</sub>	6.56	42.73	VS	
36.55	M <sub>II</sub>	6.15	42.70	MS	
37.61	M <sub>III</sub>	4.98	42.59	S	

Table IV. (Cont.)

Electron energy (keV)	Subshell	Binding energy <sup>a</sup> (keV)	Gamma-ray energy (keV)	Relative electron intensity <sup>b</sup> (%)	Transition intensity (%)
41.02	N <sub>I</sub> <sup>c</sup>				
	N <sub>II</sub> <sup>c</sup>	1.57 <sup>d</sup>	42.59	MS	
41.41	N <sub>III</sub>	1.26 <sup>d</sup>	42.67	W-MW	
42.39	O's, etc.	≈0.39 <sup>d</sup>	≈42.78	MW	
		Best Value	42.6 M1-E2		100
≈44.5	L <sub>I</sub>	25.28	≈69.8	VVVW	
≈45.4	L <sub>II</sub>	24.39	≈69.8	VVW	
50.27	L <sub>III</sub>	19.45	69.72	VW	
63.51	M <sub>II</sub>	6.15	69.66	VVVW	
		Best Value	69.7 (M1)-E2		≈ 1
45.15	L <sub>I</sub>	25.28	70.43	W	
45.94	L <sub>II</sub>	24.39	70.33	MW	
50.90	L <sub>III</sub>	19.45	70.35	MW	
63.90	M <sub>I</sub>	6.56	70.46	VVVW	
64.30	M <sub>II</sub>	6.15	70.45	VW	
≈65.2	M <sub>III</sub>	4.98	≈70.2	VVW	
		Best Value	70.4 M1-E2		≈ 3
55.60	L <sub>I</sub>	25.28	80.88	VVW	
56.45	L <sub>II</sub>	24.39	80.84	VVW	
≈61.54	L <sub>III</sub>	19.45	≈81.0	VVW	
		Best Value	80.9 M1-E2		< 1
59.90	L <sub>I</sub>	25.28	85.2	VVVW	
60.77	L <sub>II</sub>	24.39	85.2	VVVW	
		Best Value	85.2 (M1-E2)		<<1

---

---

<sup>a</sup>J. M. Hollander, M. D. Holtz, T. Novakov, and R. L. Graham,  
Ark. Fys. 28, 375 (1965).

<sup>b</sup>W = weak, S = strong, V = very, M = moderately.

<sup>c</sup>The  $N_{\text{I}}$  and  $N_{\text{II}}$  lines were too close together to be resolved well;  
since the lines were read from the high energy edge, the two lines were  
given the  $N_{\text{II}}$  position. Hence, the  $N_{\text{II}}$  binding energy is used.

<sup>d</sup>Extrapolated from Ref. a.

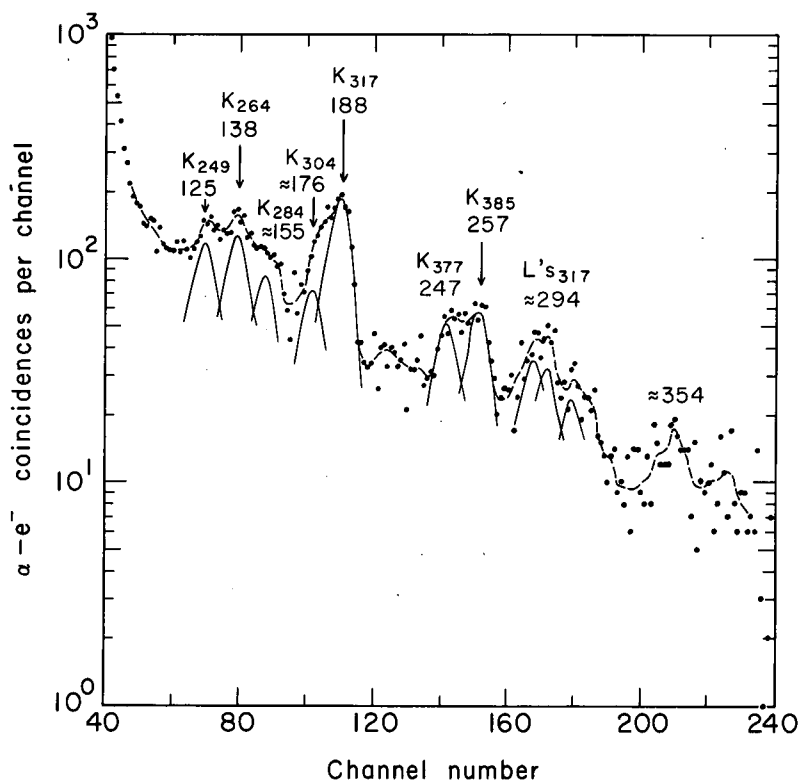
---

---

0.001-inch-thick Mylar film. This was so mounted that the electrons could reach their detector directly, while the alphas had to penetrate the film to reach theirs. Such a spectrum of electrons in fast (100 nsec resolving time) coincidence with all alphas is shown in Fig. 9. The energies and intensities of the K-conversion electrons seen in this spectrum are listed in Table V. For an energy and intensity standard  $\text{Cm}^{243}$  was used.<sup>48</sup> However, it must be emphasized that the intensities given in Table V could contain an error of up to 40%. Preparing and mounting the standard and the source to give reproducible results proved to be somewhat of a problem, but the biggest source of possible error is that the rather poor resolution ( $\approx 6\%$ ) that this detector yielded makes it difficult to resolve the peaks of Fig. 9 very precisely. The precise energies of the gamma-rays involved and standard peak shapes aided in resolving them into the correct components energy-wise, but this left the intensities somewhat uncertain. The significance of these conversion electrons and the conversion coefficients of the transitions will be discussed in Sec. II.C.5.

#### 4. Gamma-ray Spectroscopy

Two methods for detecting gamma rays were used. In Fig. 10 is a gamma spectrum obtained with a 3-inch  $\times$  3-inch NaI (Tl activated) scintillator mounted on a Dumont 6363 photomultiplier tube. In Fig. 11 is a similar spectrum obtained with a Li-drifted germanium detector. In both spectra the gamma rays were counted in coincidence with alphas detected by a ZnS-screened photomultiplier tube (Dumont 6292). Since the  $\text{Bk}^{250}$  in equilibrium in the source produces a 990-1032-keV gamma-ray complex in 86% abundance,<sup>13</sup> it was necessary to resort to fast coincidence techniques to eliminate this background. We used the Berkeley-built 11X-198 Linear Amplifier System,<sup>49</sup> and a block diagram of our method of employing it is shown in Fig. 12. This apparatus uses a "crossover" circuit to generate the fast-coincidence pulses from the crossover points on the slower pulses from the linear amplifiers, thus eliminating the need for wide-band amplifiers in the fast-coincidence circuits. We used resolving times of 100 nsec for the spectra shown.



MU-36066

Fig. 9. Conversion-electron spectrum of the low-intensity, higher-energy (200-400 keV) transitions in  $Es^{254}$  decay; obtained in fast (100 nsec resolving time) coincidence with all alphas from  $Es^{254}$ . The electron detector was a lithium-drifted silicon crystal. Energies are given in keV.

Table V. K-conversion electrons of the low-intensity, higher-energy (200-400 keV) transitions in  $\text{Bk}^{250}$  resulting from  $\text{Es}^{254}$  alpha decay. Obtained from Fig. 9.

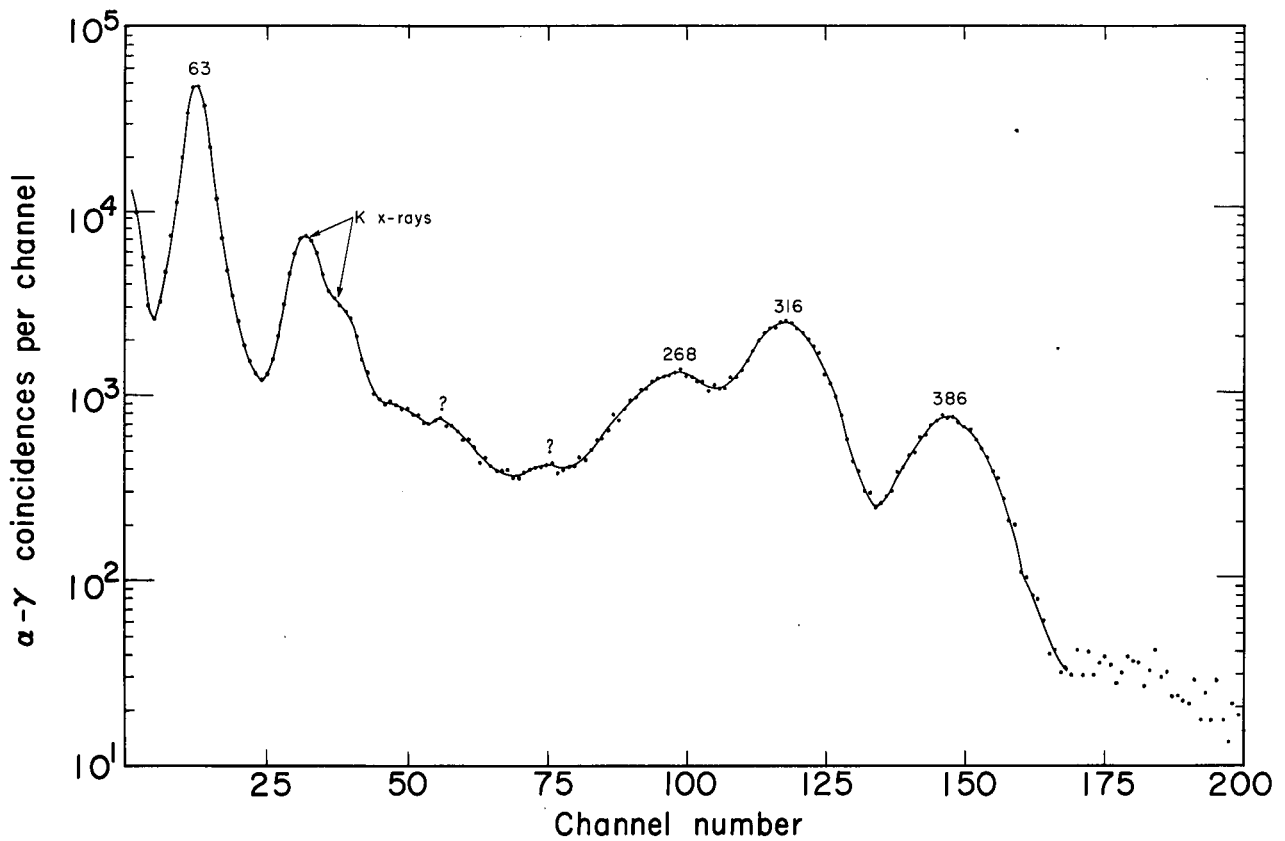
Electron <sup>a</sup> energy (keV)	Gamma-ray <sup>a</sup> energy (keV)	Electron <sup>b</sup> intensity (%)
125	249	0.04
138	264	0.06
≈155	284 (278?) incl.	≈0.025
≈176	304	0.04
188	317	0.15
247	377	0.02
257	385	0.04

<sup>a</sup>The electron energies are precise to about  $\pm 5$  keV except for the lowest ones, which may have errors of around  $\pm 8$  keV. Thus, for the gamma-ray energies and assignments the more precise numbers from Table VI are used.

<sup>b</sup>The intensities carry possible errors of about  $\pm 40\%$ .

By comparing Fig. 11 with Fig. 10 it can be seen that Li-drifted Ge detectors offer startling advances in resolution over NaI scintillators. For instance, the resolution for the 317-keV peak in Fig. 11 is somewhat less than 6-keV, or 1.8%, and we have obtained resolutions as good as 4-keV in this energy region — while in Fig. 10 the same peak is immersed in a sea of neighbors. The lithium-drifting technique starts with a "standard" p-n junction detector, i.e., a piece of p-germanium (boron acceptor) that has been doped on one surface with a donor (gallium) to produce a thin n-germanium layer. Lithium is then diffused into the detector from this side at elevated temperatures. At this point the depletion layer has moved farther into the crystal, but it is still narrow, being that small region where lithium (donor) just balances the holes produced by the acceptor. If then a reverse bias is applied at a temperature around 150° C, an ion-drift of lithium takes place, and lithium ions are transferred from the lithium-excess side of the junction to the lithium-deficient side so as to make the lithium donor almost exactly balance the acceptor over a wide region.<sup>50</sup> Thus, there is a thick depletion layer of almost intrinsic germanium, and the efficiency of the detectors for gamma rays becomes high enough to make them practicable as gamma detectors; the detectors we used had depletion layers of about 7 mm. In order to prevent gross diffusion the detectors have to be kept and used at liquid-nitrogen temperatures.

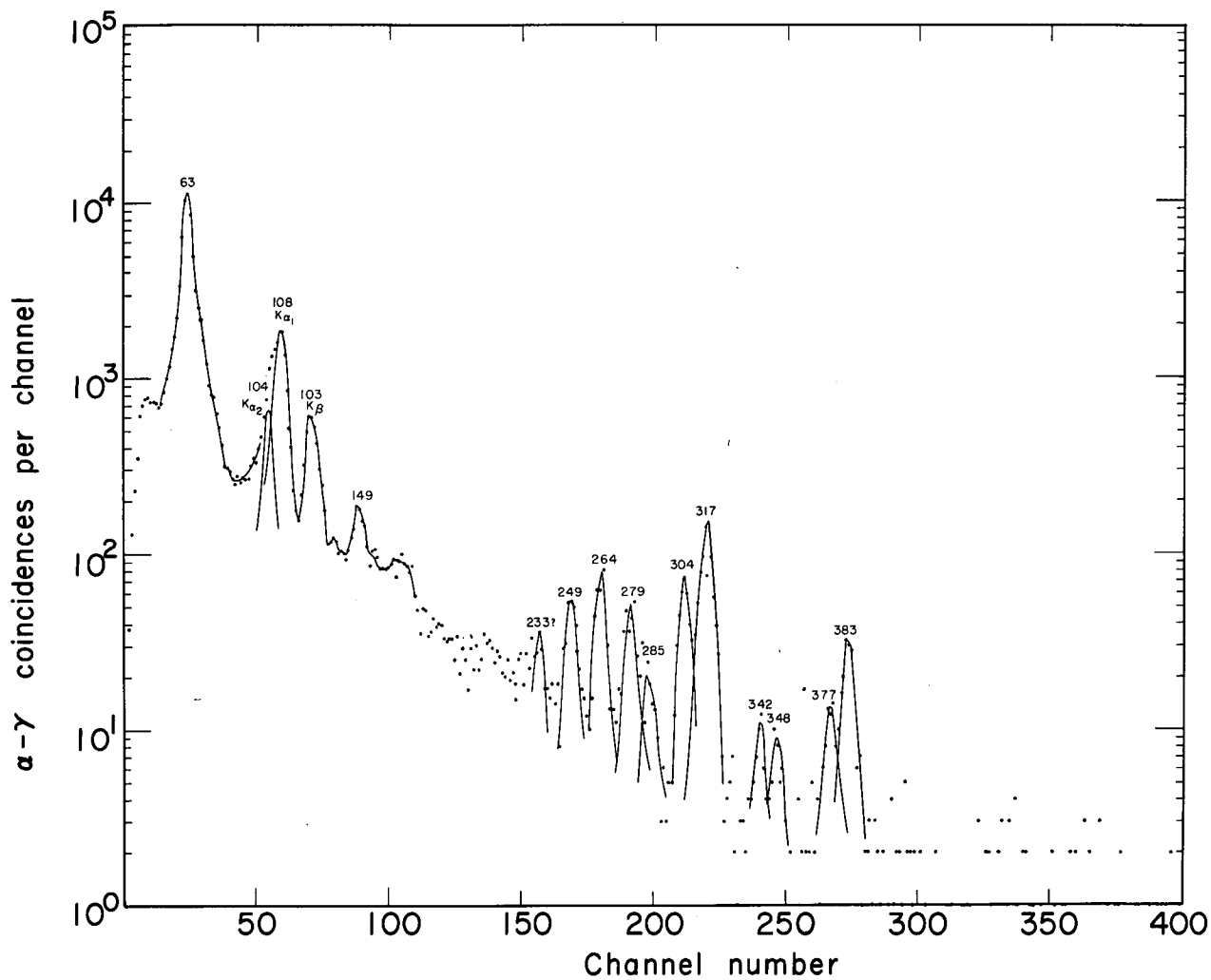
We used Lu<sup>177m</sup> as the efficiency and energy standard<sup>51</sup> for the spectrum in Fig. 11. (A number of other energy standards were also used.) The relative efficiency of the detector was also checked by comparing the sums of the peaks in Fig. 11 with the corresponding "single" peaks in Fig. 10, where the relative efficiency of the detector for gamma-ray of various energies is well known. Thus, the gamma rays identified in Es<sup>254</sup> decay are listed in Table VI together with their intensities as a percent of the alpha disintegration rate. The L-x-ray region is not shown in Figs. 10 or 11 and will be discussed later in this section. The intensity of the 63-keV gamma ray was measured as described in the following paragraph, and the remaining intensities in Table VI were measured relative to this one.



MUB-5075

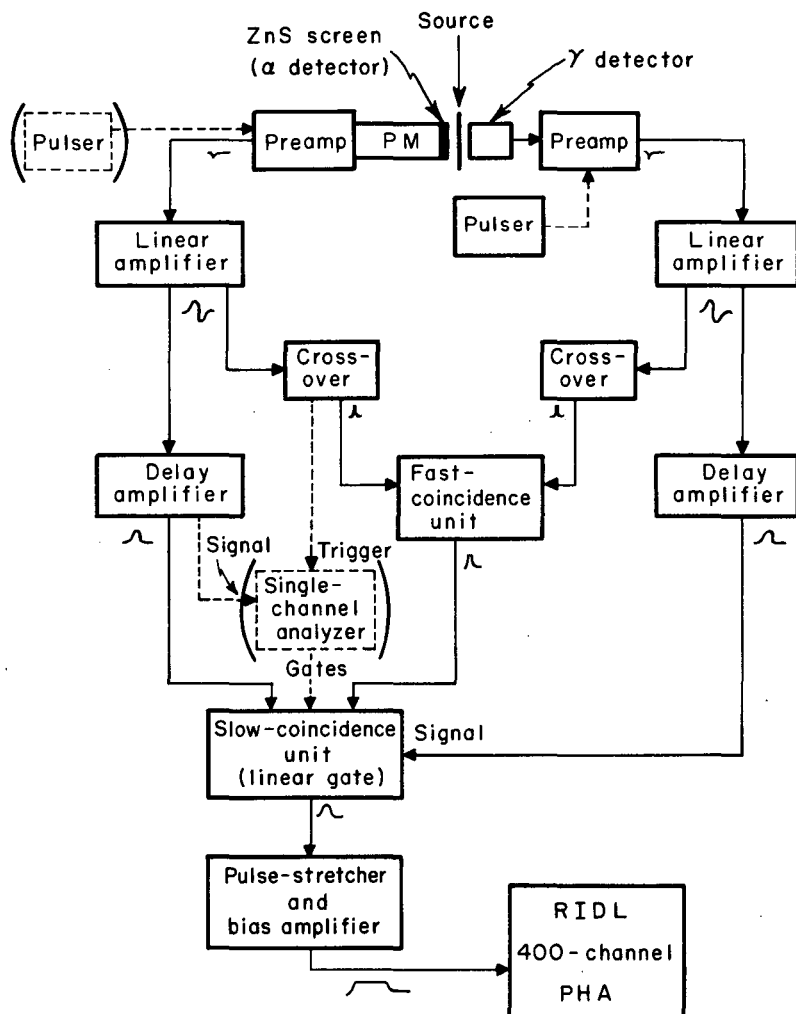
Fig. 10. Gamma-ray spectrum taken in fast (100 nsec resolving time) coincidence with all alphas from Es<sup>254</sup>. The detector used for the gamma-rays was a 3-inch × 3-inch NaI (Tl) scintillator. Gamma-ray energies are given in keV.





MUB-5074

Fig. 11. Gamma-ray spectrum taken in fast (100 nsec resolving time) coincidence with all alphas from Es<sup>254</sup>. The detector for the gamma-rays was a 1-cm-diameter, 7-mm-thick germanium (lithium-drifted) solid-state detector. Gamma-ray energies are given in keV.



MU-36059

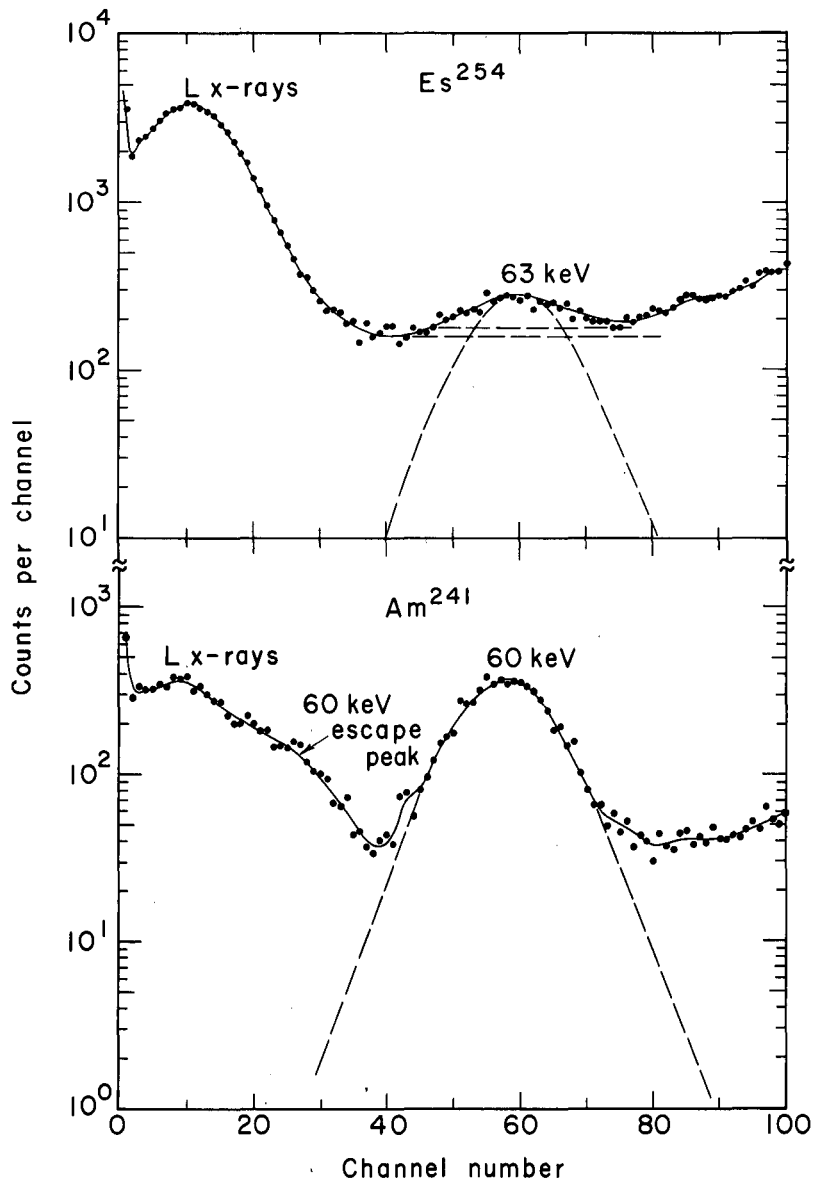
Fig. 12. Block diagram of the fast-slow coincidence circuit used for alpha-gamma (Figs. 10 and 11.) and alpha-electron (Fig. 9) coincidence spectra. The gamma-ray detector was either a NaI scintillator or a lithium-drifted germanium detector; for alpha-electron coincidences the gamma-ray detector was replaced with a silicon electron detector. The system could be used for gamma-gamma coincidences by replacing the alpha detector with a gamma detector and adding the components in parentheses. An approximate pulse shape is shown after each stage.

Table VI. Gamma rays from Es<sup>254</sup> decay.

$E_{\gamma}$ (keV)	Intensity (%)
$\approx 15-18$ (L x rays)	230 <sup>a</sup>
43	$0.3 \pm 0.1$ <sup>b</sup>
63	2.0 <sup>a</sup>
104 (K <sub><math>\alpha 2</math></sub> )	0.40
108 (K <sub><math>\alpha 1</math></sub> )	
$\approx 123$ (K <sub><math>\beta</math></sub> 's)	0.13
150 (2 $\gamma$ 's ?)	0.23
(233)	0.008
249	0.025
264	0.05
278	0.05
284	0.01
304	0.07
317	0.15
342	0.009
348	0.007
377	0.015
385	0.05

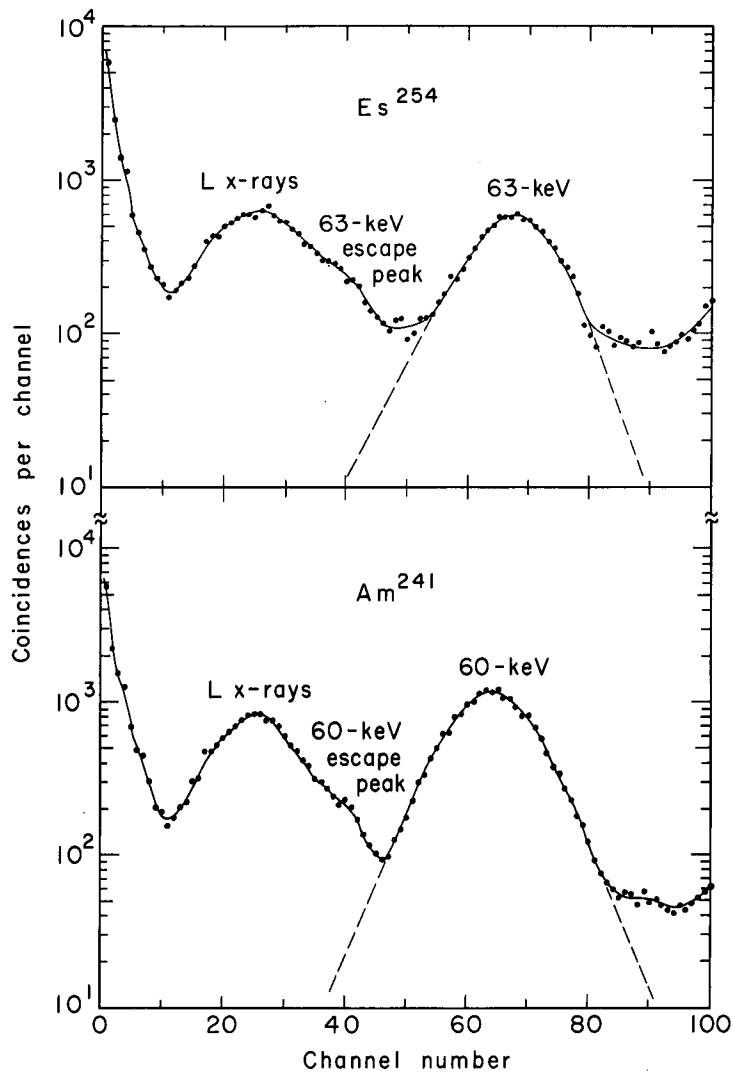
<sup>a</sup>These intensities were obtained from special experiments that compared the L x rays with those of Es<sup>253</sup> and the 63-keV  $\gamma$  with the 60-keV  $\gamma$  of Am<sup>241</sup>. The intensity under L x rays is that for L vacancies.

<sup>b</sup>This intensity was obtained from a delayed-coincidence experiment, cf. Sec. II.B.5.e. All other intensities were obtained from Figs. 10 and 11, normalized to the 63-keV  $\gamma = 2.0\%$ .



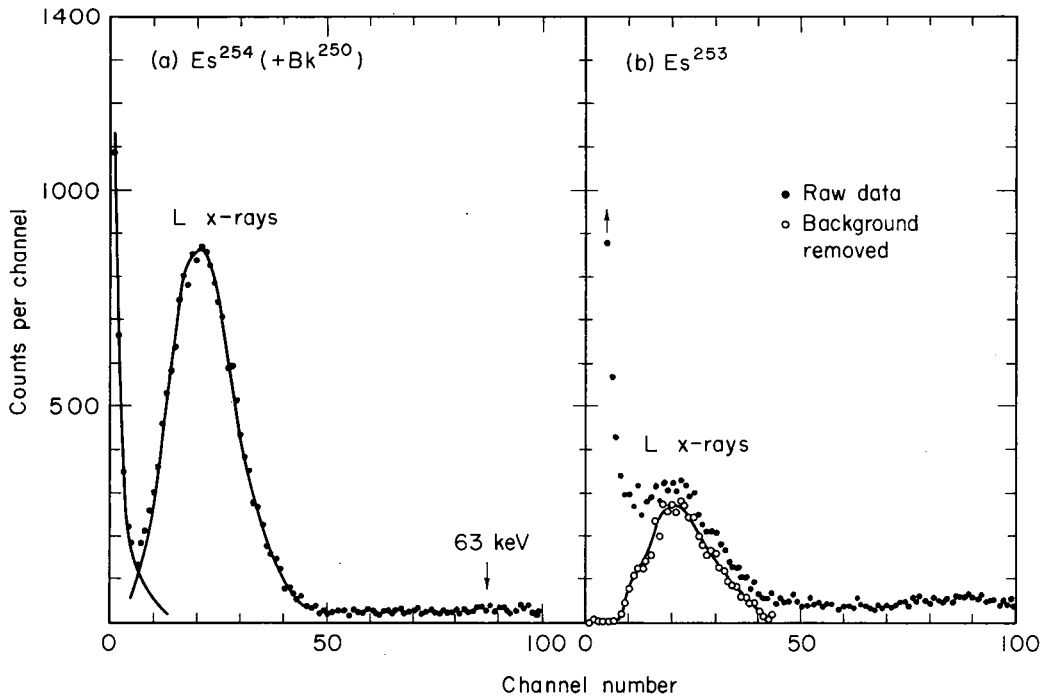
MU-36067

Fig. 13. Singles comparison between Es<sup>254</sup> and Am<sup>241</sup> to determine the intensity of the 63-keV  $\gamma$  of Es<sup>254</sup>. The top spectrum was obtained by counting an 1807- $\alpha$ /min Es<sup>254</sup> source for 80 min with a 1-inch  $\times$  1-1/2-inch NaI scintillator having a Be window; the bottom spectrum was obtained by counting a 1443- $\alpha$ /min Am<sup>241</sup> source for 20 min with the same detector and same geometry. The dashed horizontal lines in the top figure show the probable extremes that can be taken for the background. This comparison yields an intensity of  $2.3 \pm 0.5\%$  for the 63-keV  $\gamma$ .



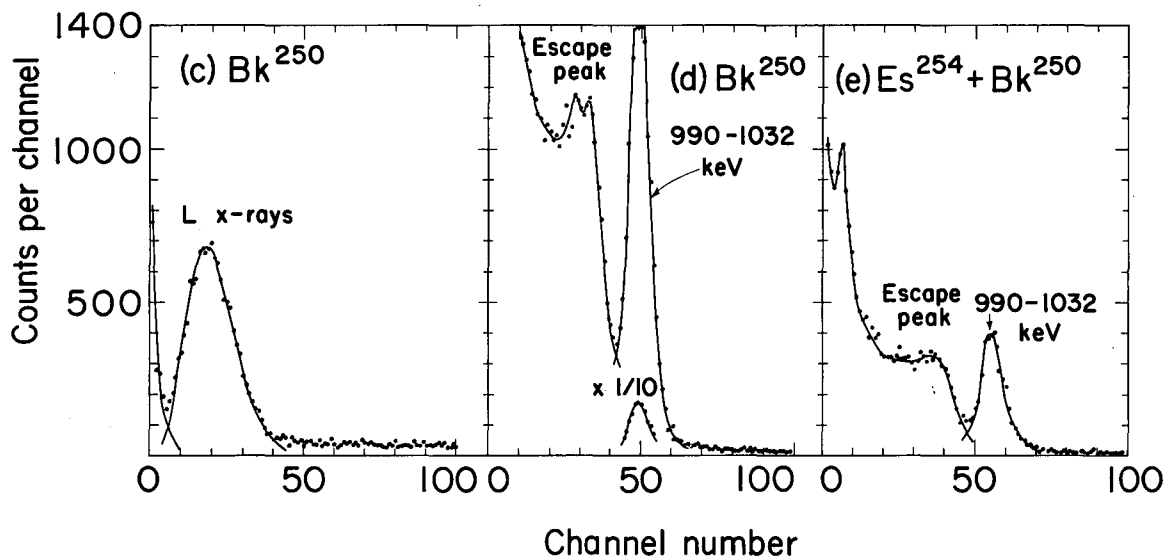
MU-3608

Fig. 14. Coincidence comparison between  $Es^{254}$  and  $Am^{241}$  to determine the intensity of the 63-keV  $\gamma$  of  $Es^{254}$ . The same sources and gamma detector were used as for Fig. 13. The top spectrum was obtained by counting gamma-rays in slow (6  $\mu$ sec resolving time) coincidence with all alphas (ZnS-screened PM as detector) from  $Es^{254}$  for 240 min; the bottom spectrum was obtained by counting the gamma-rays in slow coincidence with all alphas from  $Am^{241}$  for 50 min at the same geometry. This comparison yields an intensity of  $2.0 \pm 0.2\%$  for the 63-keV  $\gamma$ .



MU-36060

Fig. 15. Spectra involved in determining the intensity of L vacancies in Es<sup>254</sup> decay by comparing singles spectra of Es<sup>254</sup> and Es<sup>253</sup>. a) L-x-ray spectrum of Es<sup>254</sup> obtained by counting a 3200- $\alpha$ /min Es<sup>254</sup> source for 10 min with a 1-inch x 1-1/2-inch Be-windowed NaI scintillator. b) L-x-ray spectrum of Es<sup>253</sup> obtained by counting a 5310- $\alpha$ /min Es<sup>253</sup> source for 80 min with the same detector. Solid circles show raw data; open circles show them after background has been



MU-30061

Fig. 15. (cont.) c) L-x-ray spectrum of separated Bk<sup>250</sup> obtained by counting the Bk<sup>250</sup> source for 4 min with the 1-inch x 1-1/2-inch Be-windowed NaI scintillator. d) High-energy gamma-ray spectrum obtained by counting the same Bk<sup>250</sup> source for 11 min with the same detector. e) High-energy gamma-ray spectrum of Es<sup>254</sup> + Bk<sup>250</sup> obtained by counting the Es<sup>254</sup> source used in a) for 20 min with the same detector.

The energies in Table VI are expected to be precise to  $\pm 2$  keV, the intensities to about  $\pm 15\%$ .

The intensity of the 63-keV gamma ray was measured by comparison with the 60-keV gamma ray of  $\text{Am}^{241}$ , whose intensity was taken to be 0.359 per alpha disintegration.<sup>44</sup> Matching sources were prepared on Mylar film and were alpha-counted in a proportional counter, yielding 1807  $\alpha$ /min and 1443  $\alpha$ /min for the  $\text{Es}^{254}$  and  $\text{Am}^{241}$ , respectively. They were then analyzed for gamma-rays, using a 1-inch-thick  $\times$  1-1/2-inch-diameter NaI scintillator having a beryllium window. Both a singles comparison and a coincidence comparison (gamma-rays in coincidence with alphas detected by a ZnS-screened photomultiplier, 6  $\mu$ sec resolving time) were made, yielding the singles spectra of Fig. 13 and the coincidence spectra of Fig. 14. The singles comparison gave  $2.3 \pm 0.5\%$  63-keV gamma-ray per alpha disintegration, whereas the coincidence comparison gave the more precise number of  $2.0 \pm 0.2\%$ . The agreement between these numbers is worth noting, for it means that the 63-keV gamma-ray transition does not follow the long delays that will be discussed shortly.

It can be seen by comparing the  $\text{Es}^{254}$  spectra in Figs. 13 and 14 that there are many fewer L x rays in the coincidence spectrum than in the singles spectrum. The determination of the intensity of the many L x rays, or L vacancies, that follow  $\text{Es}^{254}$  alpha decay was complicated by the fact that a large fraction of these were found to follow delays that were long compared with usable resolving times (a few  $\mu$ sec). Two methods, however, were found that gave reproducible and mutually consistent results. These were: 1) a singles measurement with correction for  $\text{Bk}^{250}$  vacancies, and 2) integration under a time-to-height converter's delay curve.

The spectra involved in the singles comparison with  $\text{Es}^{253}$  are shown in Fig. 15. Matching  $\text{Es}^{254}$  (3200  $\alpha$ /min) and  $\text{Es}^{253}$  (5310  $\alpha$ /min) sources were prepared on Mylar film. Their respective L-x-ray spectra, taken with the same 1-inch  $\times$  1-1/2-inch Be-windowed NaI scintillator used for the 63-keV- $\gamma$  intensity determinations, are shown in parts a) and b) of Fig. 15. Using the value  $0.0825 \pm 0.0083$  L vacancies<sup>43</sup> per alpha



disintegration for  $\text{Es}^{253}$ , we find  $3.2 \pm 0.4$  L vacancies per alpha disintegration for  $\text{Es}^{254} + \text{Bk}^{250}$  (in equilibrium, of course). To eliminate the L vacancies coming from  $\text{Bk}^{250}$ , we separated the  $\text{Bk}^{250}$  from an  $\text{Es}^{254}$  sample by means of  $\alpha$ -hydroxy-isobutyric-acid cation exchange and took spectra of the L x rays from pure  $\text{Bk}^{250}$ , an example of which appears in part c) of Fig. 15. (In working with the  $\text{Bk}^{250}$ , one had to take care to account for its 193-min half-life. All the spectra involved in this determination were repeated a number of times and in various orders to insure consistency and reproducibility of geometry. Thus, we can truthfully claim that "typical" spectra are shown in Fig. 15.) To relate this  $\text{Bk}^{250}$  L-x-ray spectrum to the fraction of L x rays in the combined  $\text{Es}^{254}$ - $\text{Bk}^{250}$  spectrum that belongs to  $\text{Bk}^{250}$ , we carefully compared the counting rate of the  $\text{Bk}^{250}$  L x rays (Fig. 15c) with that of the  $\text{Bk}^{250}$  990-1032-keV gamma-ray complex (Fig. 15d), using the same source, counter, and position. We then counted the  $\text{Bk}^{250}$  990-1032-keV gamma-ray complex in our  $\text{Es}^{254}$  source, which had  $\text{Bk}^{250}$  in equilibrium (Fig. 15e). So, from Fig. 15c and 15d it was found that, for our counter and geometry, there were 2.38 L x rays per 990-1032-keV gamma ray; by determining the number of 990-1032-keV gamma rays in Fig. 15e this ratio could be related back to Fig. 15a, telling us that 28% of the L x rays there came from  $\text{Bk}^{250}$ , not  $\text{Es}^{254}$ , decay. Thus, there are  $2.3 \pm 0.4$  L vacancies per alpha disintegration in  $\text{Es}^{254}$ . By relating the L vacancies in  $\text{Es}^{254}$  and  $\text{Es}^{253}$  we bypassed the fluorescence yields, which are not known particularly precisely.<sup>52</sup> The entire comparison therefore rests on the assumptions that the L-subshell conversion ratios are similar for  $\text{Es}^{253}$  and  $\text{Es}^{254}$  decays and/or the variation in fluorescence yield among L subshells should not be large; we expect any discrepancy caused by these assumptions not to be greater than, say, 10%.

The second methods for determining the intensity of L vacancies involves integrating the delay curves described in Sec. II.B.5.b. We will not discuss the curves here but simply point out that the efficiency of the system for detecting L vacancies was determined by measuring an  $\text{Es}^{253}$  source (which, of course, produced only a prompt component) under identical conditions, using the above-mentioned intensity for  $\text{Es}^{253}$  L

vacancies. Separate integration of the prompt and delayed components gave  $0.035 \pm 0.005$  prompt L vacancies per alpha disintegration of  $\text{Es}^{254}$  and  $2.2 \pm 0.2$  delayed L vacancies. The total of these two is in reasonable agreement with the result derived above from the singles measurement.

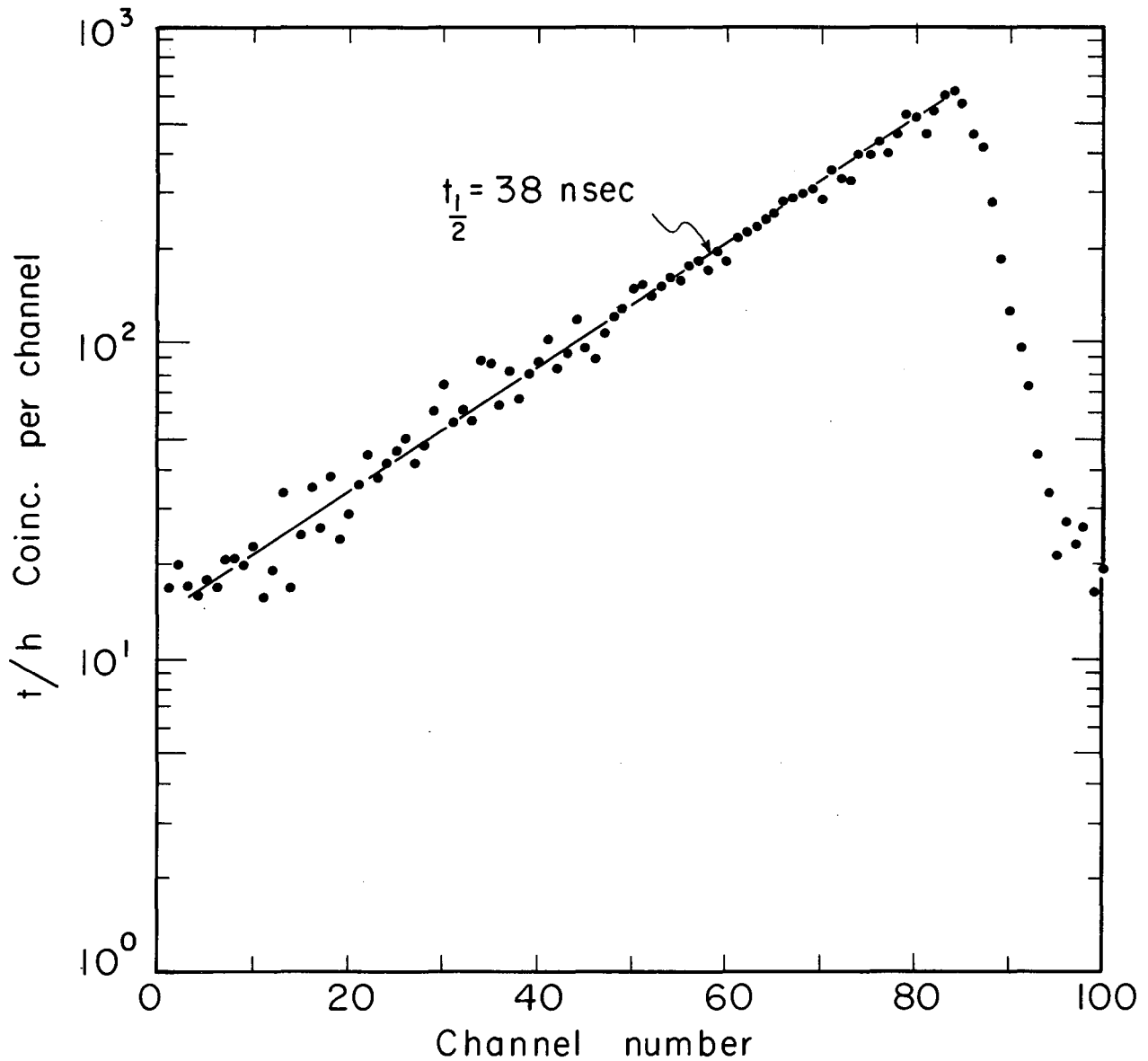
Several other rather specialized coincidence experiments involving gamma rays and, to some extent, electrons and alpha particles were made, but these will not be described in detail here. They were generally motivated by a partial knowledge of or conceived as a specialized check on some part of the decay scheme, and they will be discussed to much better purpose at the appropriate points in the discussion of the decay scheme.

#### 5. Delays and Time-to-height Coincidences

a. 63-keV Gamma Ray. Since it was known that the 63-keV gamma ray of  $\text{Es}^{254}$  is delayed,<sup>11</sup> its half-life was measured with a time-to-height converter. A 1-inch  $\times$  1-1/2-inch NaI scintillator was used to detect the gamma rays, and a ZnS-screened photomultiplier was used to detect alpha particles. The  $\text{Es}^{254}$  source (18400c/min) was prepared by vaporizing the activity onto a 0.001-inch-thick Ni backing. The 63-keV gamma-ray selected with a single-channel analyzer, was used to start the ramp generator, which had a possible sweep of about 300 nsec; the alpha pulses, after passing through a delay unit, were used to stop the ramp. The output of the time-to-height converter, analyzed with a Penco 100-channel pulse-height analyzer, produced the delay curve shown in Fig. 16. Using the half-life of the 60-keV  $\gamma$  from  $\text{Am}^{241}$  as a standard<sup>53</sup> ( $t_{1/2} = 63$  nsec), the half-life of the  $\text{Es}^{254}$  63-keV  $\gamma$  was found to be  $38 \pm 5$  nsec.

The same apparatus was used to determine whether or not the K x rays also were delayed. Within the limits of the experiment it was found that all K x rays are prompt, i.e.,  $t_{1/2} < 1$  nsec.

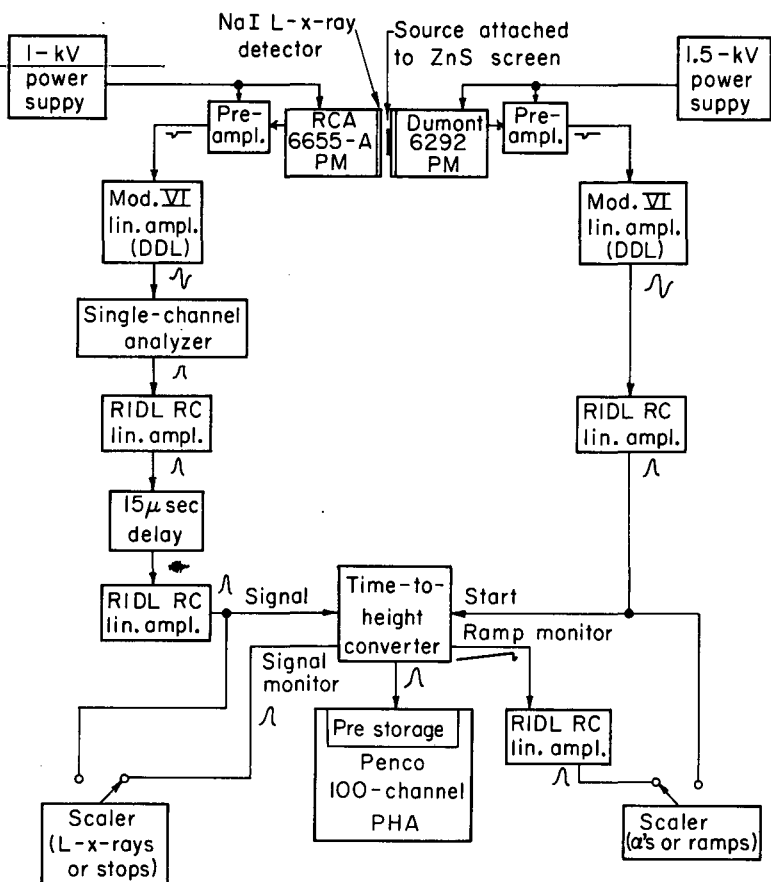
b. Alpha vs. L-x-ray Coincidences. During the course of this investigation it was found, as mentioned earlier, that most of the numerous L x rays are involved in a delay that is long compared with the usual



MUB-5460

Fig. 16. Time-to-height coincidence curve that determines the half-life of the 63-keV  $\gamma$  from  $\text{Es}^{254}$  to be  $38 \pm 5$  nsec. This curve was obtained by starting a time-to-height converter with pulses (single-channel analyzed from a NaI detector) from the 63-keV  $\gamma$  and stopping the time-to-height converter with alpha pulses (from a ZnS detector) that had been delayed electronically.

resolving time of 6  $\mu$ sec. To measure the half-life of this delay, another time-to-height converter, with a ramp rise-time adjustable from microseconds to seconds, was used.<sup>54</sup> Alpha pulses from a ZnS-screened photomultiplier were used to start the ramp generator, and single-channel-analyzed L-x-ray pulses from a 1-inch-diameter, 1-mm-thick, Be-windowed NaI scintillator were used to stop the ramp. Since it was easy to jam the time-to-height converter when long ramp rise-times were used, we had to use a very weak source, 8800c/min  $\text{Es}^{254}$  vaporized onto 0.001-inch thick Ni. This source was also used in the subsequent time-to-height coincidence experiments. Since there is more than one L vacancy per alpha disintegration, pulses can be lost due to the dead-time of the analyzer used. For this reason a Penco 100-channel analyzer with the provision of storing one pulse while analyzing another was used. In order to get the prompt edge of the delay curve into the range of the analyzer, it was necessary to introduce a delay into the L-x-ray side of the apparatus, thereby effectively adding a constant threshold to all the pulses produced by the time-to-height converter. For best results it was found that a delay of about 15  $\mu$ sec was needed, and, since an active electronic delay unit also introduces a dead-time between pulses approximately equal to the length of the delay itself, we used a series of three standard passive 5- $\mu$ sec inductance delays into this side of the circuit. This, in turn, necessitated adding a pulse-shaper both before and after the delay units. It should be borne in mind that this experiment and the ones just following were destined to uncover a most interesting decay sequence, but they did so in a rather indirect fashion; this is why it was necessary to make certain that we were not losing a significant number of pulses through instrumental dead-time, etc. As a check on the intensities observed in the delay curves and on their consistency with the overall intensities, arrangements were made to count the incoming pulses on both sides and also the ramps and gates (i.e., stopping pulses) manufactured by the time-to-height converter from what it saw as the incoming pulses. It was thus necessary to add other pulse-shapers so the scalers could recognize such pulses as the saw-tooth-shaped ramps. A block diagram of the overall setup is shown in Fig. 17.

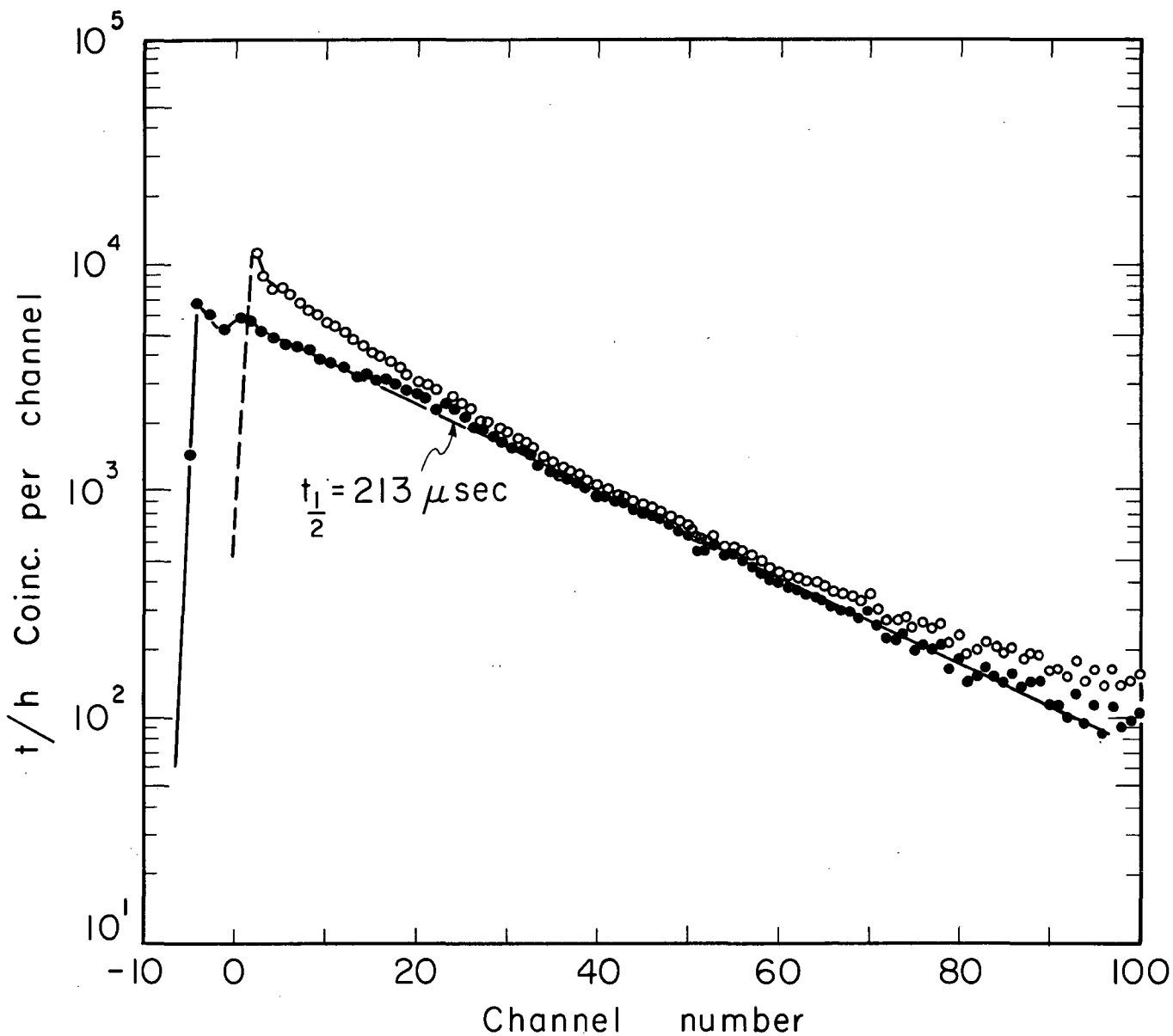


MU-36062

Fig. 17. Block diagram of the apparatus used to obtain delayed coincidence curves with a time-to-height converter. The set-up shown was used to obtain the spectra of Figs. 18 and 19. For the L-x-ray vs. L-x-ray and  $^{63}\text{-keV-}\gamma$  vs. L-x-ray spectra, the alpha-detection side was replaced with a suitable gamma-detection system similar to the L-x-ray side shown. An approximate pulse shape is shown after each stage. The small RIDL RC-shaping linear amplifiers were used as pulse shapers. The pulse height analyzer had the added provision of storing one pulse while it analyzed another.

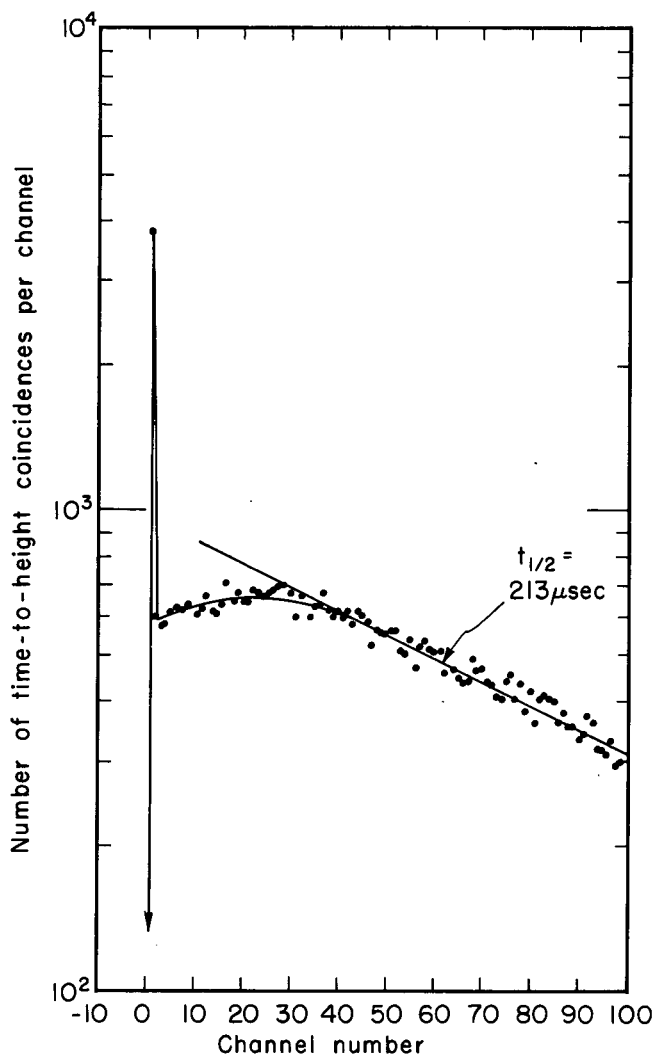
A delay curve obtained by using a setting of the time-to-height converter so that the ramp sweep could run to a maximum of 2 msec is shown in Fig. 18. A Tektronix type 180A Time-Mark Generator was used to calibrate the time scale, and, since the time-to-height converter was found to be non-linear at low pulse-height output, a randoms time-to-height "delay curve" with  $\text{Am}^{241}$  alphas replacing the  $\text{Es}^{254}$  alphas for pulses to start the ramp ( $\text{Es}^{254}$  L-x-ray pulses still stopped it) was used to improve the calibration further by giving each channel an "effective channel width." The points in Fig. 18 are shown both before and after this correction and that of having background removed. From this delay curve it was found that the half-life of the delay is  $213 \pm 8$   $\mu\text{sec}$ . This, by the way, was the delay curve used to obtain intensities of  $0.035 \pm 0.005$  prompt and  $2.2 \pm 0.2$  delayed L vacancies per alpha disintegration of  $\text{Es}^{254}$  as discussed in Sec. II.B.4.

In Fig. 18 there appears something like a "dip" immediately following the prompt side of the curve. To look more carefully at this portion immediately following the prompt edge, essentially the same experiment was repeated with the scale expanded, as is shown in Fig. 19, where the possible ramp sweep was 500  $\mu\text{sec}$ . This shows clearly that there is a dip following the prompt peak, a situation that implies a second, somewhat shorter, delay. This is consistent with the L-vacancy intensity data, which imply there are two L-converted transitions following the main body of favored alpha decay; now the implication is that two separate delayed transitions follow the main body of favored alpha decay—these may or may not be the same as the L-converted transitions. The data from Fig. 19 uniquely determine the order of the two delays, as can be demonstrated by a comparison with Fig. 20. If the shorter delay were to precede the 213- $\mu\text{sec}$  delay, a condition of no equilibrium would arise, analogous to the similar case on a longer time scale when the half-life of a parent nuclide is shorter than that of its daughter. A predicted curve for this situation is shown in Fig. 20a. If, on the other hand, the shorter delay were to follow the 213- $\mu\text{sec}$  delay, a condition of transient equilibrium would arise. The predicted curve for this situation is given in Fig. 20b.



MUB-5461

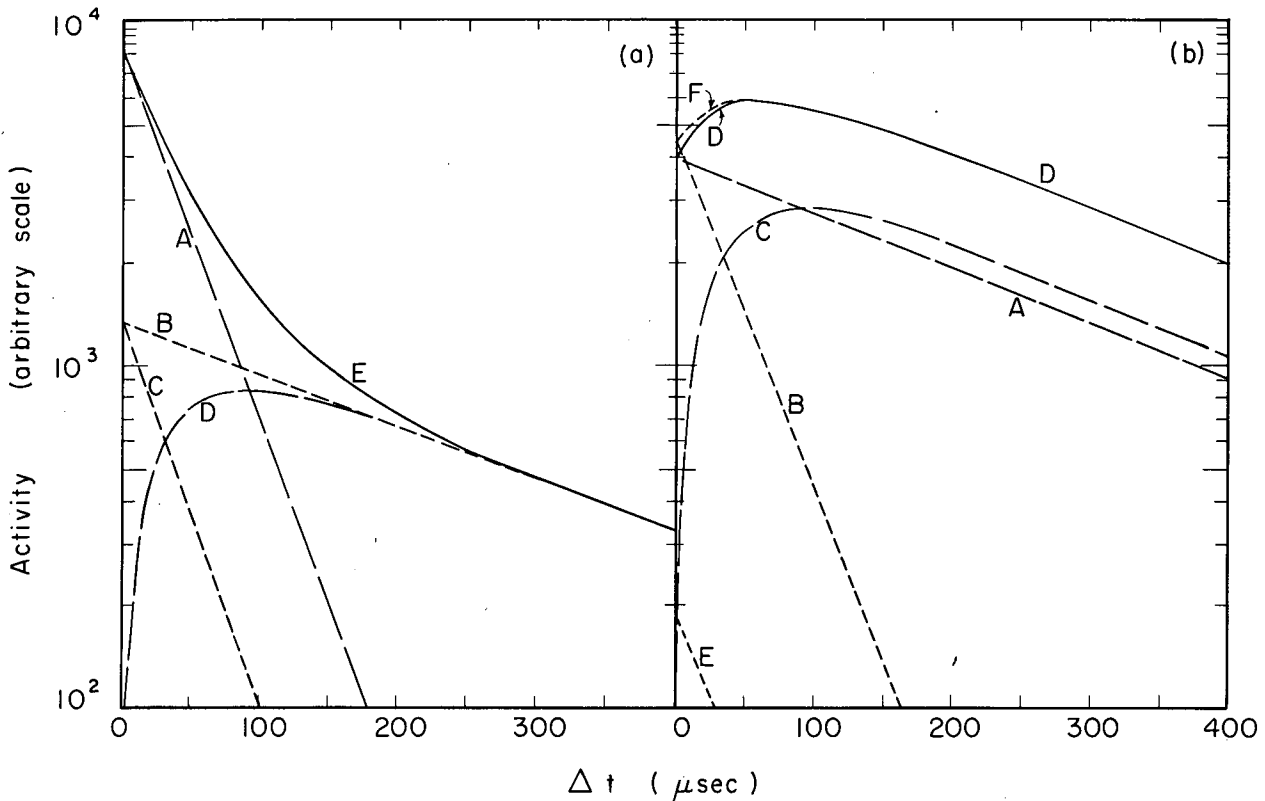
Fig. 18. The time-to-height-coincidence delay curve that establishes the longer delay in the L x rays to have a half-life of  $213 \pm 8 \mu\text{sec}$ . The curve was obtained by starting a time-to-height converter that had a possible ramp sweep of 2 msec with alpha pulses and stopping it with L-x-ray pulses. The raw data are plotted as open circles; filled circles show these corrected for channel width and background.



MU-33045

Fig. 19. Delay curve obtained by starting a time-to-height converter with alpha pulses and stopping it with L-x-ray pulses. The possible ramp sweep was  $500 \mu\text{sec}$ , each channel being  $3.41 \mu\text{sec}$ . Points have been corrected for channel width and background. This curve determines, as discussed in the text, that two delays occur among the L x rays, a shorter one that follows a longer one.



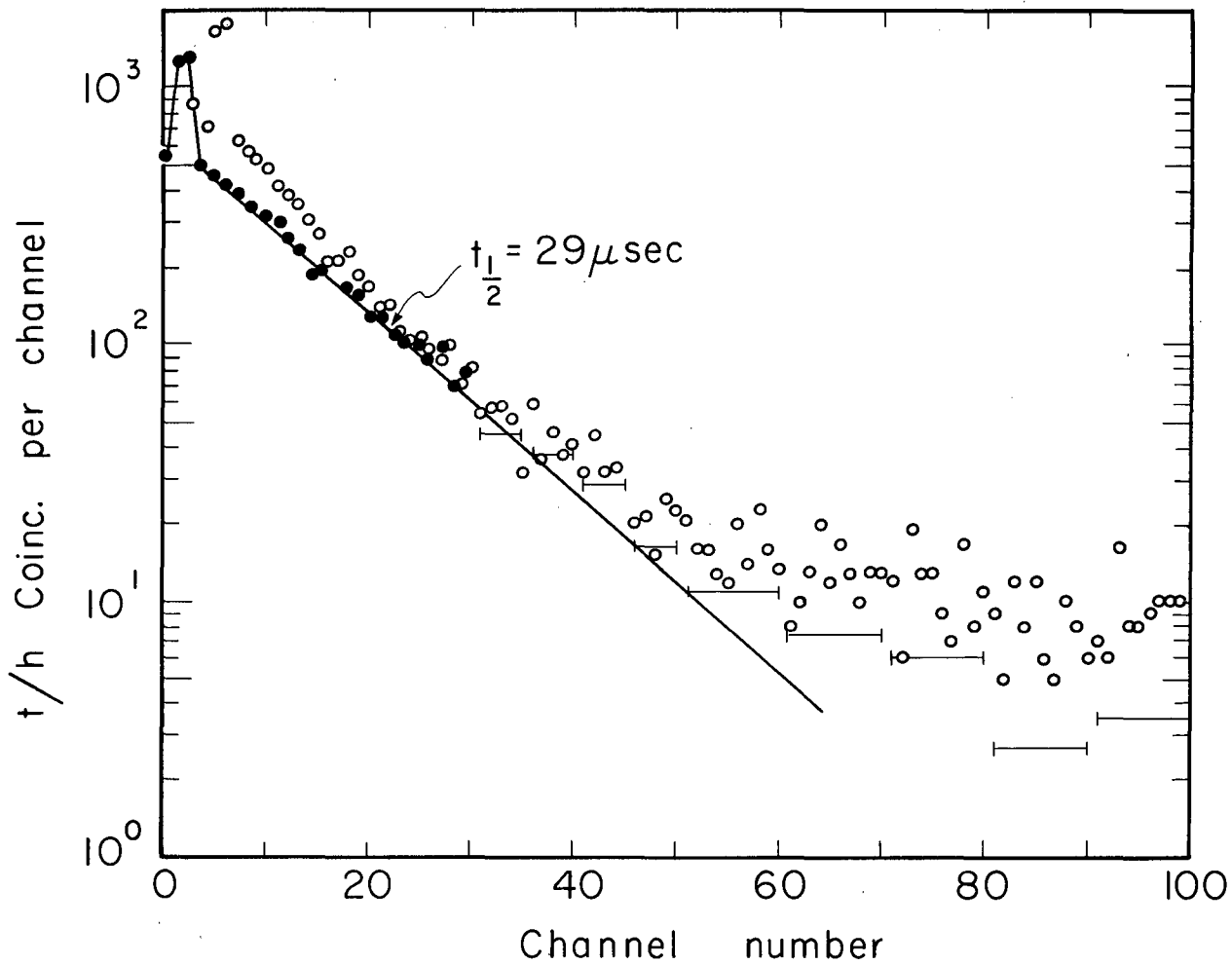


MUB-5462

Fig. 20. Predicted curves for two delayed transitions in cascade. a) The case of no equilibrium when the longer delay follows the shorter one. Line A has a 29- $\mu$ sec half-life. Line B shows a hypothetical 213- $\mu$ sec activity of the same integrated intensity as A. Line C shows a 29- $\mu$ sec activity starting at the same initial intensity as B. Curve D ( $= B - C$ ) shows the growing in of a 213- $\mu$ sec activity following a 29- $\mu$ sec activity. Curve E ( $= A + D$ ) shows the resultant activity detected. b) The case of transient equilibrium when the longer delay precedes the shorter one. Line A shows the 213- $\mu$ sec activity. Line B shows the (hypothetical) 29- $\mu$ sec activity starting at  $\lambda_{29}/(\lambda_{29}-\lambda_{213})$  the initial activity of A. Curve C ( $= [\lambda_{29}/(\lambda_{29}-\lambda_{213})] A - B$ ) shows the growing in of 29- $\mu$ sec activity following a 213- $\mu$ sec activity. Curve D ( $= A + C$ ) shows the resultant activity detected. Actually, in our experimental case about 4% of the 29- $\mu$ sec activity started early because of cross-over transitions (represented by E), and this filled the initial dip somewhat (as at F).

It can be seen that the data of Fig. 19 fit the second (transient equilibrium) curve in Fig. 20 rather well, even to the dip's being slightly filled in because of cross-over transitions. Thus, following most of the alpha decay of  $\text{Es}^{254}$  there are two delayed transitions, the first with  $t_{1/2} = 213 \mu\text{sec}$ , the second with a somewhat shorter half-life. It might be mentioned that, were it not for the cross-over transitions, the half-life of the second delay could have been determined directly from Fig. 19. As it is, the situation is analogous to one where the background to be subtracted from a simple half-life determination is uncertain. To correct for the crossover transitions and determine the half-life for the shorter delay, we would first have to know an approximate half-life for the delay. The half-life used in constructing Fig. 20 was borrowed out of order from the next section.

c. L-x-ray vs. L-x-ray Coincidences. To determine the actual half-life of the shorter delayed transition, L-x-ray vs. L-x-ray time-to-height coincidences were used. The same apparatus was used as for the alpha vs. L-x-ray coincidence studies, except that a second 1-inch-diameter, 1-mm-thick Be-windowed NaI scintillator was substituted for the alpha detector, and the signals from this were single-channel analyzed for L-x-ray pulses before being used to start the ramp generator. The time scale was again calibrated with the Time-Mark Generator and by means of a randoms spectrum that determined individual channel widths, and a careful check on intensities was made with the aid of scalers as before. The resulting delay curve is shown in Fig. 21, where again both the raw data and those corrected for channel width and background are given. With a possible ramp sweep of 500  $\mu\text{sec}$ , the half-life of this transition was found to be  $29 \pm 2 \mu\text{sec}$ . Although the statistics are not so good for this experiment as for those of the previous section, a comparison of the time-to-height-converter output, the L-x-ray counting rates on both sides, and the alpha counting rate of the source did indicate that the transition whose half-life is 29  $\mu\text{sec}$  does occur in essentially 100% of the disintegrations. There are also a small number of prompt L-x-ray vs. L-x-ray coincidences, but it is difficult



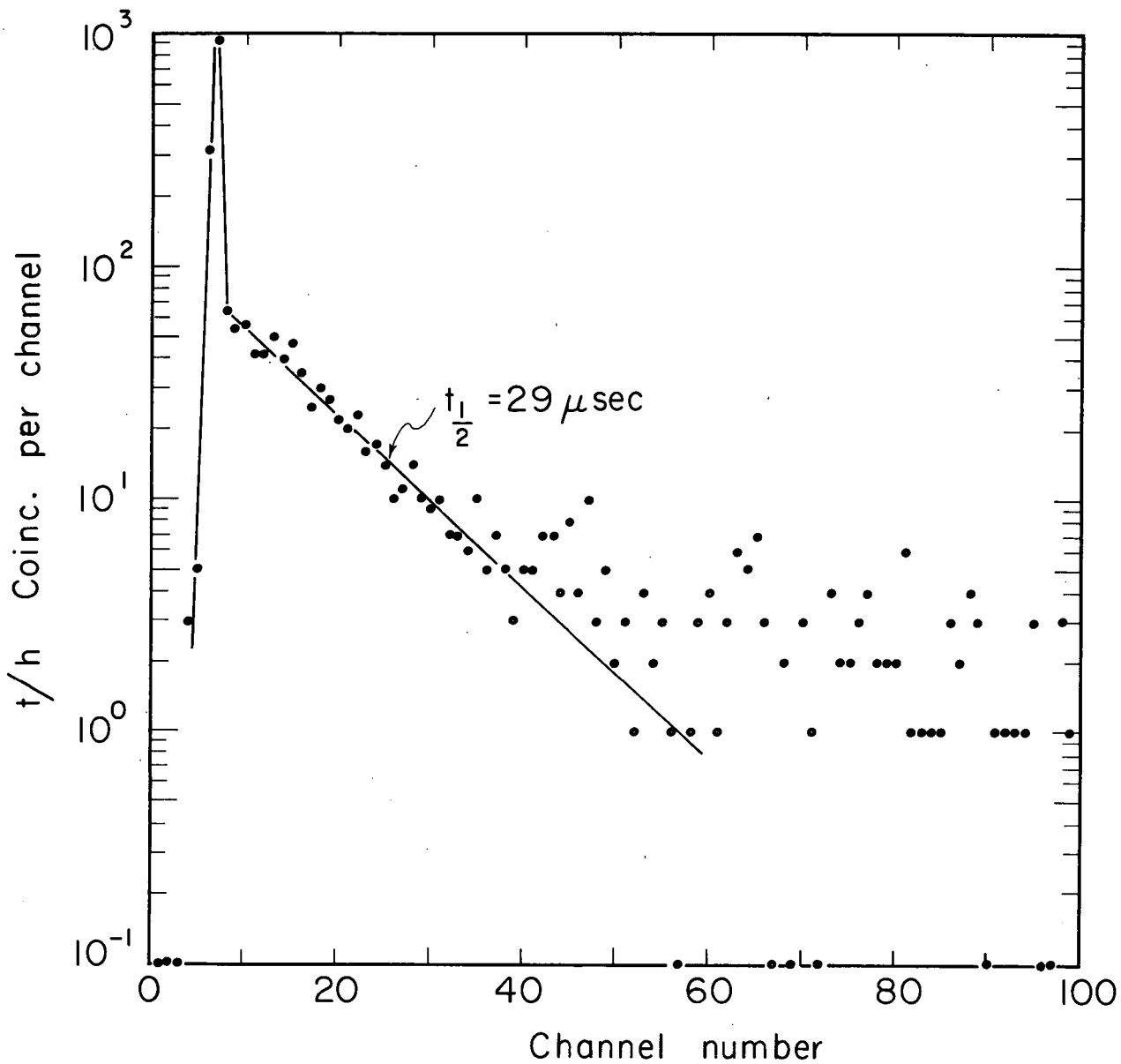
MUB-5463

Fig. 21. Delay curve that establishes the half-life of the shorter delay in the L x rays to be  $29 \pm 2 \mu \text{sec}$ . The curve was obtained by starting and stopping a time-to-height converter with L-x-ray pulses (from separate detectors). The open circles show the raw data; the filled circles show them corrected for channel width and background; the horizontal bars show the corrected data averaged over five or ten channels.

to tell just how many of these come from Es<sup>254</sup> decay (remember that Bk<sup>250</sup> is in equilibrium). It is important to note, however, that there is no prominent 213- $\mu$ sec component in this delay curve (upper limit 20% of the 29- $\mu$ sec component). This means that no prominent source of L x rays precedes the 213- $\mu$ sec delay.

d. 63-keV-Gamma vs. L-x-ray Coincidences. It would, of course, be of interest to investigate the number and particularly the delay of the L x rays following each of the gamma rays listed in Table VI. This would give considerable evidence on which of the lower bands in Bk<sup>250</sup> is the termination point of the particular gamma ray examined. Unfortunately, the only gamma ray of sufficient intensity to make this practicable is the one of 63 keV. For this transition the measurement was made using a 1-inch-thick x 1-1/2-inch-diameter NaI crystal with a Be window to detect the 63-keV  $\gamma$ . The output from this detector was single-channel analyzed for the 63-keV  $\gamma$  and then used to start the time-to-height converter. The L-x-ray side was the same as in the previous two sections. Again a possible ramp sweep of 500  $\mu$ sec was used. The resulting spectrum is shown in Fig. 22. This shows that the 29- $\mu$ sec delayed transition follows the 63-keV  $\gamma$ , but the 213- $\mu$ sec delayed transition does not. There is a sizeable prompt coincidence peak, some of which very likely indicates prompt 63-keV- $\gamma$  vs. L-x-ray coincidences, but there is also a background underneath the 63-keV line (compare Fig. 10, for example, where the background shows up even though it has been reduced by the coincidence experiment), largely from the 990-1032-keV peak of Bk<sup>250</sup> decay, and this can also contribute these prompt coincidences.

e. The Cascade Shown Graphically. As a conclusion to the experimental section on Es<sup>254</sup>, let us recapitulate what the previous coincidence experiments have told us and then see if it is possible to get a clearer picture of the delay-transition cascade and perhaps observe some of the gamma-rays that are involved. From the L-x-ray intensities we know that two transitions that convert essentially 100% in the L and outer electron shells are involved in depopulating the favored-alpha-decay level down to



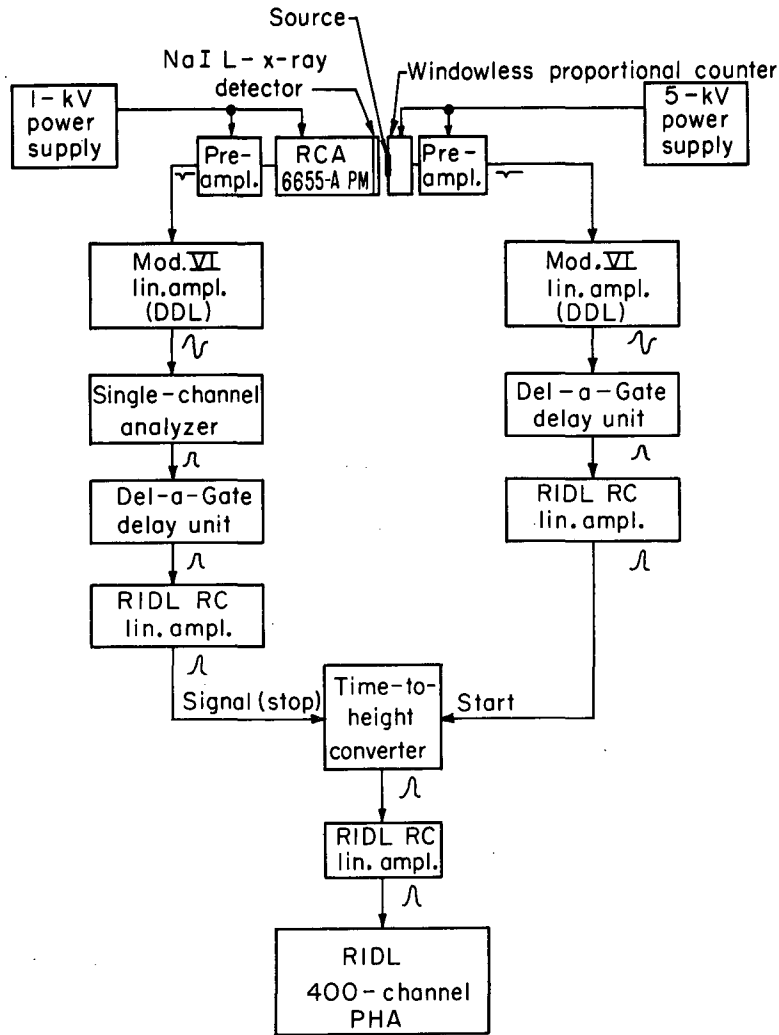
MUB-5464

Fig. 22. Time-to-height-coincidence delay curve establishing that the 29- $\mu\text{sec}$  delayed transition follows the 63-keV  $\gamma$ , but the 213- $\mu\text{sec}$  delayed transition does not. This curve was obtained by starting the time-to-height converter with pulses from the 63-keV  $\gamma$  and stopping it with L-x-ray pulses. Zero events are plotted at one-tenth.

the Bk<sup>250</sup> ground state. And from the time-to-height coincidence curves we know there are two delayed transitions, one with a 29- $\mu$ sec half-life following (not necessarily directly) one with a 213- $\mu$ sec half-life. From the conversion-electron intensities in Table III we find that only two transitions, the 35.5-keV M2 and the 42.6-keV M1-E2, are of sufficient intensity to be a major mode of depopulation from the level receiving favored alpha decay; we can perhaps grudgingly admit the 34.4-keV M1-E2 transition ( $\approx 30\%$ ), but it is more likely that it occurs in combination with another transition in the main sequence. As for the gamma rays themselves, the K-x-ray intensity is far too low for any important transition in the main sequence to have an energy greater than the K binding energy (131.6 keV<sup>46</sup>), and this leaves the 63-keV  $\gamma$  as the only possibility experimentally seen thus far. However, with a photon intensity of 2%, the 63-keV  $\gamma$  could appear in the main sequence only as an M1—the predicted<sup>55</sup> total L-shell conversion coefficients for this energy are 0.36, 26.3, 150, and 750 for E1, M1, E2, and M2 transitions, respectively, which lead to estimates of 0.5, 38, 215, and 1070 for the total conversion coefficients. There is too much photon intensity for E2 or M2 and too little for E1. However, we did not see conversion electrons for a 63-keV transition, and they would have been readily seen if it were anything other than an E1. It is most likely, then, an E1 transition that depopulates a minor branch of the decay, and until now we have not observed any photons from the main sequence. What this all leads to is the conclusion that the main sequence of depopulation from the state receiving favored alpha decay consists of two transitions that convert in the L shells, and these have to be the 35.5-keV M2 and the 42.6-keV M1-E2 transitions, as well as two delayed transitions, which may or may not be the same ones. If there are more than two transitions, the extra ones have energies below the L edge, i.e.,  $< 19.5$  keV.

A rather elaborate experiment was next performed to search for any other transitions. A transition below the L edge would convert primarily in the M subshells, giving rise to M x rays and M conversion electrons. One cannot readily detect M x rays ( $\approx 5$  keV), but with a

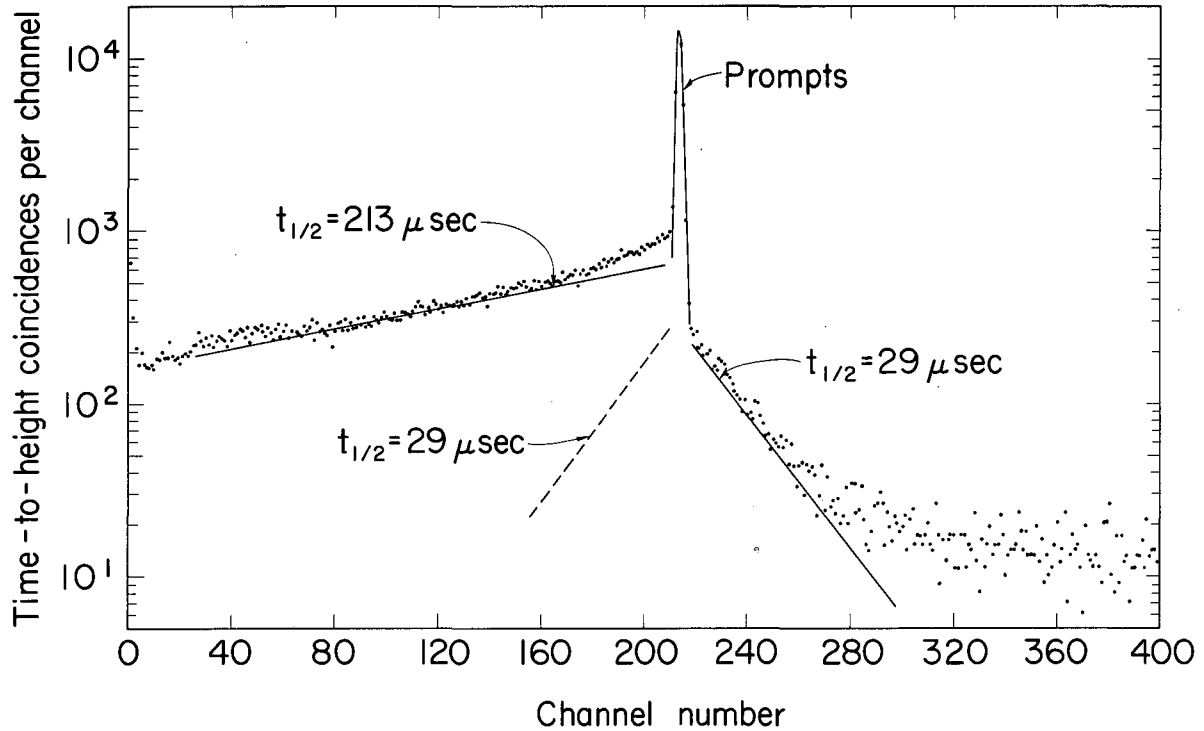
windowless proportional counter one might be able to detect Miel's providing the transition energy is at least a few keV above some of the M binding energies. The experiment consisted of a time-to-height converter started with L-x-ray pulses and stopped with pulses from a windowless proportional counter. A source was prepared that consisted of 800  $\alpha$ /min Es<sup>254</sup> on 0.001-inch aluminized Mylar film, and this was mounted as the window of the counter, with the activity on the inside. This counter could be expected to detect alpha particles, L electrons (from the two transitions already known), and M electrons (from known or unknown transitions); it turned out that the success of this experiment did not depend on the detector's being able to detect M electrons explicitly, but in a later experiment with Es<sup>253</sup> it was found that the detector did pick up M electrons from the 8.8-keV transition in Bk<sup>249</sup>, i.e., with energies at least as low as 3.8 keV. The L-x-ray detector would pick up L x rays from the two transitions already known and presumably nothing else. Since the time-to-height converter was being started with pulses not necessarily from the beginning of the main decay sequence, provision was made for introducing long (hundreds of  $\mu$ sec) delays into both sides of the system; passive delays are not practicable in this range, so Del-a-gate active delay-and-gate units were used, although this meant we were in danger of losing a good portion of the pulses. Furthermore, a RIDL 400-channel pulse-height analyzer was used that could not store one pulse while analyzing another; thus, it might lose a few more pulses. A block diagram of the apparatus is shown in Fig. 23 and a delay curve obtained when 500- $\mu$ sec delay was introduced into the proportional-counter side is shown in Fig. 24. In this spectrum there is graphic support of the preceding findings, namely that the main sequence of decay involves a long, 213- $\mu$ sec delay followed by a shorter, 29- $\mu$ sec delay. It can be seen that our forebodings about swallowed pulses were borne out; only the 213- $\mu$ sec component shows anything like 100% intensity. It should be noted that the reasoning associated with this experiment can be considered safe only because the previous time-to-height delay curves have already proved that the transitions involved are indeed all 100% transitions; not just small



MU-36063

Fig. 23. Block diagram of the apparatus used to obtain the L-x-ray vs. windowless-proportional-counter-pulses time-to-height delay curve. An approximate pulse shape is shown after each stage. The small RIDL RC-shaping linear amplifiers were used as pulse shapers.





MU-36132

Fig. 24. Delay curve that graphically shows the components of the main sequence that depopulates the levels receiving favored alpha decay in  $\text{Bk}^{250}$  down to the ground state. This curve was obtained using the apparatus of Fig. 23. with  $500 \mu\text{sec}$  more delay introduced into the proportional-counter side than in the L-x-ray side.

branches. Furthermore, Fig. 24 demonstrates that the 29- $\mu$ sec transition is one that converts in the L subshells. This is shown as follows: L-x-ray pulses from either of the transitions would see L electrons from their own transition as prompt, and the prompt components would all line up in the middle of the curve as shown. The delay curve resulting from starting the time to height converter with L x rays from the longer delay would look essentially like the curve as first collected. However, if the time-to-height converter is started with L x rays from the shorter delay, the resulting delay curve should consist of 1) a prompt component preceded by 2) a reversed 29- $\mu$ sec delay preceded by 3) a reversed 213- $\mu$ sec delay. And in Fig. 24 one can see that there is a 29- $\mu$ sec component under the large 213- $\mu$ sec component. This experiment thus corroborates our previous findings, but it must be left to the discussion section to demonstrate that the main-decay sequence has a third component in addition to these two.

Finally, is it possible to observe any of the main sequence photons directly? "Any", unfortunately, is limited to the 42.6-keV M1-E2 $\gamma$ . The theoretical L-conversion coefficients<sup>55</sup> for a 42.6-keV M1 or E2 are 78 and 920, respectively, which imply (assuming L-conversion to be 70% of the total) total conversion coefficients of approximately 110 and 1300. One would expect the gamma-ray intensity to lie between 0.9% and 0.08%, depending on the M1-E2 mixing ratio, and one should be able to detect the gamma-ray. On the other hand, the predicted L-conversion coefficient<sup>55</sup> for a 35.5-keV M2 transition should be 3800, implying a total conversion coefficient around 5400; the predicted gamma-ray intensity should be less than 0.02%, making it unlikely that one could observe the gamma ray. Similarly, if one considers the 34.4-keV M1-E2 transition as a possibility in the main sequence, he finds the predicted gamma-ray intensity to lie between 0.15% and 0.01%, making it also an unlikely possibility.

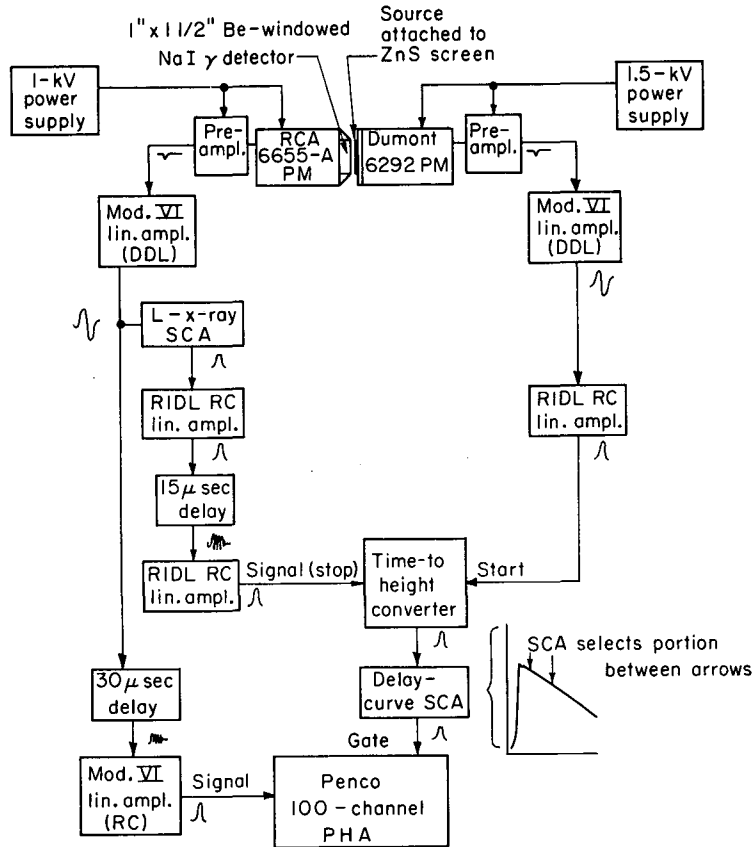
A spectrum of delayed gamma rays was obtained as follows: we used apparatus similar to that in Fig. 17 to obtain a time-to-height delay curve similar to that in Fig. 18. Then, instead of sending the output of the time-to-height converter to the multi-channel analyzer, it was sent through

a single-channel analyzer that selected that portion of the curve just following the prompt edge but not the prompt edge itself. The signal from this single-channel analyzer was used as gate for the original gamma-ray signal, which had been sent through an extra 15- $\mu$ sec passive delay, a pulse shaper, and into the signal input of the pulse-height analyzer. For a block diagram of this apparatus, see Fig. 25; the scalers are not indicated in this drawing, but they were used very much as in Fig. 17. The delayed-gamma-ray spectrum is shown in Fig. 26. It can be seen that sending the gamma-ray signal through a pulse-distorting inductance delay did not exactly improve the resolution, but we do see the 42.6-keV  $\gamma$  in this spectrum, and its intensity is  $0.3 \pm 0.1\%$ . The 63-keV  $\gamma$  appears in this spectrum probably because the single-channel analyzer was set a little too close to the prompt edge of the delay curve (the farther one moves it away from this edge, the more passive delay one has to put into the gamma-ray signal path and the more the efficiency of the apparatus is reduced), so it sent through a few prompt pulses.

### C. Discussion

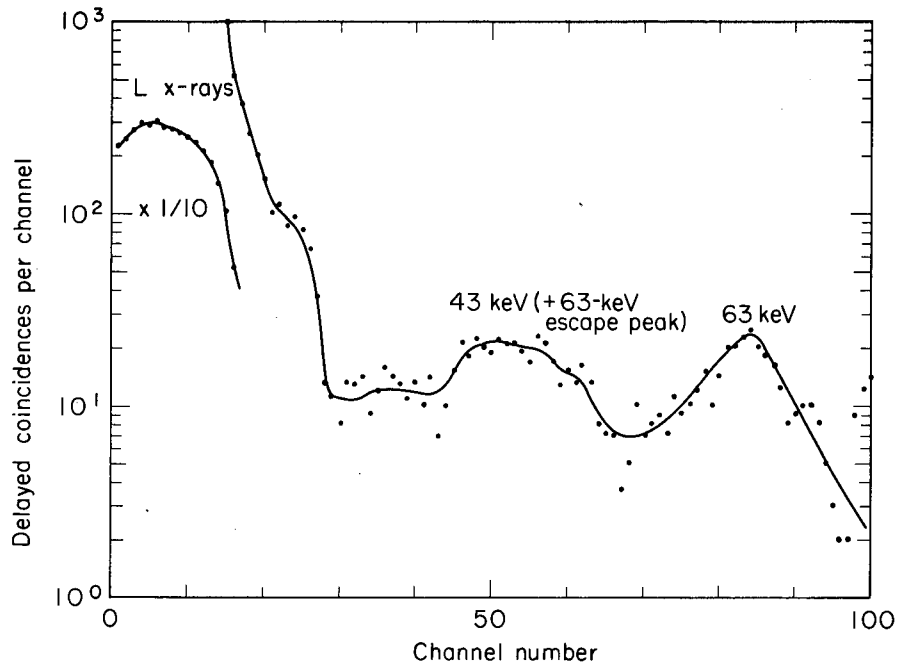
#### 1. Decay Scheme

In this section we will establish the simplest level scheme consistent with the experimental data just described. Just as complex arrangements of capacitors and resistors in a "black box" can be reduced effectively to "delta" or "tee" configurations, it is possible that some very complex procedures cause the phenomena we have observed in  $\text{Es}^{254}$  decay, but we have found nothing to warrant a more complex scheme than the one developed below. In construction of this level scheme it is not necessary to introduce any detailed interpretation of the nature of the levels, although, as we will later show, the agreement between the scheme and the predicted levels of  $\text{Bk}^{250}$  is remarkably good. The only assumption we will make, other than the scheme be no more complicated than necessary to explain the data, is the existence of rotational bands, the occurrence of which is well established in this region.<sup>3</sup>



MU-36064

Fig. 25. Block diagram of the apparatus used to obtain a delayed gamma-ray spectrum. Alpha pulses started and single-channel-analyzed L-x-ray pulses stopped a time-to-height converter. Its output was sent through a single-channel analyzer that selected that portion of the delay curve just following the prompt edge (see inset) to act as gates for the original gamma-ray pulses, which had been delayed to meet the gates. An approximate pulse shape is shown after each stage. The small RIDL RC-shaping amplifiers were used merely as pulse shapers.



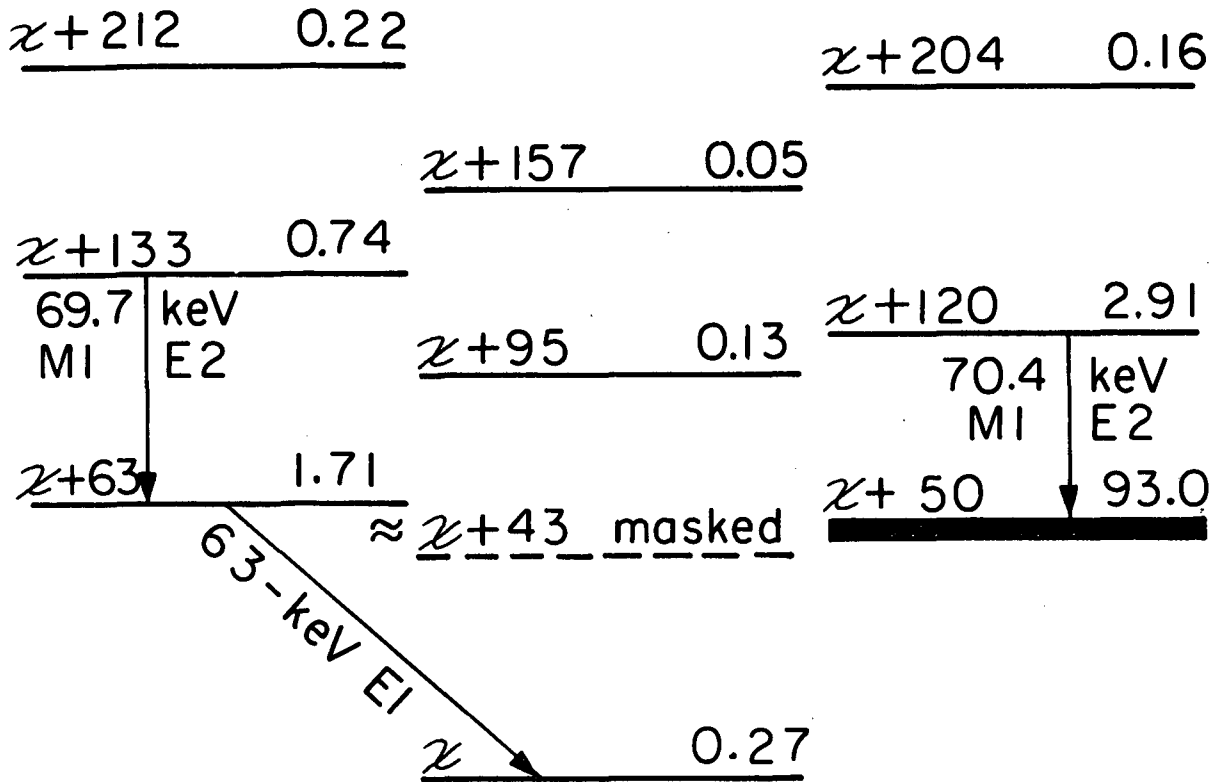
MU-36065

Fig. 26. Delayed gamma-ray spectrum obtained with the apparatus in Fig. 25. This spectrum shows the 42.6-keV  $\gamma$  from  $\text{Es}^{254}$  directly, and in an abundance of  $0.3 \pm 0.1\%$ .

The higher-energy alpha groups listed in Table III (and centered in Fig. 6) can be rather convincingly divided into three rotational bands, as sketched in Fig. 27, where the position of the  $Bk^{250}$  ground state with respect to these bands is not yet known. The intensities as well as the relative energies of the alpha groups have been used in this division. The second member of the lowest of these bands (at energy  $\approx x + 45$  keV) is not observed in the alpha spectra, but one would expect it to be obscured by the nearby very intense group.

Three of the observed gamma-ray transitions can be placed in this basic scheme immediately. The two M1-E2 transitions at about 70 keV (Table VI) fit very well as the lowest rotational transitions in two of the bands, and these have been duly entered in Fig. 27. The low intensity of these lines is consistent with the fact that  $\approx 95\%$  of the alpha decay goes to levels below these transitions. The stronger of the two, at 70.4 keV, is placed following the larger alpha population, i.e., between the  $x + 120$ - and  $x + 50$ -keV levels. The weaker then connects the  $x + 153$ - and  $x + 63$ -keV levels. The intensity of these two sets of lines, both relative to each other and in an absolute sense, seems correct for these placements, and, of course, the M1-E2 character is that expected for such rotational transitions.

The 63-keV gamma ray fits between the levels of energy  $x$  and  $x + 63$  keV. We previously decided this transition must be an E1 from a side branch in the decay scheme, since no conversion electrons were observed from it, and, assuming a normal conversion coefficient for it ( $\alpha_L = 0.36 \Rightarrow \alpha_{total} \cong 0.5$ ),<sup>55</sup> its total intensity of  $\approx 3.0\%$  is in good agreement with the total population of the band based on the level at  $x + 63$  keV (2.7%). This placement of the 63-keV transition implies that the 38-nsec half-life associated with this transition belongs to the  $x + 63$ -keV level, but, of considerably more importance at this point, it also implies that the  $x$ -keV level is not the ground state, because the 29- $\mu$ sec delay was found to follow the 63-keV transition. Thus, either the level at  $x$  keV or some lower level must have this 29- $\mu$ sec half-life, and the former (simpler) possibility turns out to be consistent with all our data.



$Bk^{250}$  -----  
 Ground state

MUB-5465

Fig. 27. Trial decay scheme for  $Es^{254}$ . The energies of the levels are given in keV on the left sides; the  $x$  indicates that the position of these with respect to the ground state is not yet known. Alpha populations are given in % on the right sides.

Considering now the band based on the  $x + 50$ -keV level, we find that  $\approx 96\%$  of all the alpha decay populates this band; therefore, all the intense transitions must be associated with its depopulation down to the ground state. And, of course, all the comments in the previous section about the two L-converted transitions now apply to the transitions that de-excite the  $x + 50$ -keV level. One of these was shown to follow the 29- $\mu$ sec delay, and one was found to precede it. Since we have tentatively assigned the 29- $\mu$ sec half-life to the  $x$ -keV level, this means that the depopulation of the  $x + 50$ -keV level must pass through the  $x$ -keV level. Remembering that the 42.6-keV M1-E2 and the 35.5-keV M2 transitions must be the L-converted transitions in the main sequence, we find that neither has the requisite energy to connect the  $x$ - and  $x + 50$ -keV levels directly, so a third transition is required. However, the 42.6-keV transition is very near the expected energy of the rotational transition connecting the  $x + 43$ - and  $x$ -keV levels. Its M1-E2 character also suggests such an assignment as a rotational transition. This would indicate that the first and unobserved transition is one of some 7 keV connecting the  $x + 50$ - and  $x + 43$ - keV levels, and such a transition would, indeed, have escaped our detection because of its low energy. The 213- $\mu$ sec half-life would then belong to the  $x + 50$ -keV level. The 35.5-keV M2 transition then is left to take part in the de-excitation of the  $x$ -keV level. As it is not necessary to assume further complication, this transition can connect it directly with the ground state. Its M2 character is consistent with the ground state. Its M2 character is consistent with the 29- $\mu$ sec half-life given to the  $x$ -keV level. Thus, the energy,  $x$ , in Fig. 27 becomes 35.5 keV. The only important feature not included here is the 34.4-keV M1-E2 transition, and its placement will be shown to fit into this scheme later. We believe this is the simplest scheme accounting for the observed data, apart, of course, from the weakly-populated, higher-energy excited states.

Since the placement of the 63 keV- $\gamma$  was crucial in the working out of this part of the level scheme, particularly in establishing the  $x$  (35.5)-keV level as the one having the 29- $\mu$ sec half-life, an experiment specifically designed to check its placement was made. This consisted of observing on a



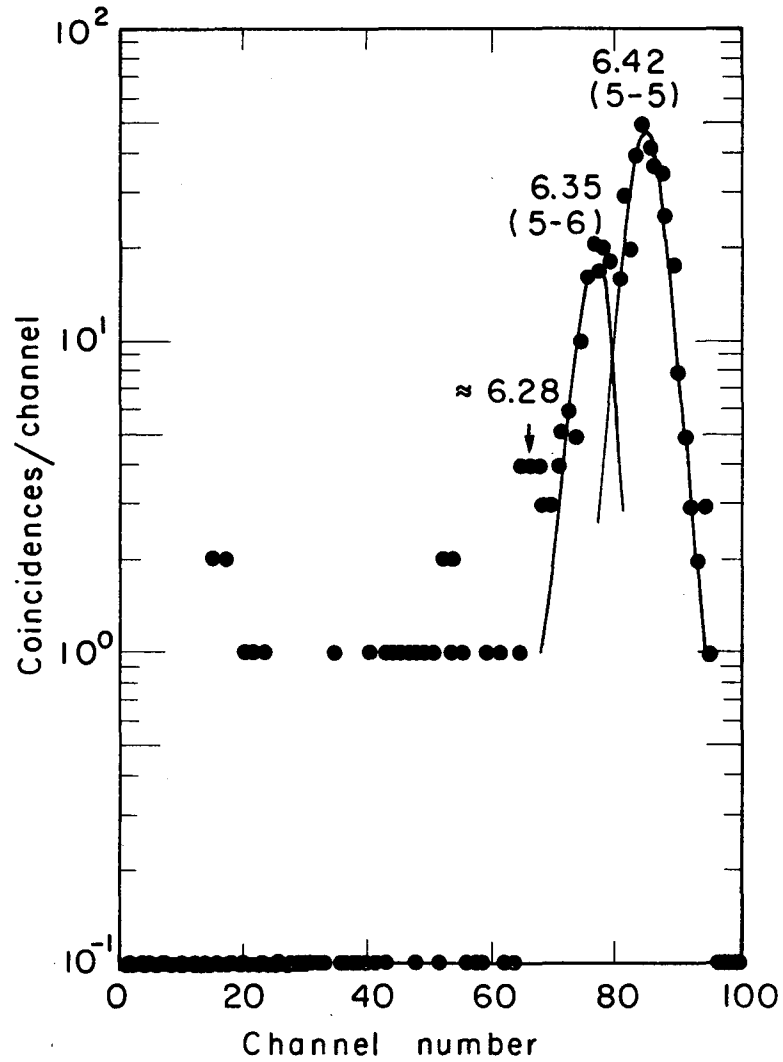
solid-state detector the alpha groups in coincidence with the 63-keV  $\gamma$ . Apparatus similar to that in Fig. 12 was used.<sup>56</sup> A spectrum obtained with a 12-hr run, using a  $10^4$   $\alpha$ /min Es<sup>254</sup> source is shown in Fig. 28. The statistics were rather poor, but groups at 6.42 and 6.35 MeV are clear, in a relative abundance of 1.0 and 0.4, respectively. Both the energies and intensities are in excellent agreement with the first two members of the  $x + 63$ - (i.e., 99) keV bands, as the scheme in Fig. 27 requires. It might be noted that even if an error in alpha-energy calibration occurred, such that the two levels could be the members of the  $x + 50$ -keV band (only 13 keV away), the relative intensities of the two groups would be in total disagreement with this band. The 63-keV transition appears, therefore, to be correctly placed in Fig. 27.

## 2. Spin and Nilsson-Level Assignments

A complete decay scheme based on the conclusions of the preceding section is shown in Fig. 29. Included here are also spin, parity, and Nilsson-level assignments and some higher-energy states, all of which will be developed in this section.

We will consider first the spin assignments of the lower bands. This will be done in two parts, the first consisting of a brief discussion of plausible spins independent of the expected states, and the second then being a detailed comparison of the observed bands with the expected bands. The result is a set of rather unambiguous spin assignments for the four lowest rotational bands.

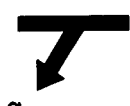
The ground state of Bk<sup>250</sup> has been assigned  $K\pi I = 2-2$  in order to account for the beta-decay properties<sup>13</sup> of this nucleus to the gamma-vibrational band in Cf<sup>250</sup>. With this assignment, the 34.4-keV M1-E2 transition, unplaced in the previous section, can be placed as the rotational transition de-exciting the 2-3 member of the ground state band; i.e., it is a transition in parallel with the 35.5-keV M2, which was suspected from the sum of their conversion lines (see Table IV) being  $\approx 100\%$  in intensity. The population of this proposed 2-3 level must be via an unobserved 1.1-keV E1, M2, or mixed transition from the 35.5-keV level. The pure M2 crossover transition from this 35.5-keV level to the



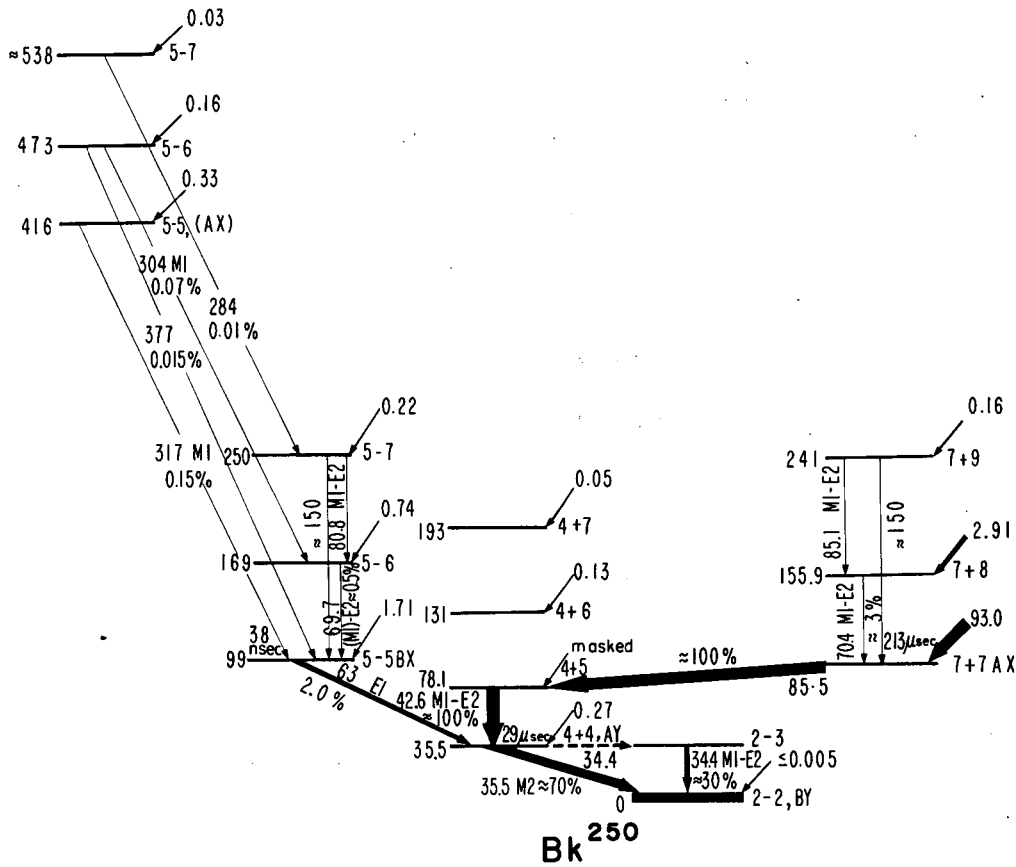
MU-36107

Fig. 28. Alpha particles observed in fast coincidence ( $\approx 50$  nsec resolving time) with the 63-keV  $\gamma$  from  $\text{Es}^{254}$  decay. This spectrum was obtained as a specially designed check on the placement of the 63-keV  $\gamma$  in the decay scheme of Fig. 27. It corroborates that placement. Alpha energies are given in MeV. Zero events are plotted at one-tenth.

Legend: %  $\alpha$  population  
 keV above ground K $\pi$ I, Proton state-neutron state

**Es<sup>254</sup>**  
  
 7+7, AX  
 $\alpha$   
 > 20 groups

Proton states	Neutron states
A 7/2+ [633 $\uparrow$ ]	X 7/2+ [613 $\uparrow$ ]
B 3/2- [521 $\uparrow$ ]	Y 1/2+ [620 $\uparrow$ ]



MUB-6632

Fig. 29. The decay scheme of Es<sup>254</sup>.

ground state suggests spin  $0^+$  or  $4^+$  for it, and the branching to the 3-member of the ground band makes  $4^+$  the reasonable choice.

Since the 63-keV transition is E1, the 99-keV level must then have spin  $3^-$ ,  $4^-$ , or  $5^-$ , and the lack of any population to the ground-band 2- or 3- states, in spite of the 38-nsec half-life of this level, makes  $5^-$  the most likely assignment. The 78-keV level, as the first rotational state based on the  $4^+$  (35.5-keV) level, should be assigned  $4^+$ . Since the 86-keV level has a half-life of 213- $\mu$ sec, it is unlikely that the 7-keV transition, which connects this level with the one at 78-keV, has a multipolarity higher than two. The spin of the 86-keV level would then lie between 3 and 7, with the parity unknown. However, the lack of any detectable transition to the  $4^+$  (35.5-keV) level rather strongly suggests a spin larger than 5 (or  $> 6$  if the 7-keV transition has  $L = 2$ ). Thus, the 86-keV level probably has a spin of 6 or 7. The above assignments are obviously only probable ones, based solely on the interband transitions and the previous 2-2 ground-state assignment. In the rest of the section we will compare in detail the properties of the expected bands in  $\text{Bk}^{250}$  with these assignments.

We will first construct a hypothetical level scheme for the odd-odd nucleus,  $\text{Bk}^{250}$ , from the properties of the appropriate odd-mass nuclei. This construction is based on the assumption of complete independence of the two odd particles. That such a treatment works so well is one of the most surprising conclusions coming from the study of odd-odd nuclei. Fortunately, two of the four neighboring odd-mass nuclei,  $\text{Bk}^{249}$  and  $\text{Cf}^{251}$  (having the same odd proton<sup>34</sup> and neutron<sup>12</sup> respectively, as  $\text{Bk}^{250}$ ), have been well studied. Their respective level schemes are shown in Figs. 30 and 31. The single-particle states identified in these nuclei are, of course, the most likely Nilsson single-particle states for constructing the two-particle states of  $\text{Bk}^{250}$ . The respective Nilsson diagrams themselves,<sup>4</sup> showing all the available single-proton and single-neutron states for this region are presented in Figs. 32 and 33. They show the effect of a prolate spheroidal deformation on the shell-model states, which split into twofold-degenerate components. The relative energy of these components

### $E^{253}$ decay scheme

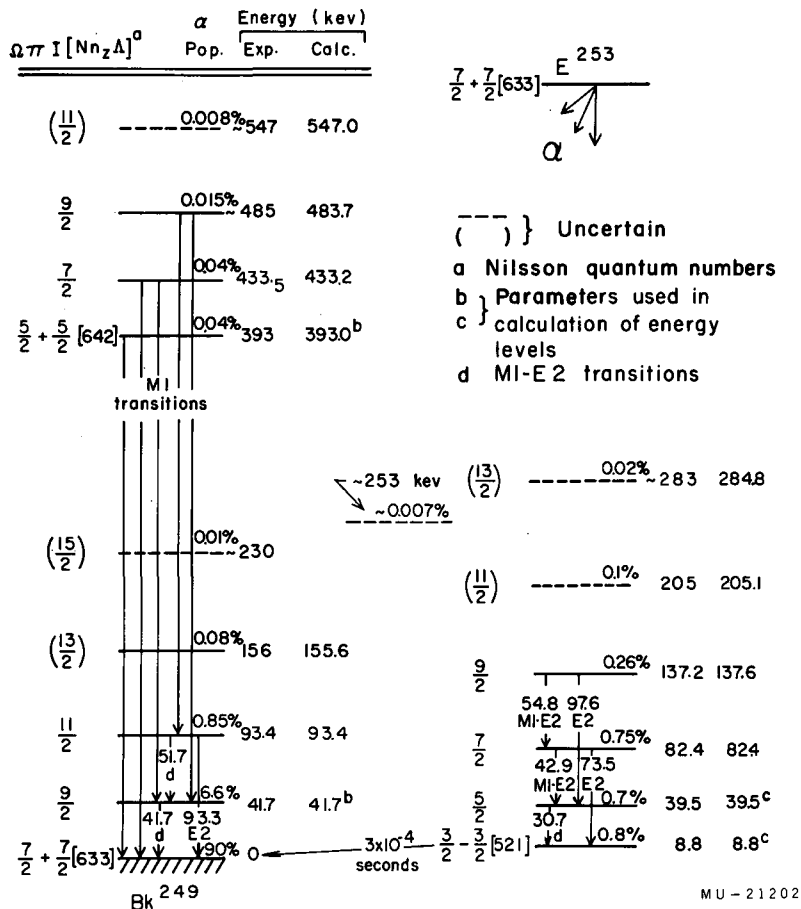


Fig. 30. The decay scheme of  $Es^{253}$ , showing the levels in  $Bk^{249}$ , which should be the "most available" single-proton states to be used in constructing the odd-odd states in  $Bk^{250}$ . From Ref. 34.

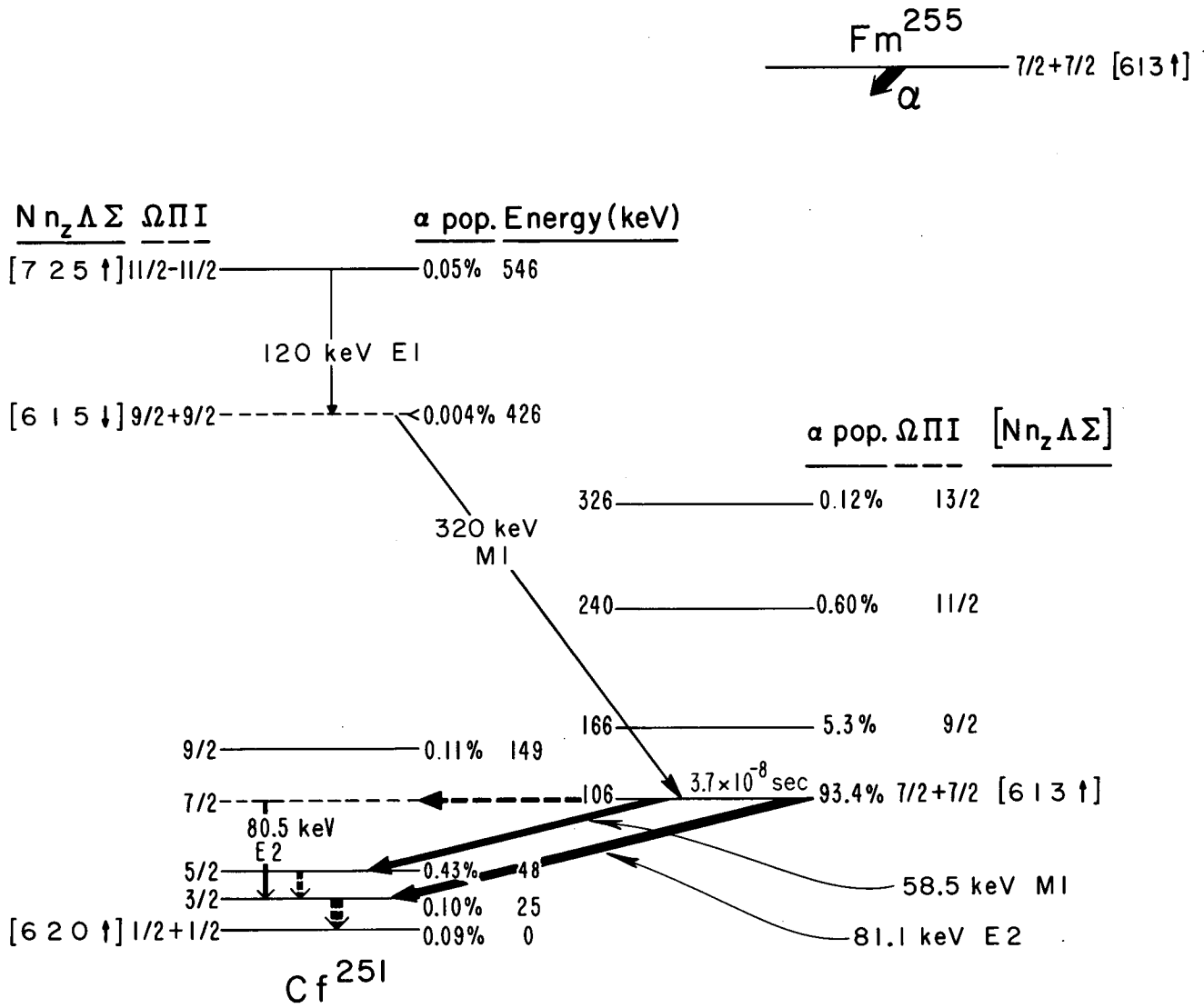
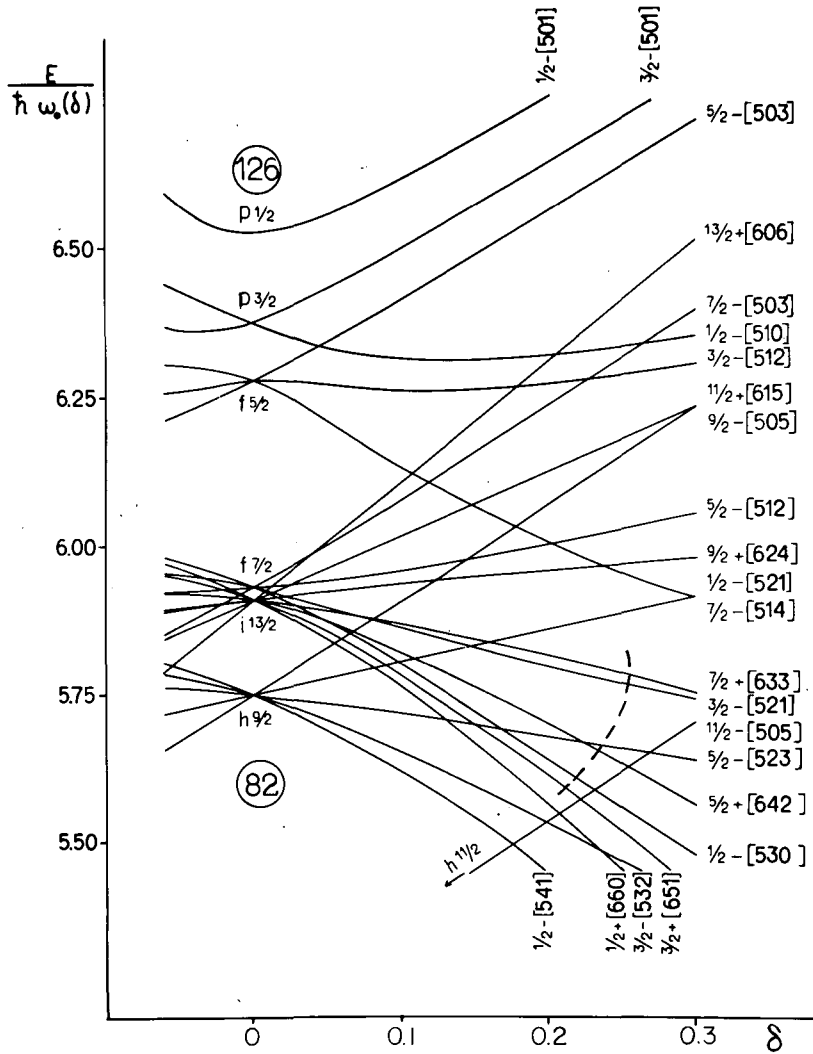
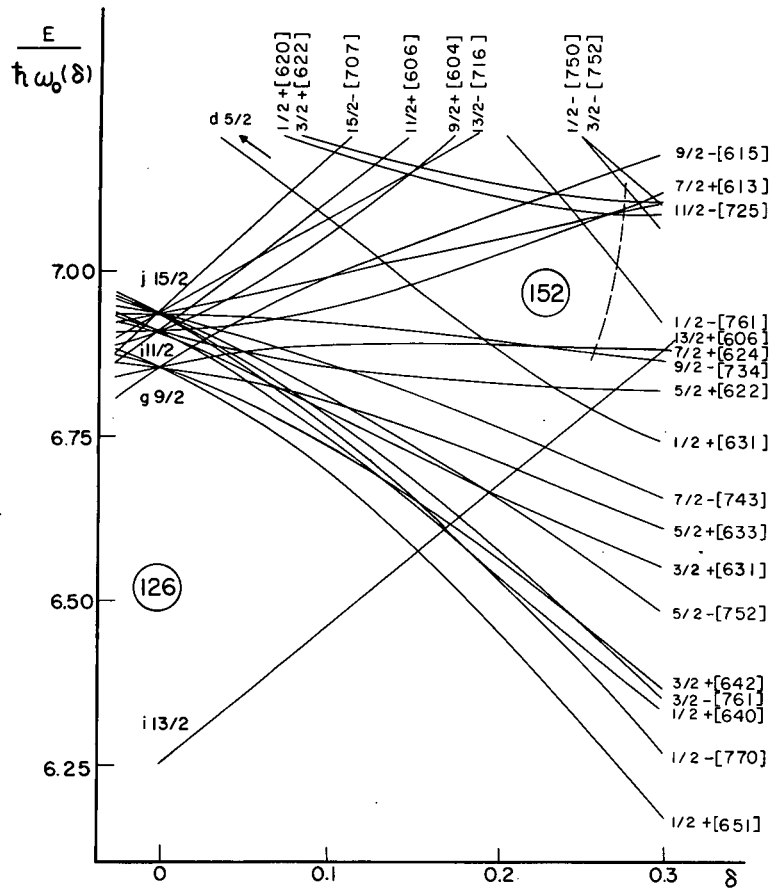


Fig. 31. The decay scheme of  $Fm^{255}$ , showing the levels in  $Cf^{251}$ , which should be the "most available" single-neutron states to be used in constructing the odd-odd states in  $Bk^{250}$ . From Ref. 12.



MU-15745

Fig. 32. Nilsson diagram showing single-proton states' relative energy plotted against nuclear deformation. The region of interest is indicated by the dashed line. Quantum numbers identifying the states are  $\Omega$ , projection of the particle spin (i.e.,  $j$ ) on the nuclear symmetry axis;  $\pi$ , parity;  $N$ , total number of nodes in the wave function;  $n_z$ , number of nodal planes perpendicular to the symmetry axis;  $\Lambda$ , projection of particle orbital angular momentum;  $\Sigma$  (not in the figure but used in the text), projection of the particle intrinsic spin. From Ref. 57.



MU-15744

Fig. 33. Nilsson diagram showing single-neutron states' relative energy plotted against nuclear deformation. The region of interest is indicated by the dashed line. This diagram shows clearly the neutron subshell at 152 neutrons caused by an accidental energy gap between neutron states at large deformations. The quantum numbers are explained in the caption to Fig. 32. From Ref. 57.



is plotted against the nuclear deformation,  $\delta$ , defined as (major radius - minor radius)/(average radius). The regions of interest for this study are indicated by dashed lines in each figure. The Nilsson states are identified by the following quantum numbers:  $\Omega\pi[N n_z \Lambda \Sigma]$ , where  $\Omega$  is the projection of the particle angular momentum,  $j$ , on the nuclear symmetry axis,  $\pi$  is the parity,  $N$  is the principal oscillator quantum number (the total number of nodes in the wave function),  $n_z$  is the number of nodal planes perpendicular to the nuclear symmetry axis, and  $\Lambda$  and  $\Sigma$  are the orbital and intrinsic-spin components of  $\Omega$  such that  $\Omega = \Lambda \pm \Sigma$ , depending on a parallel (spin-up,  $\uparrow$ ) or anti-parallel (spin-down,  $\downarrow$ ) arrangement of  $\Lambda$  and  $\Sigma$ .

Our method of constructing the properties of the odd-odd nucleus will be illustrated using the ground states of  $\text{Bk}^{249}$  and  $\text{Cf}^{251}$ , which have  $K\pi$  values of  $7/2+$  and  $1/2+$ , respectively; i.e., these are the Nilsson single-particle  $7/2+$   $[633\uparrow]$  proton and  $1/2+$   $[620\uparrow]$  neutron states. These can be combined to give two-particle states with  $K\pi$  values of  $4+$  and  $3+$ , of which the Gallagher and Moszkowski coupling rules<sup>58</sup> would predict the  $4+$  (triplet coupling,  $\Sigma = 1$ ) to lie lower in energy. We do not guess as to the splitting of these levels (50 - 100 keV in most cases known), but we will take the predicted energy of the lower level simply to be the sum of the energies of the band heads in the odd-mass nuclei, zero in this instance. The expected value of  $\hbar^2/2\mathcal{I}$  for these bands (presumably equal) is obtained by adding the values of  $2\mathcal{I}/\hbar^2$  for the appropriate bands in the odd-mass nuclei and then subtracting a value representing the nearby even-even nuclei (taken<sup>59</sup> from  $\text{Cf}^{250}$  to be  $1/7.03 \text{ keV}^{-1} = 142 \text{ MeV}^{-1}$ ; in this manner we empirically add the increase in the moment of inertia,  $\mathcal{I}$ , over that of the even-even core that is caused by each odd particle, and then we subtract out the value of the core so as not to include it twice. For the  $4+$  and  $3+$  bands under consideration, this gives:  $216 + 156 - 142 = 230 \text{ MeV}^{-1}$ , or  $\hbar^2/2\mathcal{I} = 4.36 \text{ keV}$ . Higher-order terms will be considered later, but we will make predictions here as to the sign of  $B$ , the coefficient of the  $I^2(I+1)^2$  term in the rotational-energy equation. This

coefficient is probably small and negative for the neutron band but larger and positive for the proton band (Sec. II.C.6 or, for a complete explanation, Sec. V), so it should be expected to be positive for the composite  $4+$  and  $3+$  bands. These predictions are listed in Table VII for all the expected low-energy bands in  $\text{Bk}^{250}$ . At the intersection of column and row for the proton and neutron states the composite states are listed, with the higher-lying singlet coupling in parentheses, and under these are listed the other predictions.

We also can estimate the alpha population to some of the various bands in  $\text{Bk}^{250}$ , due to the fortunate circumstance that the alpha-emitting state in  $\text{Es}^{254}$  is very likely a  $K\pi = 7+$  level (discussed later, naturally) composed of the  $7/2+ [633\uparrow]$  proton state and the  $7/2+ [613\uparrow]$  neutron state. It is just these particular proton and neutron states that are assigned as the ground states of  $\text{Es}^{253}$  and  $\text{Fm}^{255}$ , whose alpha decays have been studied<sup>34,12</sup> and provide the above-mentioned information on the levels in  $\text{Bk}^{249}$  and  $\text{Cf}^{251}$ . Thus, alpha-decay hindrance factors are known for each of the bands in  $\text{Bk}^{249}$  and  $\text{Cf}^{251}$ . (The hindrance factor is defined as the ratio of the alpha decay calculated by simple spin-independent barrier-penetration theory, i.e., to the ground state of an even-even nucleus, to the experimentally-observed alpha decay; more of this in Sec. II.C.3.) For the odd-odd nucleus, in cases where one particle remains unchanged, we will assume that the hindrance factor is simply the product of the appropriate two odd-mass hindrance factors, one being favored decay (particle unchanged) and the other generally being unfavored decay (particle changed). Two qualifications must be made to this proposal. First, hindrance factors between states where both particles change or where the relative orientation of the proton and neutron changes (i.e., between singlet and triplet states) cannot be estimated other than to guess that they will be quite large. This unpredictability comes about because the odd-odd decay will generally allow different alpha waves (L values) in different proportions than did the corresponding odd-mass decay. Second, rather than introduce at this point a discussion of alpha L-waves (Sec. II.C.3., please), we will simply take as representative of each band the state having the lowest

Table VII. Properties of rotational bands in Bk<sup>250</sup>.

Proton states	7/2 + [633↑]	3/2 - [521↑]	5/2 + [642↑]
Neutron states	<u>Predicted Properties</u>		
1/2 + [620↑]	Kπ=4+ (3+) E =0 keV ħ <sup>2</sup> /2I=4.36 keV B, positive HF=750	Kπ=2- (1-) E =9 keV ħ <sup>2</sup> /2I=5.65 keV B, negative HF, large	Kπ=3+ (2+) E =389 keV ħ <sup>2</sup> /2I=5.36 keV B, positive HF, large
7/2 + [613↑]	Kπ=7+ (0+) E =106 keV ħ <sup>2</sup> /2I=4.48 keV B, positive HF=2.0	Kπ=5- (2-) E =115 keV ħ <sup>2</sup> /2I=5.86 keV B, negative HF=90	Kπ=6+ (1+) E =495 keV ħ <sup>2</sup> /2I=5.54 keV B, positive HF=34
	<u>Experimental Properties</u>		
1/2 + [620↑]	Kπ=4+ E =35.5 keV ħ <sup>2</sup> /2I=4.26 keV B, positive HF=1270	Kπ=2- E = 0 keV ħ <sup>2</sup> /2I=5.73 keV B, ? HF>1.3 × 10 <sup>5</sup>	not observed
7/2 + [613↑]	Kπ=7+ E =85.5 keV ħ <sup>2</sup> /2I=4.40 keV B, positive HF=2.9	Kπ=5- E =99keV ħ <sup>2</sup> /2I=5.83 keV B, negative HF=136	Kπ=6+ E =434 keV ħ <sup>2</sup> /2I=4.6 keV B, ? HF=160

hindrance factor (not necessarily the lowest member of the band). The error introduced by using this particular state generally should be small and should rarely, if ever, exceed a factor of two. For the  $K\pi = 4+$  and  $3+$  states we have been considering, no hindrance factor is predicted for the  $3+$  state (it should be very large), because the  $\Omega\pi = 7/2+$  and  $1/2+$  neutron states are oppositely oriented in the parent and daughter relative to the unchanging  $7/2+$  proton state (i.e., it is a singlet state, whereas the parent is a triplet). A hindrance factor of 1.93 (proton,  $7/2+ \rightarrow 1/2+$ ), times 390 (neutron,  $7/2+ \rightarrow 1/2+$ ), or 750 is predicted for the  $4+$  state. The hindrance factors are included in Table VII.

We will now compare the properties of the observed bands in  $\text{Bk}^{250}$  with those estimated in Table VII. First, the ground-state band has the following observed properties:  $E = 0$  keV,  $\hbar^2/2\mathcal{I} = 5.73$  keV (for  $K = 2$ ),  $\alpha \text{HF} \geq 1.3 \times 10^5$ , and suggested spin and parity  $2-$ . The agreement with the theoretical  $2-$  band composed of the  $1/2[620\uparrow]$  neutron and the  $3/2-[521\uparrow]$  proton is, in all respects, excellent. The other possible assignment as the  $2-$  band composed of the  $3/2-[521\uparrow]$  proton and the  $7/2+[613\uparrow]$  neutron would be poorer with respect to predicted energy by more than 100 keV and in flat contradiction to the Gallagher-Moszkowski rules, which say that the  $5-$  band composed of these states should lie lower in energy than the  $2-$  band. The former assignment thus seems clearly indicated.

The band based on the 35.5-keV level has:  $E = 35.5$  keV,  $\hbar^2/2\mathcal{I} = 4.26$  keV (for  $K = 4$ ),  $\alpha \text{HF} = 1270$ , and proposed spin and parity  $4+$ . The agreement with the theoretical  $4+$  band composed of the  $7/2+[633\uparrow]$  proton and the  $1/2+[620\uparrow]$  neutron is almost unbelievably good. In particular, the unusually small predicted value for  $\hbar^2/2\mathcal{I}$  (associated largely with the  $7/2+[633\uparrow]$  proton state) is remarkably well borne out in this band.

For the band based on the 99-keV level, we find:  $E = 99$  keV,  $\hbar^2/2\mathcal{I} = 5.75$  keV (for  $K = 5$ ),  $\alpha \text{HF} = 136$ , and proposed spin and parity  $5-$ . Again the choice from Table VII is clear—the  $5-$  band composed of the  $3/2-[521\uparrow]$  proton and the  $7/2+[613\uparrow]$  neutron. The agreement is as good in this case as for the two previous bands.

We consider finally the band based on the 86-keV level. This band obviously received the favored alpha decay; therefore, it is expected to have the same configuration as the parent,  $\text{Es}^{254}$ . It is, in fact, on the basis of the properties of this band that the parent is presumed to have the 7+ configuration used in estimating the alpha hindrance factors. We find for this band:  $E = 86$  keV,  $n^2/2\mathcal{S} = 5.03$  keV (for  $K = 6$ ) or 4.40 keV (for  $K = 7$ ),  $\alpha \text{ HF} = 2.9$ , and probable  $K$  values of 6 or 7, parity unknown. The assignment as the  $K\pi = 7+$  state made up of the  $7/2+[633\uparrow]$  proton and the  $7/2+[613\uparrow]$  neutron is rather clear. The only other high-spin state near this energy is the  $K\pi = 5-$  configuration composed of the  $3/2-[521\uparrow]$  proton and the  $7/2+[613\uparrow]$  neutron. One might consider this assignment both for the 86-keV state and the  $\text{Es}^{254}$  parent state; however, the gamma-transition de-excitation pathway would be extremely unlikely on this basis. Also, the 99-keV band meets the predictions for this 5- configuration quite admirably, while, with the 7+ assignment, the 85.5-keV band shows the unusually small value for  $n^2/2\mathcal{S}$  and the positive  $B$  associated with the  $7/2+[633\uparrow]$  proton state. Finally, if the 85.5-keV level and the  $\text{Es}^{254}$  parent state were 5-, the 2- rather than the 4+ band should have received alpha population.

Before proceeding further, something should be said about the Gallagher-Moszkowski coupling rules<sup>58</sup> and why one should be able to trust them when the Nordheim coupling rules for spherical odd-odd nuclei have proved so treacherous. First of all, in deformed nuclei one does not find the wealth of possible states resulting from a given proton and neutron that one finds in spherical nuclei, for the symmetry and projection quantum numbers allow only an algebraic either-or coupling rather than the vectorial-coupling proliferation of possibilities. In spherical nuclei the energy is minimized when the orbital wave functions of the two particles are coupled anti-parallel and the intrinsic spins are coupled to a triplet (parallel). When both these requirements can be met, the so-called "strong" Nordheim rule is in effect, but when they are in competition, though the "weak" Nordheim rule predicts the triplet coupling will win out, one usually finds an intermediate coupling taking place. For deformed nuclei, not

only are such intermediate orientations eliminated, but also, because of a plane of reflection symmetry in the nucleus that makes it necessary to symmetrize the wave functions in  $+K$  and  $-K$ , for a pure  $\delta$ -function force the parallel and anti-parallel overlappings of the orbital wave functions both minimize that contribution to the energy. As one proceeds toward more complex and realistic forces, it is true that the anti-parallel coupling does become favored, but apparently not to a significant extent. Thus, the Gallagher-Moszkowski rules predict that the determining factor will be strictly the parallel coupling of the intrinsic spins, or  $\Sigma$ 's, with little or no aid or competition from the orbital coupling, and the proton-neutron triplet configuration will always lie lower in energy. So far there is no known violation of these rules in the heavy-element region, and the lone violation in the rare-earth region (in  $\text{Ho}^{166}$ ) can be explained satisfactorily by Coriolis coupling in a rather novel situation: the 0-singlet state from a  $7/2-[523\uparrow]$  proton and a  $7/2+[633\uparrow]$  neutron is pushed below the 7- triplet state because there is a wealth of higher-lying bands to interact with it but none to interact with the 7- triplet.<sup>60</sup> There is not an analogous situation in  $\text{Bk}^{250}$ , so we can safely expect the rules to hold.

Coming back to the states in  $\text{Bk}^{250}$ , the close correspondence between the predicted and observed properties of these lowest four bands is quite remarkable. This agreement, together with the independently established level scheme and proposed spins, makes the assignment of the levels, in our opinion, essentially certain. Furthermore, it indicates that the odd proton and odd neutron must behave essentially independently of each other. In the next few sections we will first examine in more detail some of the properties of the bands and then take a look at the higher-lying states.

### 3. Alpha Transition Probabilities

Hindrance factors were calculated for the alpha groups of  $\text{Es}^{254}$ , using the spin-independent equations of Preston.<sup>61</sup> Because of the scarcity of information in this region, there is some uncertainty as to what one should use for the nuclear radius. If one assumes  $r_0 \propto A^{1/3}$  and uses

9.42822 fermis<sup>62</sup> for the radius of Es<sup>253</sup>, he comes out with 9.44067 as the calculated radius of Es<sup>254</sup>. This value of  $r_0$  in the calculation yields 3.3 for the hindrance factor of the favored 6.437-MeV alpha group. However, the effective value of  $r_0$  should depend on the nuclear states as well as on  $A^{1/3}$ , and, for example,  $r_0$  for Fm<sup>255</sup> (=9.3614 fermis)<sup>62</sup> is smaller than  $r_0$  for Es<sup>253</sup>. If one takes the average of  $r_0$  for Es<sup>253</sup> and Fm<sup>255</sup>, one gets  $r_0 = 9.3948$  fermis for Es<sup>254</sup>, and this value yields 2.9 for the hindrance factor of the 6.437-MeV alpha group. Since we are interested in the relative values of the hindrance factors, we arbitrarily picked the latter value for  $r_0$ . Hindrance factors calculated with it are listed in Table VIII according to the rotational bands they populate. They were used as an aid to grouping the various levels into rotational bands, as was discussed previously.

The alpha decay of an odd-mass nucleus to a rotational band in the daughter that has the same intrinsic configuration as the parent is known as "favored" decay and is very similar to the decay of an even-even nucleus ( $K = 0$ ) to the ground-state rotational band ( $K = 0$ ) of its daughter. It has been shown that hindrance factors for alpha waves of the same angular momentum are very nearly the same for both situations.<sup>63</sup> Again, little is known concerning odd-odd cases, but the successful predictions of Table VII make it seem worthwhile to extend this favored-decay concept to odd-odd nuclei along with the other odd-mass properties.

Alpha transition probabilities to the various states in a rotational band receiving favored alpha decay are given by:

$$P = \frac{P_E}{N} \sum_{L=0,2,4,\dots} \frac{\langle I_i L K_i (K_f - K_i) | I_i L I_f K_f \rangle^2}{HF_L}$$

where  $P_E$  is the alpha transition probability expected from simple (spin-independent) barrier-penetration theory,  $HF_L$  is the hindrance factor from the closest even-even (or, in this case, the neighboring odd-mass) nuclides for alpha emission with angular momentum  $L$ , and the Clebsch-Gordon coefficient couples the spin of the parent nuclear state with the alpha particle

Table VIII. Alpha hindrance factors for Es<sup>254</sup> decay.

<u>K<math>\pi</math>I of final state</u>	<u>Excited-state energy (keV)</u>	<u>Alpha energy (MeV)</u>	<u>Intensity (%)</u>	<u>Hindrance factor</u>
7+7	85.5	6.437 $\pm$ 0.005	93.0	2.9
7+8	155.9	6.367 $\pm$ 0.005	2.91	43
7+9	241	6.284 $\pm$ 0.005	0.16	310
7+10	$\approx$ 334	6.193 $\pm$ 0.010	0.08 <sup>a</sup>	$\approx$ 240 <sup>a</sup>
5-5	99	6.424 $\pm$ 0.005	1.71	136
5-6	169	6.355 $\pm$ 0.005	0.74	150
5-7	249	6.276 $\pm$ 0.005	0.22	210
5-8	$\approx$ 327	6.200 $\pm$ 0.010	0.05 <sup>a</sup>	$\approx$ 340 <sup>a</sup>
4+4	35.5	6.486 $\pm$ 0.005	0.27	1700
4+5	78.1	masked	----	----
4+6	131	6.392 $\pm$ 0.005	0.13	1300
4+7	193	6.331 $\pm$ 0.005	0.05	1700
4+8	270	6.255 $\pm$ 0.010	0.01	3900
2-2	0	6.524 $\pm$ 0.010 $\leq$	0.005	$\geq 1.3 \times 10^5$
2-3	34.4	masked, if present	----	----
5-5	416	6.113 $\pm$ 0.005	0.33	23
5-6	473	6.068 $\pm$ 0.005	0.16	25
5-7	$\approx$ 538	6.00 $\pm$ 0.02	0.03	60
( 6+6	434	6.089 $\pm$ 0.005	0.08	160 )
( 6+7	$\approx$ 498	masked	----	----

<sup>a</sup>These two groups, and possibly a third, were not resolved in our alpha spectra; therefore, these hindrance factors are, if anything, too small.



spin (together with their respective K values) to form the spin of the daughter state (and its K). N generally has a value between 1 and 2 and is treated as a parameter to be determined empirically, although it can be calculated from a detailed knowledge of the nuclear wave function.<sup>64</sup> For our purposes here it can be set = 1.

These calculated alpha transition probabilities are compared with the experimental intensities in Table IX. Relative hindrance factors of 1:3.85:36.8 for L = 0:2:4 were used, an average of those given for Es<sup>253</sup> (1:3.7:43.5)<sup>34</sup> and Fm<sup>255</sup> (1:4:30).<sup>12</sup> The hindrance factor for the L = 6 wave<sup>65</sup> is approximately 1300, so this wave should have a negligible contribution. Calculations were originally made for all K values between 4 and 9 as an aid in assigning the spin of the 85.5-keV band. It is pointless still to pretend that we have not assigned a spin to that band, so the complete calculations are included only for the correct  $K_{\pi} = 7+$  assignment; the fit is reasonably good. For comparison, the predicted intensities to the first three members of the band are included for all the other K values. It can be seen that there is a monotonic change with K, with the lower K-values predicting far too much population to the upper members, while K = 7, 8, and 9 all give reasonable fits, K = 8 being the best, in fact.

Although the agreement in Table IX is reasonably good, it could be improved by using a lower relative hindrance factor for the L = 2 alpha wave; however, not only would it be useless to try to improve the simple theory without a clear physical basis, juggling the numbers could easily cloud the issue until one was not at all sure as to what they meant. Of more significance is the ratio of the population to the 7+9 member to that to the 7+8 member. Our experimental ratio is 34% lower than the calculated value; however, it is generally found that the experimental ratio is 20-30% lower than the calculated one, and in Fm<sup>255</sup> decay it is 36% lower.<sup>12</sup> Usually this is interpreted as an interaction of the nuclear quadrupole moment with the outgoing alpha wave.<sup>66</sup> Considering the extrapolation to an odd-odd nucleus, our agreement is not bad. It would also be possible to consider the effects of band mixing due to the Coriolis interaction,

but, except for some unexpected interference between alpha waves of different angular momenta, this should not change the predictions in Table IX much.  $K = 6$  and  $K = 8$  would be the main added components, and it can be seen that their alpha-intensity distributions do not vary that much from that of  $K = 7$ .

One could perform similar calculations for the alpha decay to the other bands, using the relative hindrance factors that are found for the corresponding single-particle bands in  $Bk^{249}$  and  $Cf^{251}$ . However, this is becoming increasingly esoteric, and it is probably more meaningful to force the predicted intensities to fit the experimental intensities to the first two levels in a band, and from this to obtain the relative mixtures of alpha  $L$  waves populating each band. This is done for the 5- and 4+ bands in Table X.

A reasonably good fit is obtained for alpha population to the 5- band if one uses a mixture of 71%  $L = 3$  and 29%  $L = 5$  alpha waves. This means the hindrance factors for these alpha waves to this band are approximately 67 and 160, respectively. The corresponding hindrance factors for  $L = 3$  and  $L = 5$  alpha waves to the 3/2- band in  $Bk^{249}$  are 32 and 230.<sup>34</sup>

For the population to the 4+ band one can obtain a fit by using 51%  $L = 4$  and 49%  $L = 6$  alpha waves, with respective hindrance factors of about 570 and 600. The hindrance factor for the  $L = 4$  wave, in particular, seems large—it is only 160 for the analogous transition to the 1/2+ band in  $Cf^{251}$ .<sup>12</sup> In that nucleus the Coriolis mixing of the 7/2+ (same as parent) and 1/2+ bands was particularly severe because of an accidental superposition of their 7/2+ members. Still, it is not obvious why the hindrance factor for the  $L = 4$  wave to the 4+ band in  $Bk^{250}$  should be so large, especially why it is almost as large as that for the  $L = 6$ .

A less empirical approach to alpha-decay theory has been developed by Rasmussen, Mang, and Poggenburg,<sup>102</sup> but as of yet their calculations have not been extended to cover odd-odd decay. It will be interesting and worthwhile to apply their calculations to these einsteinium nuclei as soon as it becomes possible.

Table IX. Calculated alpha populations for Es<sup>254</sup> favored alpha decay.

Excited-state energy (keV)	I	Calculated intensities (%)				Σ L	Experimental intensities (%)
		L = 0	L = 2	L = 4			
<u>for K = 7</u>							
85.5	7	78.7 (norm)	13.7	0.55	93.0 (norm)	93.0	
155.9	8	-----	2.83	0.41	3.24	2.91	
241	9	-----	0.16	0.11	0.27	0.16	
≈334	10	-----	-----	0.012	0.012	0.05 <sup>a</sup>	
≈451	11	-----	-----	0.0005	0.0005	not obs.	
<u>for K = 8</u>							
85.5	8	78.1 (norm)	14.3	0.64	93.0 (norm)	93.0	
155.6	9	-----	2.60	0.41	3.01	2.91	
241	10	-----	0.12	0.09	0.21	0.16	
<u>for K = 9</u>							
85.5	9	77.6 (norm)	14.7	0.72	93.0 (norm)	93.0	
155.9	10	-----	2.36	0.40	2.76	2.91	
241	11	-----	0.10	0.09	0.19	0.16	
<u>for K = 4</u>							
85.5	4	81.9 (norm)	10.8	0.21	93.0 (norm)	93.0	
155.9	5	-----	4.10	0.33	4.43	2.91	
241	6	-----	0.39	0.16	0.55	0.16	

Table IX. (Cont.)

Excited-state energy (keV)	I	Calculated intensities (%)				Σ L	Experimental intensities (%)
		L = 0	L = 2	L = 4			
<u>for K = 5</u>							
85.5	7	80.6 (norm)	12.1	0.34	93.0 (norm)	93.0	
155.9	6	-----	3.59	0.37	3.96	2.91	
241	7	-----	0.27	0.14	0.41	0.16	
<u>for K = 6</u>							
85.5	6	79.6 (norm)	13.0	0.45	93.0 (norm)	93.0	
155.9	7	-----	3.18	0.40	3.58	2.91	
241	8	-----	0.21	0.12	0.33	0.16	

<sup>a</sup>This group and the one populating the 5-8 level at  $\approx 327$  keV were not resolved, so the experimental intensity is only approximate.

Table X. Calculated alpha populations to the unfavored bands in Bk<sup>250</sup>.

Excited-state energy (keV)	I	Calculated Intensities (%)			Experimental intensities (%)
		L = 3 (71%)	L = 5 (29%)	$\frac{\Sigma}{L}$	
<u>K = 5- band:</u>					
99	5	1.56	0.15	$\frac{1.71}{L}$ (norm)	1.71
169	6	0.57	0.17	$\frac{0.74}{L}$ (norm)	0.74
249	7	0.10	0.09	0.19	0.22
≈327	8	0.011	0.024	0.035	0.05 <sup>a</sup>
≈435	9	0.0006	0.0003	0.0009	not obs.
<u>K = 4+ band:</u>					
		L = 4 (51%)	L = 6 (49%)	$\frac{\Sigma}{L}$	
35.5	4	0.24	0.03	$\frac{0.27}{L}$ (norm)	0.27
78.1	5	0.17	0.07	0.24	masked
131	6	0.064	0.066	$\frac{0.13}{L}$ (norm)	0.13
193	7	0.015	0.037	0.052	0.05
263	8	0.002	0.012	0.014	0.01
≈350	9	0.0002	0.0005	0.0007	not obs.

<sup>a</sup>This alpha group was not resolved from the one populating the 7+10 level and possibly another, so the experimental intensity is only approximate.

#### 4. Gamma-Ray Transition Probabilities

Three of the observed interband transitions have half-lives sufficiently long to be easily measurable. For these it is of interest to compare the observed half-lives with the single-particle estimates<sup>17</sup> and, especially, with whatever may be known about the analogous transitions in the neighboring odd-mass nuclei. In Table XI these delayed gamma transitions are listed with their half-lives, the corresponding single-particle estimates of their half-lives, and their retardations (the ratio of the experimental half-life to the single-particle estimate).

Considering first the 35.5-keV M2 transition, we find the partial half-life for the decay of the 4+4 level by this branch to be about 40  $\mu$ sec (including conversion). This is hindered by a factor of about 30 over the single-particle estimate. According to the assignments already made, this transition involves no change in the neutron state, but the proton state changes from 7/2+[633 $\uparrow$ ] to 3/2-[521 $\uparrow$ ]. In Bk<sup>249</sup> this same transition occurs in the opposite direction with an energy of 8.8 keV and a half-life of 0.3 msec (Fig. 30). The 35.5-keV transition in Bk<sup>250</sup>, if corrected to an energy of 9 keV ( $t_{1/2}(\text{M2 photon}) \propto E\gamma^{-5}$ , but toward lower energies the internal conversion increases greatly, making the overall half-life of a transition change rather slowly with energy), would have a half-life of about 0.18 msec. This agreement is excellent. We will not try to take into account the vector-addition coefficients either here or later in this section when comparing odd-mass and odd-odd nuclei, because the variation of transition probabilities even among different odd-mass nuclei having the same odd particle is sufficiently great to show that making such detailed comparisons would be meaningless.

In competition with this 35.5-keV M2 transition is the 1.1-keV transition to the 2-3 level. We can validly use the ratios of vector-addition coefficients here to predict the branching if the 1.1-keV transition were pure M2:<sup>67</sup>

$$\frac{(M2, I_1 \rightarrow I_2)}{(M2, I_1 \rightarrow I_2)} = \frac{(M2, 4+4 \rightarrow 3+3)}{(M2, 4+4 \rightarrow 3+3)}$$

$$\frac{G(M2, I_1 \rightarrow I_f)}{G(M2, I_1 \rightarrow I_f')} = \frac{G(M2, 4+4 \rightarrow 2-3)}{G(M2, 4+4 \rightarrow 2-2)} =$$

$$\frac{\langle I_1 K_1 (L=2) (K_f - K_1) | I_1 (L=2) I_f K_f \rangle^2}{\langle I_1 K_1 (L=2) (K_f - K_1) | I_1 (L=2) I_f' K_f \rangle^2} \cdot \frac{T_{sp}}{T_{sp}'} =$$

$$\frac{\langle 4 \ 4 \ 2 \ -2 \ 4 \ 2 \ 3 \ -2 \rangle^2}{\langle 4 \ 4 \ 2 \ -2 \ 4 \ 2 \ 2 \ -2 \rangle^2} \cdot (0.08) = \frac{0.311}{0.556} (0.08) = 0.04,$$

i.e., there should be a branch about 4% in intensity. (The ratio of the single-particle transition probabilities,  $T_{sp}/T_{sp}'$ , in the above equation shows the drastic difference conversion makes. The ratio, including conversion, is seen to be 0.08, whereas for the pure M2 photons it would be  $(1.1/35.5)^5 \approx 2 \times 10^{-8}$ .) The fact that the 1.1-keV transition is about an order of magnitude larger than 4% suggests that the transition is largely a K-forbidden E1. If so, the hindrance factor would be around  $10^6$ , not at all unreasonable for such a transition in this region. No analogous E1 transition can occur in Bk<sup>249</sup>.

The 7-keV transition connecting the 85.5-keV and 78.1-keV levels is very likely a K-forbidden E2, since an M3 would not only have a much longer half-life but would also populate the 4+4 level. As an E2 it is hindered by about  $2 \times 10^3$  over the single-particle estimate. This seems quite plausible, considering that the transition is K-forbidden. According to our assignments, this transition should involve no change in proton state but a change in neutron state from  $7/2+[613\uparrow]$  to  $1/2+[620\uparrow]$ . An analogous E2 transition was observed in Cf<sup>251</sup> between the above  $7/2+7/2$  state and the  $3/2+$  member of the  $1/2+$  band.<sup>12</sup> This transition in Cf<sup>251</sup> was found to be hindered by a factor of only 12 over the single-particle estimate, which was initially quite surprising inasmuch as it is K-forbidden. It was found, however, that in Cf<sup>251</sup> the  $7/2+$  member of the  $1/2+$  band accidentally occurred only 0.56 keV from the above  $7/2+7/2$  level. The mixing of these two levels can introduce small amounts of the collective E2

Table XI. Delayed Gamma Transitions in Bk<sup>250</sup>.

$E_{\gamma}$ (keV)	Multi-polarity	Experimental Half-life	Single particle estimate	Retardation	
7	E2	$213 \pm 8 \mu\text{sec}$	100 nsec	$2 \times 10^3$	
a {	35.5	M2	$\approx 40 \mu\text{sec}$	1.4 $\mu\text{sec}$	30
	1.1	E1	$\approx 100 \mu\text{sec}$	100 psec <sup>b</sup>	$10^6$
	63	E1	$38 \pm 5 \text{ nsec}$	100 fsec	$10^5$

<sup>a</sup>These two transitions are, of course, in competition with each other.

<sup>b</sup>Since conversion coefficients are not available for such low-energy transitions, we used that for the lowest available,  $\approx 20$  keV. This is justified by the fact that, at low energies, the overall transition rate does not change rapidly, i.e., the conversion increase just about balances the loss in photon rate; cf. Ref. 17.



transition probabilities between these two bands, and this was thought to be responsible for the relatively strong E2 transition. In Bk<sup>250</sup> there is no such accidental, close positioning of the I = 7 levels in  $K\pi = 4+$  and  $7+$  bands, and, correspondingly, the E2 transition probability is lower by over two orders of magnitude. This is quite consistent and even lends support to the above interpretation of the situation in Cf<sup>251</sup>. A similarly analogous transition has been examined very recently<sup>68</sup> in Cm<sup>249</sup>, resulting from the alpha decay of Cf<sup>253</sup>. Here there appears to be a K-forbidden E2 with a half-life of  $27 \pm 3$   $\mu$ sec and an energy not too far above the L edge leading from the  $7/2+7/2$  level to the  $1/2+3/2$  level, although a competing doubly K-forbidden M1 below the L edge leading to the  $1/2+5/2$  level cannot be definitely ruled out. This again appears consistent with what we have found for the transition in Bk<sup>250</sup>.

According to our assignments, the 63-keV E1 transition involves a change of both proton and neutron states. Such transitions are, of course, strictly forbidden on a simple single-particle picture and have no direct analogs in the odd-mass nuclei. This transition is hindered by a factor of about  $10^5$  over the single-particle estimate; however, this is not an especially large hindrance factor for a typical E1 transition in this region of the periodic table. In fact, as will be discussed below, it is not very easy to account for the strength of this transition.

It is interesting to note that the population of the  $K\pi = 2-$  and  $7+$  bands from this  $K\pi = 5-$  band can be estimated rather simply. The (unobserved) K-forbidden E2 transition from this 5-5 level to the 34.4-keV 2-3 level is, in single-particle terms, exactly the same transition as the 7-keV E2 between the  $7+7$  and  $4+5$  levels. Correcting the half-life of the 7-keV transition to the 65-keV energy difference between the 5-5 and 2-3 levels, we obtain a half-life of about 50  $\mu$ sec or a branching of about 0.1% to this level. Similarly, the (unobserved) 13.5-keV M2 transition connecting the 5-5 level with the  $7+7$  level is analogous to the observed 29- $\mu$ sec M2 transition; from this half-life a branching of 0.02% to the  $7+7$  level can be estimated. Both of these branchings are well below our limits of detection, so our failure to observe either is consistent with the expected transition half-lives.

The problem in accounting for the strength of the 63-keV E1 transition can be summarized as follows: the proton must change states from  $3/2-[521\uparrow]$  to  $7/2+[633\uparrow]$  simultaneously with the neutron change from  $7/2+[613\uparrow]$  to  $1/2+[620\uparrow]$ , and the former change (in the reverse direction) alone is at least an order of magnitude more retarded than the 63-keV E1, as evidenced by the 1.1-keV transition from the  $4+4$  to the  $2-3$  level. [An entertaining aside: the  $\text{Es}^{254}$  nuclei that decay to the  $5-$  band change their proton state from  $7/2+$  to  $3/2-$  to  $7/2+$  to  $3/2-$  on their way to the  $\text{Bk}^{250}$  ground state.] The obvious solution of introducing admixture of states to account for the E1 strength does not seem immediately attractive, since E1 transitions in the nearby odd-mass nuclei are not appreciably faster than the one under consideration. On the other hand, the interaction of the odd proton and odd neutron can introduce admixtures where no corresponding admixtures are possible in the odd-mass nuclei. Such an admixture, for example, could be of an (unobserved)  $K\pi = 5-$  band composed of the  $7/2+[633\uparrow]$  proton and a  $3/2-[752\downarrow]$  neutron into the 99-keV  $5-$  band. The E1 transition would then represent the change of this new  $3/2-$  neutron into the  $1/2+[620\uparrow]$  neutron, leaving the proton unchanged. The  $3/2-[752\downarrow]$  neutron we chose in this illustration was picked because it should lie rather near the observed neutron states in  $\text{Cf}^{251}$  according to Nilsson's calculations.<sup>57</sup> This particular state may not be of great importance in this case, but the point is that as one goes higher and higher in the  $N = 7$  oscillator shell there will be  $K\pi = 3/2-$  states having larger and larger E1 transition probabilities to the  $1/2+[620\uparrow]$  neutron state, and the proton-neutron interaction may be a rather effective way of admixing these states into the ones of interest. This 63-keV E1 transition represents the only example in  $\text{Bk}^{250}$  where a simple analogy to the odd-mass nuclei seems inadequate, and the above explanation is at least one way that might explain it. The transition probability of this E1 is, after all, quite small ( $10^{-5}$  of single-particle) and therefore presumably more subject to change because of small differences in admixed states than are the other transitions discussed.

It should be noted that this 63-keV transition is not an anomalous E1 in the sense that the  $L_I$  and  $L_{II}$  conversion coefficients are enhanced over their normal values.<sup>69</sup> Most of these anomalous transitions involve

violations of selection rules in the asymptotic quantum numbers,<sup>70</sup> such as the 60-keV E1 transition in Np<sup>237</sup>, which violates the selection rule in  $n_z$ .<sup>71</sup> These violations hinder the photon emission with respect to the conversion, specifically with respect to conversion in those electron shells with the largest density at the nucleus. Thus, the 63-keV transition could conceivably be anomalous or not, depending on the asymptotic quantum numbers of the states that were admixed into the principal states in order to make the transition go in the first place. For example, the transition in the illustration above, from the admixed  $3/2-[752\downarrow]$  neutron state to the  $1/2+[620\uparrow]$  neutron state, definitely would be predicted to be anomalous, for it violates selection rules both in  $n_z$  and in  $\Lambda$ . However, the predicted conversion coefficients for a normal E1 transition are 0.12 for each of the three L subshells,<sup>55</sup> and they do not appear to have been enhanced much. On the 380-day exposure in the permanent-magnet electron spectrograph (Fig. 8) we were unable to detect any electron lines from this transition. The  $L_I$  line could easily have been masked, but the  $L_{II}$  could not be present to an extent greater than  $\approx 0.2\%$ . Thus, it appears that, whatever be the states that are admixed, if this is the correct explanation for the 63-keV E1, most of them, at least, do not represent anomalous transitions.

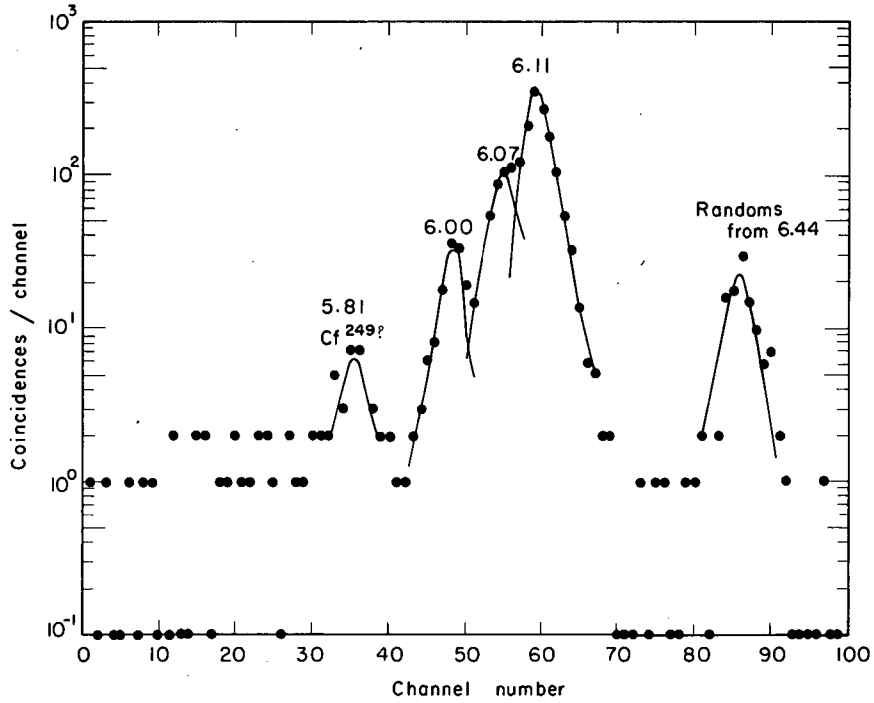
##### 5. Higher-Energy States

There are a considerable number of low-energy alpha groups, some of which are tentative, that populate levels around 400-600 keV in Bk<sup>250</sup>. There are also a number of gamma rays observed in this general energy region that undoubtedly de-excite these levels. It is our opinion, however, that only one band in this region can be established with sufficient certainty to incorporate it into the formal decay scheme. It will be discussed first in this section, and then several more aspects of this higher region will be discussed. It must be emphasized, however, that they will be considerably less than certain, so, should they be proved wrong at some later date, this should not cause suspicion on the remainder of the scheme.

The two lower-energy alpha groups of outstanding intensity are those at 6.113 and 6.068 MeV (Fig. 7). The larger of these, at 6.113 MeV,

is very near the energy of the main alpha group from  $\text{Cf}^{252}$ , but a limit placed on the spontaneous-fission decay rate of the sample showed that most of this group cannot be  $\text{Cf}^{252}$ . These two groups define levels in  $\text{Bk}^{250}$  at 416 and 473 keV, and the spacing of and similar alpha population to these levels suggests that they are members of a rotational band. One can place the gamma rays of 304, 317, and 377 keV as transitions de-exciting this new band to the first two members of the 5- band at 99 and 169 keV. To check this placement, a coincidence experiment was made in which the alpha groups in fast coincidence ( $\approx 50$  nsec resolving time) with gamma rays of energy greater than 275 keV were observed with a solid-state detector; essentially the same apparatus was used as was used to obtain the spectrum in Fig. 28.<sup>56</sup> An  $\text{Es}^{254}$  source with  $\approx 10^4$   $\alpha$ /min was used; the spectrum obtained during a 66-hr run is shown in Fig. 34. The peaks observed are at energies of 6.11, 6.07, and 6.00 MeV in relative intensities of 1.0:0.4:0.1, respectively. The first two of these are in reasonable agreement with the levels just discussed (probably the 6.089-MeV alpha group is also present, just between the 6.11-MeV and 6.07-MeV groups, but it is not resolved out), and the third suggests a level at  $\approx 538$  keV in  $\text{Bk}^{250}$ , which can be de-excited by the 284-keV  $\gamma$  transition to the 250-keV level. This state might be the third member of the rotational band under consideration, but it is less certain than the first two members of this band.

We will now find out that, although it is not difficult to characterize this new high-lying band, reconciling its characteristics with what one would expect to find from a consideration of systematics is a different matter. First of all, let us consider its spin and parity values. The most immediate attack on this is, of course, to determine the multipolarity of the gamma transitions depopulating it. Using the electron intensities from Fig. 9 and Table V, one can obtain conversion coefficients for these gamma rays, but, as was discussed in connection with the solid-state electron spectrum of Fig. 9, the electron intensities and hence the conversion coefficients carry large uncertainties with them; from them it might be difficult to decide between, say, a pure M1 and a mixed M1-E2. We can obtain independent conversion coefficients for at least three of



MU-36108

Fig. 34. Alpha particles observed in fast coincidence ( $\approx 50$  nsec resolving time) with all gammas from  $\text{Es}^{254}$  with energy greater than 275 keV during a 66-hr run. Alpha energies are given in MeV. Zero events are plotted at one-tenth.

the four gamma rays de-exciting this band, however, by making a comparison of the alpha population to the level in question versus the gamma-ray intensity depopulating it; this was done, with the result that the 304-keV and 317-keV  $\gamma$ 's can be assigned as M1, and, although the 284-keV and 377-keV  $\gamma$ 's are considerably less certain, they, too, are probably M1's—at least they are not pure electric multipoles. The conversion coefficients for all the higher-energy gamma transitions are listed in Table XII, where they are compared with theoretical conversion coefficients<sup>55</sup> for the lower multipoles and assignments are made. It can be seen that the conversion coefficients obtained by considering the alpha populations, where applicable, tend to lend a little more confidence to the imprecise ones determined by the electron measurements, so I have been bold and have assigned the multipolarities of the 249, 264, and 385-keV  $\gamma$ 's, as well as the ones depopulating our new band.

Thus, the new band has  $K\pi = 4-, 5-, \text{ or } 6-$ . For these three choices, the values of  $\hbar^2/2\mathcal{I}$  are 5.70, 4.75, and 4.07 keV, respectively. Now let us consider the hindrance factor for alpha population to this band; from Table VIII it is seen to be 23, a very low value, considering that it is not favored decay. And for a band to receive alpha population with such a small hindrance, it must be rather closely related to the parent state, or, in this nucleus, to the  $7+$  band! Here is where the difficulties start. When one considers the neutron single-particle states available, he finds none closely enough related to suggest a low enough hindrance factor; besides, it already appears that the value of  $\hbar^2/2\mathcal{I}$  might be abnormally low, and the closest neutron state that might involve such a value lies all the way below the neutron subshell. At first the proton situation looks more promising. In  $\text{Bk}^{249}$  we find a  $5/2+[642\uparrow]$  proton state at 393 keV (Fig.30), which comes from the same  $i_{13/2}$  spherical level that the  $7/2+[633\uparrow]$  does; it would be expected to undergo Coriolis mixing with the  $7/2+[633\uparrow]$  proton state, which could be expected to enhance the alpha population it receives and to compress the band, i.e., give a small value for  $\hbar^2/2\mathcal{I}$  (see Sec. IV). However, when coupled with the  $7/2+[613\uparrow]$  neutron, this proton would yield  $K\pi = 6+$ ; the properties of such a  $6+$  state are listed in Table VII. It can

Table XII. K-conversion coefficients for the higher-energy gamma rays from  $\text{Es}^{254}$  decay.

$E_{\gamma}$ (keV)	Experimental Conversion Coefficients		Theoretical Conversion <sup>a</sup> Coefficients				Assignments
	from alpha population	from electron intensity	E1	M1	E2	M2	
249	---	$1.6 \pm 0.8$	0.052	2.1	0.11	6.0	M1
264	---	$1.2 \pm 0.8$	0.046	1.8	0.098	5.1	M1
284	$2 \pm 1$	---	0.040	1.5	0.087	3.9	M1 ?
304	$1.0 \pm 0.2$	$0.6 \pm 0.4$	0.035	1.2	0.079	3.2	M1
317	$1.2 \pm 0.2$	$1.0 \pm 0.4$	0.031	1.1	0.074	2.8	M1
377	$< 1 ?$	$1.3 \pm 0.7$	0.022	0.67	0.056	1.6	M1 ??
385	---	$0.8 \pm 0.4$	0.021	0.63	0.053	1.5	M1

<sup>a</sup>from Ref. 55.

be seen that some of the properties of our new band can be partially reconciled with the predicted properties of a 6+ band; however, there are some fatal defects. Even in the unlikely event that the gamma-rays de-populating the band were E1's that we had mistaken for M1's—under our experimental conditions we would not have expected to see any conversion electrons for E1's of these energies—the gamma rays would still have to lead down to the 99-keV 5- band. Both the 5- band and the new band are populated by alpha groups with energies very near carefully determined standards, Cf<sup>250</sup> and the 6.437-MeV group, so the alpha energies should be quite accurate. Also, the gamma-ray energies are thought to be quite accurate, so it is very unlikely that the new band is de-excited down to the 7+ band, even though the 5- and 7+ bands accidentally have very similar spacing. (We did attempt a coincidence experiment with the 63-keV  $\gamma$  leading from the 5- band, but the low intensities involved made us give it up after a two-week run that was still quite indefinite as to whether or not any higher-energy gamma rays were seen.) And the hypothetical 6+ band would be expected to decay to the 7+ band not to the 5- band. The Coriolis interaction would mix enough of the 7+ band into the 6+ band to enhance the transitions collectively. We start with single-particle estimates of  $7 \times 10^{-13}$  sec and  $10^{-14}$  sec for a 300-keV M1 (to the 7+) and E1 (to the 5-) transition.<sup>17</sup> We then enhance the M1 by a conservative one order of magnitude and retard the E1 by a factor of  $10^5$ , which is what one would expect for E1's in this region; this yields  $7 \times 10^{-14}$  for the M1 and  $\approx 10^{-9}$  for the E1—so the 6+ state should have a very small branching to the 5- band. Also, if the new band were the 6+, it would have a value of 4.07 keV for  $\hbar^2/2\mathcal{I}$ ; the predicted value in Table VII is 5.54 keV, and there is no easy way to explain why the value could be so low as 4.07, keV, i.e., lower than for the 7+ band itself (again, see Sec.IV).

The only other proton state closely related to the 7/2+ [633 $\uparrow$ ] is the 9/2+[624 $\uparrow$ ], which should appear in Bk<sup>249</sup> somewhere in the vicinity of 1 MeV. It can be ruled out easily, for, even if by some quirk the Fermi surface could have been moved to lie between the 7/2+[633 $\uparrow$ ] and 9/2+[624 $\uparrow$ ] protons in order to bring the latter down to this energy (in Bk<sup>249</sup> the Fermi surface lies between the 7/2+[633 $\uparrow$ ] and the 5/2+[642 $\uparrow$ ] protons, with the latter



being the hole state), it would face the same difficulties of assignment as did the 6+ trial (i.e.,  $5/2+[642\uparrow]$  proton), plus impossibly close spacings in the experimental band for  $K = 8$  ( $9/2+[624\uparrow]$  proton +  $7/2+[613\uparrow]$  neutron):

Since intrinsic states are eliminated, the new band is probably some type of vibrational band based on the 7+ band. Assuming this to be true, it should have roughly the same rotational properties as the 7+ band, and this allows us to select  $K\pi = 5-$ , for  $\hbar^2/2\mathcal{I} = 4.75$  keV is the most reasonable value for a band similar to and lying above the 7+ band, where  $\hbar^2/2\mathcal{I} = 4.40$  keV. The most obvious way of interpreting a negative parity band based on a positive parity band is to consider it an octupole vibration. Octupole vibrations have moved very far down in energy in some parts of the heavy-element region—for example, in  $\text{Pa}^{227}$  there is what is thought to be a 1- octupole vibration within 65 keV of its intrinsic state.<sup>72</sup> However, in order to form a 5- band based on a 7+ band, it would have to be a 2- octupole vibration.<sup>2</sup> One of these was hinted at in  $\text{U}^{236}$ , a 2-2 level at 687 keV.<sup>73</sup> The hindrance factor for alpha decay from  $\text{Pu}^{240}$  to the 2-3 (?) level that feeds it was found to be 65, which indicates that alpha decay to such states may not be greatly hindered. A better example is the 2-2 band at 842 keV in  $\text{Cm}^{246}$  populated by the beta decay of  $\text{Am}^{246}$ .<sup>96</sup> It seems well established as a 2- octupole vibration. However, until more information becomes available on these states, we had better content ourselves with saying just that the band starting at 416 keV in  $\text{Bk}^{250}$  probably has  $K\pi = 5-$  and is closely related to the 7+ band.

Assuming the 5- assignment, we can calculate the alpha transition probabilities to the various levels in this band in the same manner as it was done for unfavored alpha decay to the lower bands in Sec. II.C.3. This is done in Table XIII both for pure  $L = 3$  and for mixed  $L = 3$  and  $L = 5$  alpha waves. One can obtain a good fit either way; perhaps it is slightly better for pure  $L = 3$  normalized to the population reaching the first level, but the alpha-wave hindrance factors may be somewhat more likely when one uses 74%  $L = 3$  and 26%  $L = 5$ , normalized to the population hitting the first two members. Interestingly enough, this particular mixture of  $L = 3$  and  $L = 6$  alpha waves is very similar to the mixture that gave the

Table XIII. Calculated alpha populations to the 416-keV band in Bk<sup>250</sup>.

Excited-state energy (keV)	I	Calculated Intensities (%)			Experimental intensities (%)
<u>Pure L=3</u>					
416	5	0.33 (norm)			0.33
473	6	0.14			0.16
≈538	7	0.03			0.03
≈610	8	0.003			not obs.
<u>Mixed L=3 and L=5</u>					
		<u>L=3</u> (74%)	<u>L=5</u> (26%)	<u>Σ</u> <u>L</u>	
416	5	0.304	0.028	0.33 (norm)	0.33
473	6	0.129	0.033	0.16 (norm)	0.16
≈538	7	0.026	0.018	0.04	0.03
≈610	8	0.003	0.005	0.008	not obs.

best fit for alpha population to the 99-keV 5- band. The actual alpha-wave hindrance factors were  $HF_3 = 17$  for pure  $L = 3$ , and  $HF_3 = 12$  and  $HF_5 = 33$  for the mixture fit.

There are two gamma transitions observed de-exciting the 5-6 member of the band (at 473 keV). Presuming them both to be M1's (the 377-keV transition is unsure), we find for the ratio of reduced transition probabilities,

$$\frac{B(M1, 377)}{B(M1, 304)} = \frac{0.015\%}{0.07\%} \cdot \left(\frac{304 \text{ keV}}{377 \text{ keV}}\right)^3 = 0.11 \pm 0.04.$$

If the transitions are relatively unhindered, one might expect a ratio of vector-addition coefficients to give the correct relative reduced transition probabilities; and that they are indeed unhindered, i.e., fast, is evidenced by their successful competition with the rotational transitions within the band itself. The vector-addition coefficients give,

$$\frac{B(M1, 377)}{B(M1, 304)} = \frac{\langle 6510 | 6155 \rangle^2}{\langle 6510 | 6165 \rangle^2} = \frac{0.141}{0.595} = 0.237.$$

This is not good agreement, but neither is it particularly meaningful as disagreement. First, we do not know that the 377-keV transition is pure M1; second, we do not know enough about the properties of the band to warrant an attempt at explaining the disagreement.

There is some evidence that we did find the 6+ band based on the above-mentioned  $5/2+[642\uparrow]$  proton state and the  $7/2+[613\uparrow]$  neutron state. The small alpha group at 6.089 keV defines a level in  $Bk^{250}$  at 434 keV. This could be de-excited to the 7+7 level by the 348-keV  $\gamma$ . If so, then one might suspect that the 342-keV  $\gamma$  could de-excite the second member of this band, a 6+7 level at 498 keV, to the 7+8 level; the alpha group defining such a state would, of course, be hopelessly masked by the  $Cr^{250}$  in the source. Remembering that the 6+ band should be rather badly mixed with the 7+ band, one would expect the 6+7 state to receive an abnormally large amount of alpha population because the mixing would allow some "favored"

$L = 0$  alpha wave to hit it; this might be an explanation for the high intensity of the 342-keV  $\gamma$  relative to the 348-keV  $\gamma$ . The experimental properties of this band are entered in Table VII in parentheses; the fit with the predicted properties is neither particularly good nor particularly bad. There is far too little evidence to warrant placing this band in the decay scheme, but it is mentioned as an interesting possibility.

Finally, the 385-keV  $\gamma$ . An M1. If one examines the Fm<sup>255</sup> decay scheme in Fig. 31, he finds that an  $11/2+[725\uparrow]$  neutron state at 546 keV receives 0.05% alpha population, implying a hindrance factor of only 25. This state de-excites by a 120-keV E1  $\gamma$  to a  $9/2+[615\downarrow]$  state at 426 keV that does not receive observed alpha population; the  $9/2+$  state decays to the  $7/2+[613\uparrow]$  state at 106 keV by a 320-keV M1  $\gamma$ . Now, in Bk<sup>250</sup> one would expect a 9- state composed of the  $11/2-[725\uparrow]$  neutron coupled with the  $7/2+[633\uparrow]$  proton to exist somewhere in the same general vicinity as the  $11/2+$  state, and it should be expected to receive alpha population with a hindrance factor of approximately  $(2.9)(25) \cong 75$ . However, in Bk<sup>250</sup> the intermediate state composed of the  $9/2+[615\downarrow]$  neutron and the  $7/2+[633\uparrow]$  proton would be the singlet coupling of these states; the Gallagher-Moszkowski rules predict the  $1+$  triplet coupling to lie lower in energy, in this case in the general vicinity of 426 keV, while the  $8+$  singlet would lie, say, 50-100 keV higher. Thus, the E1 transition connecting the 9- and  $8+$  levels in Bk<sup>250</sup> would most likely have its energy reduced from the 120 keV that the analogous transition in Cf<sup>251</sup> has, while the M1 connecting the  $8+$  and  $7+7$  levels in Bk<sup>250</sup> should have its energy increased. Perhaps the 385-keV  $\gamma$  is this transition. The facts are that no observed levels at high enough energies in Bk<sup>250</sup> receive sufficient alpha population to enable them to produce this 385-keV  $\gamma$ ; therefore, the level that produces it must be in the region masked by the Cf<sup>250</sup> groups—and this is exactly where we would predict the 9- level to be. Again, unfortunately, we must stop with this hopeful but inconclusive analysis. The  $8+$  level itself would receive even less alpha population than the (unobserved) population to its analogous state in Cf<sup>251</sup> because it is a singlet; there is no hope of seeing it directly. One might perform a coincidence experiment with the 385-keV  $\gamma$ , hoping to see the E1 above it, but this E1 probably has an energy in or not far above the L-x-ray region, so such an

experiment would tell one nothing. Finally, one just might use the 385-keV  $\gamma$  to start a time-to-height converter, using L x rays to stop it; if one obtained the complex 213- $\mu$ sec, 29- $\mu$ sec delay curve, it would mean that the 385 did indeed feed the 7+ band. However, this would require a huge sample and even more patience. All we can do is conclude by saying that it should be there, otherwise it would be necessary to find or invent an explanation as to why it was not.

Thus ends the evidence on the higher-lying states in Bk<sup>250</sup>. They are not nearly so well defined or understood as the lower-lying bands. And some of the gamma rays, those at 249, 264, and 278 keV, have not been placed even in hypothesis. However, some evidence has been found that the higher as well as the lower single-particle states from neighboring odd-mass nuclei can be used in the extrapolation to odd-odd systems.

#### 6. Rotational Spacings

The problem of accounting for moments of inertia in odd-odd nuclei is in principle very similar to the corresponding problem in odd-mass nuclei, which has been rather successfully considered in terms of the motion of the individual nucleons. Very briefly, one calculates the moment of inertia of the even-even core, using Nilsson wave functions and the cranking model<sup>74</sup> but including effects due to the pairing correlations. Reasonable agreement with experimental moments have been obtained by several groups.<sup>75</sup> With an odd particle, one modifies the calculation slightly because of the level blocked by the odd particle, and then one adds in explicitly the effects due to the Coriolis couplings of the particular odd particle.<sup>35</sup> The effect in general is to increase the moments of inertia by some 20% over the even-even values. For two odd particles, one should simply carry out the above procedure for each odd particle; if the two particles move independently, then, to lowest order, the changes from the even-even value of  $\hbar^2/2\mathcal{I}$  due to each particle should just be additive. This is the justification for the estimates of  $\hbar^2/2\mathcal{I}$  given in Table VII. More will be said about this and about the Coriolis interaction, in particular, in Sec. IV, but, to bring the discussion of Es<sup>254</sup> decay to a close, we will include a phenomenological treatment of the behavior of the

rotational bands in  $Bk^{250}$ , and to make this clear a little will have to be said in advance about the Coriolis interaction.

Since the Coriolis couplings of the odd particles are put in explicitly, the moments of inertia vary depending on the properties of the particular odd particles involved. For example, it has been known for some time that certain states have particularly large Coriolis couplings and therefore produce unusually large moments of inertia.<sup>77</sup> These states originate from the high- $j$  shell-model orbitals, which, because of the large spin-orbit coupling have dropped down into a given major shell from the next higher harmonic-oscillator shell. Thus, the Nilsson states coming from these orbitals form small groups of states of opposite parity from the parity of their surrounding states, and, since the Coriolis interaction does not involve states of differing parity, these states form closed groups as far as the interaction is concerned. Also, since the Coriolis matrix elements are proportional to  $[j(j+1) - \Omega(\Omega \pm 1)]^{1/2}$ , as well as  $[I(I+1) - K(K \mp 1)]^{1/2}$ , the matrix elements between these high- $j$  states are unusually large—although  $j$  is not a good quantum number and the Nilsson states are linear combinations of several  $j$ 's, the original  $j$  remains the dominant component. In the observed levels in  $Bk^{250}$  no neutron states of this type are involved; however, the  $7/2+[633\uparrow]$  proton state is of this type, here an even-parity state originating from the  $1_{13/2}$  spherical state and surrounded by odd-parity states. The bands in  $Bk^{250}$  that have large moments of inertia ( $\hbar^2/2\mathcal{I} \approx 4.5$  keV;  $K\pi = 4+, 7+, 416\text{-keV } 5-?$ ) all involve this proton state. The second-order contribution coming from these states is the introduction of a positive term in  $I^2(I+1)^2$  into the rotational-energy spacings, so that in order to get good fits with the experimental levels, one must use the full equation,

$$E_I = E_0 + \frac{\hbar^2}{2\mathcal{I}} I(I+1) + B I^2(I+1)^2$$

This positive term is large enough to offset the smaller negative term in  $I^2(I+1)^2$  that is introduced by the rotation-vibration interaction, i.e.,

centrifugal stretching of the nucleus at high angular momentum values. The negative term is found in the fit for "normal" rotational bands, for example, the 99-keV 5- band, which has little or no observed Coriolis mixing.

In Table XIV the rotational spacings are calculated both with and without the  $I^2(I+1)^2$  term, and the fits are compared with the experimental spacings. It can be seen that the fits are better when the full equation is used. In order to obtain a moderately precise value for B, it is necessary to obtain very precise energies for three levels in a band, which can prove difficult. In Table XIV the values of B for the 7+ and 99-keV 5- bands are reasonably good, that for the 4+ band is less precise—but none of them should be taken quantitatively, for an error of, say, 1 keV in the position of the third member of the band can make a considerable change in B. For the 2- and the 416-keV 5- bands one cannot obtain meaningful B values.

#### 7. Conclusion

All the states observed in the alpha decay of Es<sup>254</sup> are those based on the lower-lying, triplet-couplings of the doublets formed by coupling the odd proton and neutron states. For the particular single-particle states involved in forming the Bk<sup>250</sup> nucleus, it just turns out that each triplet is also the higher-spin combination; therefore, alpha decay to these levels is enhanced threefold over the singlets, by energy considerations, by spin considerations (Es<sup>254</sup> having large spin), and by the selection rule saying that  $\Sigma$  should not change.<sup>77</sup> Thus, it was to be expected that we did not see any of the singlet couplings. Some information can undoubtedly be obtained on these by studying the alpha branching of Es<sup>254m</sup>, which, although it, too, is probably a triplet, would populate some of the singlets by virtue of its low spin. Knowing the experimental behavior of these, especially the 0+ band (the singlet corresponding to the 7+ triplet), could enable one to go far toward a knowledge of the nucleon-nucleon residual forces. More will be said about this in Sec. IV.

To conclude the section of  $\text{Es}^{254}$  decay, I must say that, although our decay scheme is already quite complex, much remains to be accounted for, especially in the higher-energy regions. Techniques are available now for sorting out the properties of the higher-lying states from the formidable background and interference from the lower states and the  $\text{Bk}^{250}$  background, so, when more intense sources of  $\text{Es}^{254}$  become available, further study of it should prove rewarding. If further information from it can be coupled with information obtained from  $\text{Es}^{254m}$  alpha decay, the  $\text{Bk}^{250}$  nucleus could easily become one of the most important experimental searchlights into nuclear structure.



Table XIV. Rotational-energy spacing in the bands of Bk<sup>250</sup>, calculated and experimental.

KπI	Energy of level (keV)		
	$E_I = E_0 + \frac{\hbar^2}{2\mathcal{I}} I(I+1)$	$E_I = E_0 + \frac{\hbar^2}{2\mathcal{I}} I(I+1) + BI^2(I+1)^2$	Experimental
for 7+ band:	$E_0 = -160.9\text{keV}$ $\frac{\hbar^2}{2\mathcal{I}} = 4.40\text{keV}$	$E_0 = -121.0\text{keV}$ $\frac{\hbar^2}{2\mathcal{I}} = 3.14\text{keV}$ $B = +0.0098\text{keV}$	
7+7	85.5 (norm)	85.5 (norm)	85.5
7+8	155.9 (norm)	155.9 (norm)	155.9
7+9	235.1	241.1 (norm)	241.1
7+10	323.1	343.0	≈334 <sup>a</sup>
7+11	419.9	464.3	not obs.
for 99-keV 5- band:	$E_0 = -75.9\text{keV}$ $\frac{\hbar^2}{2\mathcal{I}} = 5.83\text{keV}$	$E_0 = -82.0\text{keV}$ $\frac{\hbar^2}{2\mathcal{I}} = 6.17\text{keV}$ $B = -0.0046\text{keV}$	
5-5	99 (norm)	99 (norm)	99
5-6	169 (norm)	169 (norm)	169
5-7	251	249 (norm)	249
5-8	344	338	≈327 <sup>a</sup>
5-9	449	436	not obs.
for 4+ band:	$E_0 = -49.5\text{keV}$ $\frac{\hbar^2}{2\mathcal{I}} = 4.26\text{keV}$	$E_0 = -45.6\text{keV}$ $\frac{\hbar^2}{2\mathcal{I}} = 3.94\text{keV}$ $B = +0.0064\text{keV}$	
4+4	35.5 (norm)	35.5 (norm)	35.5
4+5	78.1 (norm)	78.1 (norm)	78.1
4+6	129.3	131 (norm)	131
4+7	190	194	193
4+8	257	271	270
4+9	334	360	not obs.

Table XIV. (Cont.)

K $\pi$ I	Energy of level (keV)	
	$E_I = E_0 + \frac{\hbar^2}{2\mathcal{I}} I(I+1)$	Experimental
for 2- band:	$E_0 = -34.4 \text{ keV}$	
	$\frac{\hbar^2}{2\mathcal{I}} = 5.73 \text{ keV}$	
2-2	0 (norm)	0
2-3	34.4 (norm)	34.4
2-4	80.2	not obs.
2-5	137.5	not obs.
for 416-keV 5- band:	$E_0 = 273.5 \text{ keV}$	
	$\frac{\hbar^2}{2\mathcal{I}} = 4.75 \text{ keV}$	
5-5	416 (norm)	416
5-6	473 (norm)	473
5-7	539	$\approx 538$
5-8	615	not obs.

<sup>a</sup>These two groups were not resolved from each other and possibly from a third group; therefore, the energies are only approximate.

III. Es<sup>252</sup>

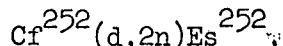
A. Experimental Procedure

1. Source Preparation

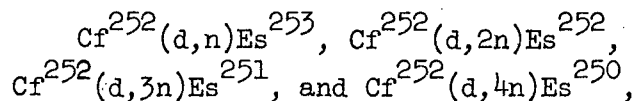
Unfortunately, Es<sup>252</sup> cannot be prepared by neutron irradiation, because Cf<sup>253</sup> is the lowest-mass californium isotope that is a  $\beta^-$  emitter (cf. Fig. 3). Es<sup>252</sup> was first produced by the reaction,



which has a peak cross-section of about 1 mb with 30-MeV alpha particles.<sup>78</sup> We decided to produce Es<sup>252</sup> by the reaction,



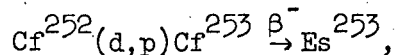
because Cf<sup>252</sup> was somewhat more available than Bk<sup>249</sup> (although more difficult to work with because of its spontaneous fission), and because, although no measurements were available, one could estimate that the latter reaction would have a larger cross-section, perhaps at least 10 mb. The Q's for the various (d,xn) reactions,



are approximately -2.1, +4.3, 9.6, and 16.4 MeV, respectively,<sup>79</sup> so one would want to bombard with deuterons just above the Coulomb barrier ( $\approx 14$  MeV) in order to maximize the (d,2n) reaction.

For the actual bombardment, 7  $\mu\text{gm}$  Cf<sup>252</sup> was electroplated onto a gold foil in a 0.01-cm<sup>2</sup> area. A 13.5-MeV beam of deuterons from the Berkeley HILAC was focussed down to hit a spot 0.02-cm<sup>2</sup> in area, so that the 0.5  $\mu\text{amp}$  beam produced a flux of 25  $\mu\text{amp}/\text{cm}^2$  on the target region.<sup>80</sup> The bombardment was carried out continuously for five days in June 1964.

After the bombardment the initial separation of the einsteinium fraction from the target californium and the fission products was carried out by remote control in water-shielded "caves"; the procedure was very similar to that used for the Es<sup>254</sup> source (cf. Sec. II.B.1.). Es<sup>253</sup>, which just happens to have almost identically the same energy for its principal alpha group as does Es<sup>252</sup> (Es<sup>253</sup>: 6.640 MeV<sup>34</sup>; Es<sup>252</sup>: 6.639 MeV)<sup>78</sup> and consequently presents a major problem as a contaminant, is produced by the Oppenheimer-Phillips reaction,



in high yield as well as by the (d,n) reaction, so the separation of the einsteinium fraction from the californium fraction was carried out as soon as possible after the bombardment; hopefully, before too much of the Cf<sup>253</sup> ( $t_{1/2} = 17.6 \pm 0.2 \text{ d}$ )<sup>81</sup> had time to decay to Es<sup>253</sup>. After the initial separations, the einsteinium was further purified by additional  $\alpha$ -hydroxyisobutyric-acid, alcoholic-HCl, and "clean-up" ion-exchange columns. The source was then thought to consist primarily of Es<sup>253</sup>, Es<sup>252</sup>, and Es<sup>251</sup>.

Some preliminary gamma-ray measurements were made in order to catch the Es<sup>251</sup>, a 1.5-d  $t_{1/2}$  species that decays primarily by electron capture.<sup>78</sup> We saw some evidence of an 81-keV  $\gamma$ , but not a 58-keV  $\gamma$ , that decayed with the correct half-life. Since the levels in the daughter, Cf<sup>251</sup>, are known from the alpha decay of Fm<sup>255</sup> (cf. Fig. 31), this gamma-ray information alone would indicate that Es<sup>251</sup> populates the 1/2+[620 $\uparrow$ ] band, but not the 7/2+[613 $\uparrow$ ] band, in Cf<sup>251</sup>. If so, then the ground state of Es<sup>251</sup> is probably the 3/2-[521 $\uparrow$ ] proton state and not the 7/2+[633 $\uparrow$ ] proton state that forms the ground states of Bk<sup>249</sup> and Es<sup>253</sup>. However, more study needs to be made on Es<sup>251</sup> before one can assert this definitely or produce a decay scheme.

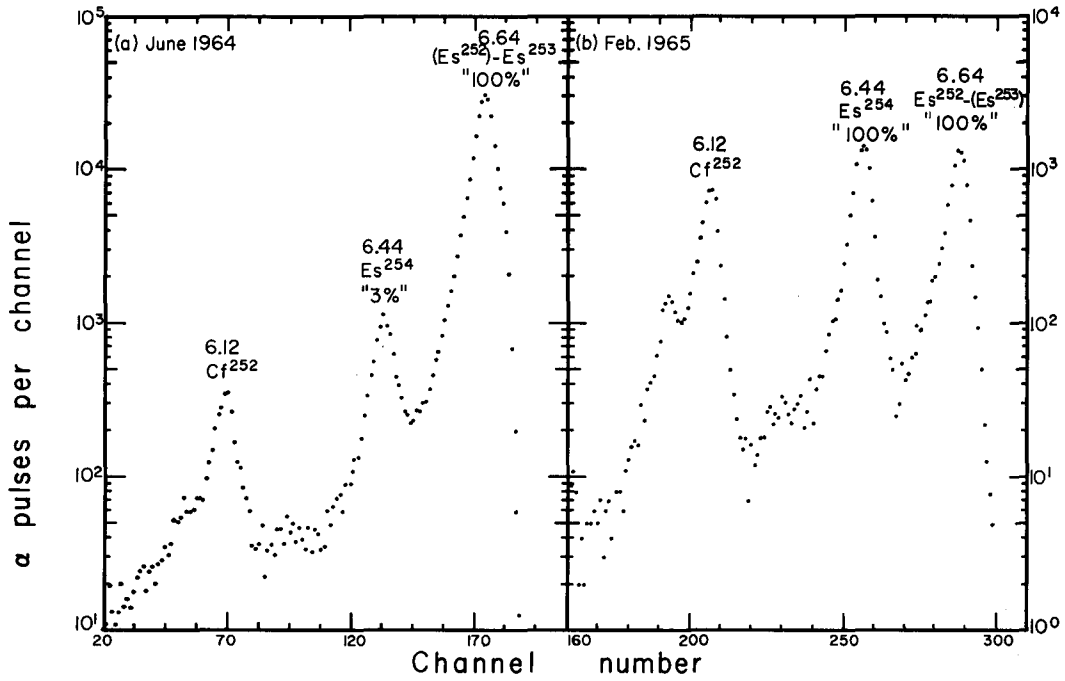
Before quantitative measurements could be performed on the Es<sup>252</sup> ( $t_{1/2} \cong 140 \text{ d}$ )<sup>78</sup>, it was necessary to let the source stand until the obstructing Es<sup>253</sup> ( $t_{1/2} = 20.03 \pm 0.01 \text{ d}$ )<sup>28</sup> had decayed away. However, to check on the relative yields of Es<sup>252</sup> and Es<sup>253</sup> and to determine when the source

was pure enough  $\text{Es}^{252}$  to take the measurements, periodic alpha spectra were taken on a small (800  $\alpha$ /min initially) portion of the source in a Frisch grid chamber. These were taken intermittently from June 1964 to Feb. 1965; two typical ones, though from time extremes, are shown in Fig. 34. It can be seen that there is an unexpected component at 6.44 MeV; the half-life of this peak was found to be  $250 \pm 50$  d—this and its energy means that it must be  $\text{Es}^{254}$ . The  $(d, \gamma)$  reaction, which is the only plausible mechanism for producing  $\text{Es}^{254}$  from  $\text{Cf}^{252}$ , should have an extremely small cross-section compared with those for particle emission, so we concluded that the  $\text{Es}^{254}$  must have been residual in the original  $\text{Cf}^{252}$  target material. Unfortunately, as will be shown later, this  $\text{Es}^{254}$  obscured a fairly important portion of the  $\text{Es}^{252}$  alpha spectrum. From these grid-chamber alpha spectra we determined that approximately twenty times as much  $\text{Es}^{253}$  activity was produced as  $\text{Es}^{252}$  activity. As for the  $\text{Es}^{252}$ , on 15 December 1964 we had approximately 4000  $\alpha$ /dis/min, corresponding to a cross-section of approximately 7 mb for its formation. The bombarding energy of the deuterons (13.5 MeV) may have been slightly below the barrier.

To remove further  $\text{Cf}^{252}$  (seen in Fig. 35), the source was given a penultimate chemical purification in December and electroplated onto a 0.0005-inch thick nickel backing; it could thus act both as an alpha source and as a gamma source, since the thin nickel would not attenuate even L x rays very much. This was used for all subsequent measurements, although a final chemical separation, discussed in the next section, was performed in connection with the alpha spectroscopy.

## 2. Alpha Spectroscopy

Since we had so little  $\text{Es}^{252}$ , it was not feasible to use the magnetic alpha spectrograph with its low transmission. However, by using a small gold-doped, lithium-drifted silicon alpha detector (0.25-cm square, 0.5-mm thick) and a digital gain stabilizer<sup>82</sup> to hold the amplification steady, and by using a rather low geometry to avoid pile-up from electrons or other radiations, we were able to obtain resolutions as good as 17.2 keV (FWHM) at 1-2% geometry. A spectrum that has almost this resolution is shown in Fig. 36, where the stabilizer held the gain steady for the entire run time of



MU-36186

Fig. 35. Alpha-particle spectra of a small portion of the Es<sup>252</sup> source after the first round of purifications. These two spectra are typical of a series that was obtained from June 1964 to Feb. 1965 with a Frisch grid chamber. Es<sup>252</sup> and Es<sup>253</sup> have almost the same principal alpha energies, so they show up as one peak, which was mostly Es<sup>253</sup> in (a) and mostly Es<sup>252</sup> in (b). Each run was for 8 hr.

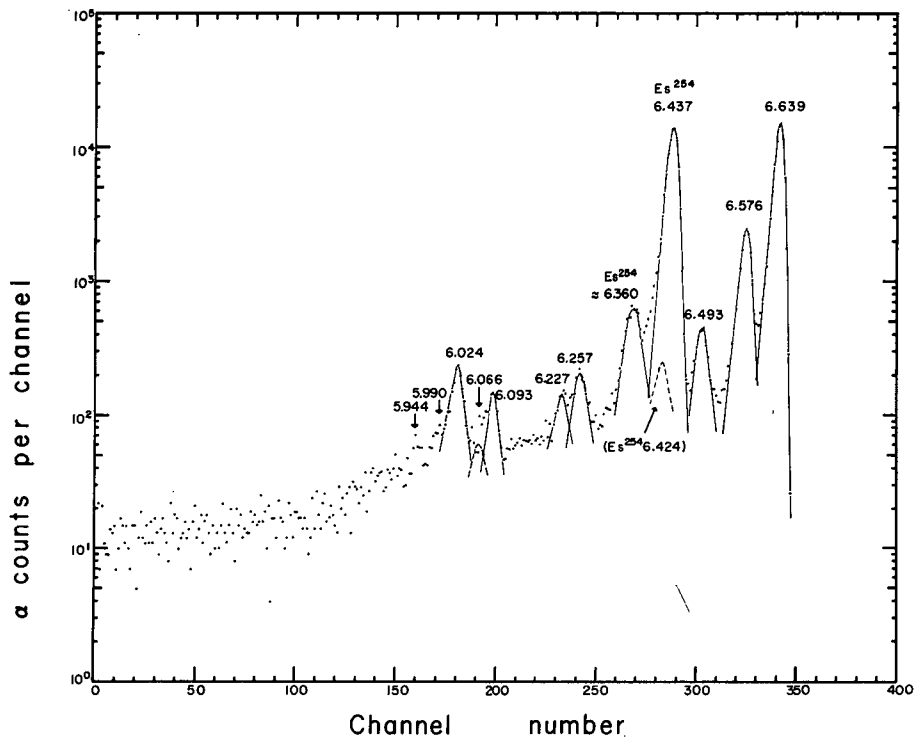


Fig. 36. Es<sup>252</sup> alpha-particle spectrum taken with a solid-state alpha detector at low geometry and with a digital stabilizer to hold the gain steady. This was a 94-hr run.

94 hr. The energy calibration for this spectrum was made very much as that for the Es<sup>254</sup> runs, a pulser-produced straight line being normalized to known standards. This spectrum was obtained after a final chemical purification was performed on the source and it was again electroplated onto 0.0005-inch nickel. The reason for this was to make certain that the peak(s) at 6.093 MeV did not belong to Cf<sup>252</sup>. On spectra before the final separation from Cf<sup>252</sup>, the peak in this vicinity was much more intense, so it is expected that the present peak comes primarily from Es<sup>252</sup>. The alpha groups, their intensities, and the species from which they originate are given in Table XV.

### 3. Electron Spectroscopy

Similarly, our small sample of Es<sup>252</sup> precluded the use of high-resolution (low-transmission), permanent-magnet electron spectrographs. However, a 7-hr run was made using the same solid-state electron detector described in Sec. II.B.3. Again, electrons were observed in fast (100 nsec resolving time) coincidence with all alpha particles. The resulting spectrum is not pictured, for its content can be summarized in few words: electron groups at 98, 117, 144, and 164 keV, relative to the Cm<sup>243</sup> standard.<sup>78</sup> These can be interpreted as L and M conversion electrons of a  $\approx 123$ -keV transition (the 98- and 117-keV electrons) and L and M electrons of a  $\approx 169$ -keV transition (the 144- and 164-keV electrons); these assignments are indicated by the spread-out peak shape of the L electrons, corresponding to the 5-keV spread between L<sub>I</sub> and L<sub>III</sub> binding energies, as well as by the simple energy separations of the groups. The intensity calibration for this run was rather poor, as we did not risk re-preparing our source to make it a good electron-emitting source, but the intensity of each L-conversion peak (at 98 and 144 keV) was at least 1%, implying a transition intensity of at least  $\approx 5\%$  in both cases. No other highly converted transitions with energies greater than 100-keV were observed.

### 4. Gamma-Ray Spectroscopy

Again, because of the small source, higher-resolution methods of detection (i.e., Ge gamma-ray detectors) were ruled out. Gamma-ray spectra were obtained only with NaI scintillators. To eliminate the ever-present Bk<sup>250</sup> background, these spectra were taken in fast coincidence with all alpha particles from the source (detected with a ZnS-screened photomultiplier), using the same electronics described in Sec. II.B.4 and shown in Fig. 12.



Table XV. Es<sup>252</sup> alpha groups and their intensities; obtained from the spectrum in Fig. 36.

Alpha-particle energy (MeV)	Intensity <sup>b</sup> (relative)	Excited-state energy <sup>c</sup> (keV)
6.639 ± 0.005 <sup>a</sup>	100	0
6.576 ± 0.010	15.3	64
6.493 ± 0.010	2.8	148
Es <sup>254</sup> : 6.437 ± 0.005 <sup>a</sup>	100	d
Es <sup>254</sup> : 6.360 ± 0.010	3.15	d
6.257 ± 0.010	0.96	388
6.227 ± 0.010	0.40	419
6.093 ± 0.010	0.70	556
6.066 ± 0.013 ?	0.14	≈582
6.024 ± 0.010	1.3	625
5.990 ± 0.010 ?	0.09	659
5.944 ± 0.013 ?	0.11	706

<sup>a</sup>The 6.639-(Ref. 78) and 6.437-(Ref. 39) MeV groups were used as energy standards.

<sup>b</sup>Since the Es<sup>254</sup> groups obscure an unknown amount of Es<sup>252</sup> groups, the intensities are given relative to the 6.639-MeV group = 100, instead of in percentages of the total decay.

<sup>c</sup>These energies are given relative to the 6.639-MeV group; it is not certain that this group populates the ground state of Bk<sup>248</sup>, so there may be a constant addend for these energies.

<sup>d</sup>From this it can be seen that Es<sup>252</sup> groups populating states in the region 175-300 keV (cf. note c) would be obscured.

Most of the measurements were performed with a commercially-mounted (Harshaw) 3-inch  $\times$  3-inch NaI scintillator that had a potential 6% resolution. In order to pick out any delays that might occur in connection with the transitions in Bk<sup>248</sup>, separate resolving times of 110, 50, 20, and 10 nsec were used. A 10-d run with a 110-nsec resolving time and a 6-d run with a 20-nsec resolving time are shown in Figs. 37a and 37b, respectively. It can be seen that no delays within the experimental range were found with these spectra, other than the expected delay associated with the 63-keV  $\gamma$  from the Es<sup>254</sup> in the source. (When this 63-keV  $\gamma$  was suppressed somewhat with the 20-nsec resolving time, the 74-keV  $\gamma$  from Es<sup>252</sup> shows up clearly, as in Fig. 37b). Thus, there are probably no delays associated with photons having energies greater than about 50 keV. However, delayed transitions with half-lives less than a few nanoseconds would not show up, nor would delays with half-lives of microseconds or longer—in the latter case we would very likely not have seen the photons unless the transitions were very intense. Also, delays associated with high-converted transitions would not have been detected for the same reason. The energies of the Es<sup>252</sup> gamma rays and their intensities relative to the 63-keV  $\gamma$  from Es<sup>254</sup> (intensity = 2.0%) are listed in Table XVI. The energies therein are expected to be precise to about  $\pm$  4 keV, except where they are noted to be less precise, and the intensities are expected to be precise to about  $\pm$  10%.

The intensity of L vacancies in Es<sup>252</sup> decay was measured in a set of singles comparisons very similar to those used for measuring the intensity of the Es<sup>254</sup> vacancies (Sec. II.B.4), except that this time the Es<sup>252</sup> L vacancies were compared with the Es<sup>254</sup> vacancies themselves. The series of spectra look very much like those in Fig. 15, so there is little point in reproducing them. Suffice it to say that when we compared our Es<sup>252</sup> source (containing 45% Es<sup>254</sup>, with all this implies about Bk<sup>250</sup>, etc.) with a similarly prepared source of pure Es<sup>254</sup>, we found the Es<sup>252</sup> source to contain 84% as many L x rays per disintegration as the Es<sup>254</sup> source. Assuming 320% L vacancies for the Es<sup>254</sup> source (including Bk<sup>250</sup>), this leaves 123% L vacancies in the Es<sup>252</sup> source that do not come from

Table XVI. Gamma rays from Es<sup>252</sup> decay.

<u>E <math>\gamma</math> (keV)</u>	<u>Intensity (%)<sup>a</sup></u>
$\approx 15-18$ (L x rays)	$(< 123 \pm 20)^b$
74	0.29
$\approx 105$ (K <sub><math>\alpha</math></sub> )	2.2
$\approx 123$ (K <sub><math>\beta</math></sub> )	0.07
154	0.08
198	0.23
228	0.21
278	1.1
398 complex	0.15
$\approx 515$	0.14
$\approx 565$	

<sup>a</sup>The intensities (except for L vacancies) were obtained from the spectra of Fig. 37, normalized to the 63-keV  $\gamma$  from Es<sup>254</sup> (intensity = 2.0%, Sec. II. B. 4).

<sup>b</sup>This intensity was obtained from a singles comparison with L x rays from Es<sup>254</sup> (+ Bk<sup>250</sup>), and it is the intensity for the L vacancies from Es<sup>252</sup> decay plus Bk<sup>248</sup> decay. Since there is some question as to what to use for the Bk<sup>248</sup> intensity (see text), the combined number is given as an upper limit for the Es<sup>252</sup>. If the 16-hr Bk<sup>248</sup> is the daughter of Es<sup>252</sup>, the intensity of Es<sup>252</sup> L vacancies becomes  $70 \pm 20\%$ .

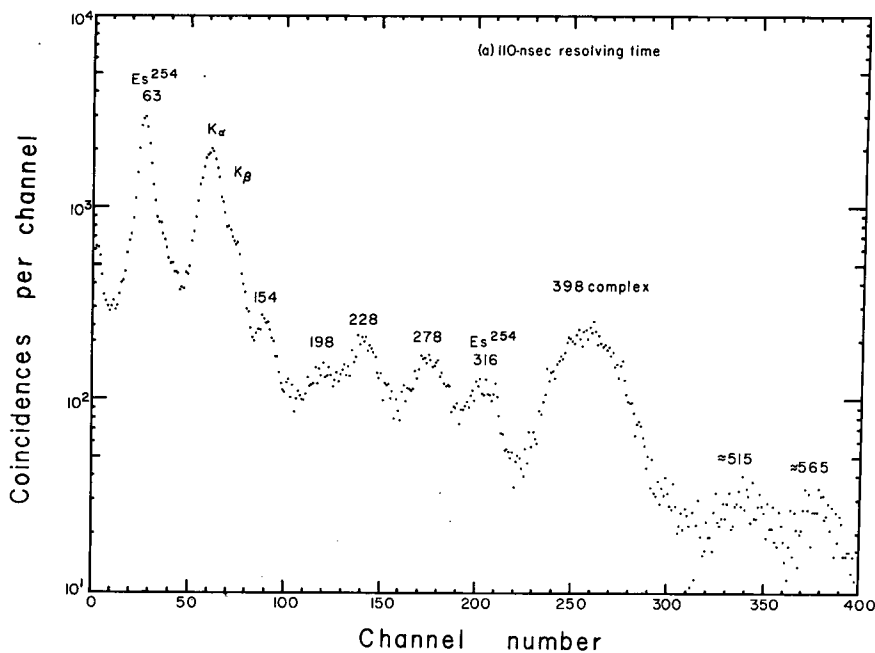


Fig. 37.  $Es^{252}$  gamma rays observed in fast coincidence with all alpha particles from the source. A 3-inch  $\times$  3-inch NaI scintillator was used as the gamma-ray detector; a ZnS-screened photomultiplier was used as the alpha-particle detector. Gamma-ray energies are given in keV.  
a) Spectrum obtained in 10 days with a 110-nsec resolving time.

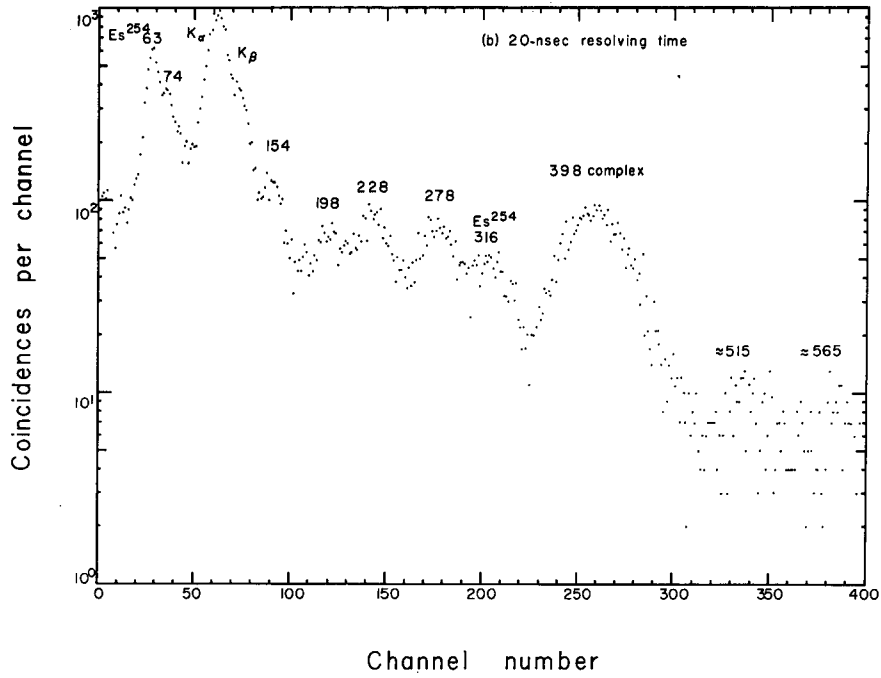


Fig. 37. (cont.) b) Spectrum obtained in 6 days with a 20-nsec resolving time.

Es<sup>254</sup> or Bk<sup>250</sup> decays. Presumably these come from Es<sup>252</sup> and Bk<sup>248</sup> decays. There is some difficulty concerning the Bk<sup>248</sup>, which will be discussed in Sec. III.B.3, and there is reason to suspect that we do not see the standard 16-hr Bk<sup>248</sup> as the main daughter of Es<sup>252</sup>. IF the 16-hr Bk<sup>248</sup> were considered to be in equilibrium with the Es<sup>252</sup>, then it accounts for 26% of the L x rays,<sup>83</sup> or approximately 52% of the L vacancies, depending on the fluorescence yields, which are not well known.<sup>52</sup> In this case the Es<sup>252</sup> decay should produce about  $70 \pm 20\%$  L vacancies, but the only reasonably certain number remains the combined one,  $123 \pm 20\%$  L vacancies for Es<sup>252</sup> and its immediate daughter activities. This comparison has made the same assumptions about comparing vacancies as did the Es<sup>254</sup>-Es<sup>253</sup> comparison, i.e., it was assumed that either the L subshell conversion ratios were similar in the two nuclides or, if not, the fluorescence yields in the different subshells were similar. The error this could introduce should be small compared with the uncertainty concerning the Bk<sup>248</sup> contribution.

## B. Discussion

### 1. Decay Scheme

There are two major difficulties confronting an attempt to formulate a decay scheme for  $\text{Es}^{252}$  at this point: First, the relative lack of data, both in quality and in quantity, as compared with that for  $\text{Es}^{254}$ , which results from having such a small source with which to work. Second, the fact that a major portion of the alpha spectrum, covering states in  $\text{Bk}^{248}$  from 175 to 300 keV (relative to the 6.639-MeV alpha group populating a state at 0 keV), is obscured by the  $\text{Es}^{254}$  that cannot be removed from the source. However,  $\text{Es}^{252}$  and  $\text{Bk}^{248}$  are sufficiently important to make it worthwhile to analyze what information we do have as far as is possible. Also, this information and analysis turns out to be novel enough to merit its being set out as clearly as possible, i.e., in a partial decay scheme. The assignments that will be made in the coming pages will be rather few as compared with those made for  $\text{Es}^{254}$  decay, but those made will be reasonably secure and possibly even more enlightening than those for  $\text{Es}^{254}$  decay.

Again, the only initial assumptions that will be made are that the decay scheme be no more complex than necessary to explain the data (for this nucleus this assumption does not amount to much) and that there are indeed well-defined rotational bands in this region of elements. You will see that it is ultimately necessary to lean somewhat heavily on theoretical predictions about the particular single-particle states that are likely possibilities for forming the compound odd-odd states in order to make some of the assignments. But, the success we had with these in the  $\text{Es}^{254}$  decay scheme and the success with them in the  $\text{Am}^{242m}$  decay scheme<sup>18</sup> make them seem rather dependable. The use of these predictions will be deferred until the next section, however, and in this section we shall see just how far we can get by using just general systematics.

The alpha groups populate levels in  $\text{Bk}^{248}$  that can be divided rather easily into four distinct rotational bands, based on the states populated by the 6.639-, 6.257-, 6.093-, and 6.024-MeV alpha groups. Before the energies of these levels in  $\text{Bk}^{248}$  can be assigned, a further assumption

of sorts must be made: A careful examination of the high-energy portion of the alpha spectra failed to reveal any alpha groups with energies greater than the 6.639-MeV group, so we have no direct evidence that there are states in  $Bk^{248}$  below the level populated by this group. However, as will soon be seen, this level and the rotational band based on it do not have the characteristics assigned to the known ground state<sup>84</sup> of  $Bk^{248}$ . In fact, with our assignments, the level populated by the 6.639-MeV alpha group is predicted to lie below levels having assignments similar to the known "ground state." Just what is the ground state of  $Bk^{248}$  will be dealt with in Sec. III.B.3. In the meantime, in the absence of conflicting data and for the purposes of our partial decay scheme the level in  $Bk^{248}$  populated by the 6.639-MeV alpha group will be placed at "0 keV," and all other energies will be assigned relative to this. Thus, the four rotational bands obtained from the alpha spectra are based on states at 0, 388, 556, and 625 keV. This large range is quite reasonable and exactly what one would expect if it is remembered that  $Es^{252}$  with its 153 neutrons lies above the neutron subshell at 152 neutrons,<sup>1</sup> while  $Bk^{248}$  with only 151 neutrons lies below this subshell; thus,  $Es^{252}$  alpha decay crosses the subshell, and one would expect the favored decay to populate states rather high-lying in  $Bk^{248}$ . This proves to be the case, and in this partial decay scheme we obtain the first quantitative measure of the energy gap caused by the subshell.<sup>85</sup>

As an aid to weeding out doubtful and spurious states from these rotational bands, the alpha-decay hindrance factors will be invoked here instead of in the section on alpha transitions probabilities. These were calculated, as in the case for  $Es^{254}$ , with the spin-independent equations of Preston.<sup>61,62</sup> Unfortunately, very little is known about even-even or odd-mass states immediately surrounding  $Es^{252}$ , so these could not give much help with choosing a nuclear radius, which is dependent on the nuclear states as well as on  $A^{1/3}$ . Since we were interested primarily in the relative values of the hindrance factors within  $Es^{252}$  alpha decay, instead of making assumptions about the  $Es^{252}$  nuclear radius, we simply used the  $Es^{253}$  radius ( $=9.42822$  fermis<sup>62</sup>). This is probably larger than the  $Es^{252}$



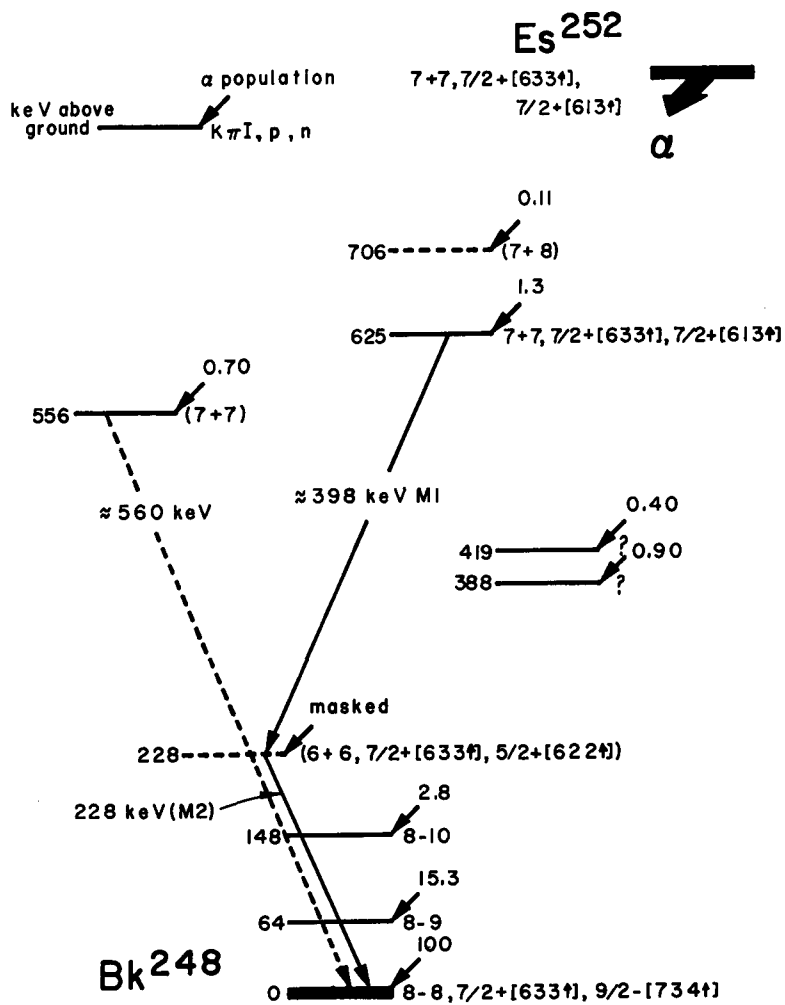
radius (both from considerations of  $A^{1/3}$  and from the fact that the  $Es^{253} r_0$  is larger than that for  $Fm^{255}$  and, presumably, for  $Es^{254}$ ), but its use very likely increases all the hindrance factors by a factor of 1.5 at most, which may be less of an error than the fact that a considerable portion of the alpha decay (obscured by  $Es^{254}$ ) may have not been included in the calculation. Anyway, the hindrance factors are listed in Table XVII according to the rotational bands they populate. Here we see the first astonishing piece of information about  $Es^{252}$  decay—the hindrance factors are all startlingly low! However, they are reasonably consistent for each band, and with their use we can probably eliminate the questionable state at 582 keV from the band starting at 556 keV, but perhaps we can include the questionable state at 706 keV in the band starting at 625 keV, throwing out the 659-keV questionable state as not belonging to this band. (It will be corroborated later that the 659-keV state cannot be the second member of this band, although the 706-keV level is not definitely proven to be the second member.) Thus, the first rotational band contains members at 0, 64, and 148 keV; the second contains those at 388 and 419 keV; the third contains the one at 556 keV; and the last contains the one at 625 keV and probably the one at 706 keV. These can be seen in more graphic form in the partial decay scheme itself, which is inserted early as Fig. 38.

Now let us consider the rotational bands individually. First, the lowest. We know that it does not receive the favored alpha decay for a number of reasons: first, as was mentioned before, the low-lying bands in  $Bk^{248}$  should be made from neutron states below the neutron subshell, and, thus, none of their levels should be the same as the ground state of  $Es^{252}$ , no matter what that turns out to be; second, the hindrance factors for alpha decay to this band are by no means the lowest hindrance factors in Table XVII; and third, the relative alpha populations to the three members of this band are totally wrong for favored alpha decay—since the  $L = 0$  alpha wave in favored decay hits only the first member of a rotational band, this first member usually gets about thirty times as much alpha

Table XVII. Alpha hindrance factors for Es<sup>252</sup> decay.

Excited-state energy (keV)	Alpha energy (MeV)	intensity <sup>a</sup> (%)	Hindrance factor
0	6.639 ± 0.005	82.1	16
64	6.576 ± 0.010	12.6	53
148	6.493 ± 0.010	2.3	120
388	6.257 ± 0.010	0.79	26
419	6.227 ± 0.010	0.33	43
556	6.093 ± 0.010	0.57	5.1
625	6.024 ± 0.010	1.1	1.2
≈706	5.944 ± 0.013 (?)	0.09	5.4
≈582 ?	6.066 ± 0.013 2	0.11	19
≈659 ?	5.990 ± 0.010 ?	0.07	12

<sup>a</sup>These intensities are listed simply because they are the intensities used for calculating the hindrance factors. They are not to be considered final figures, because an unknown amount of alpha population was probably obscured by Es<sup>254</sup> in the source. The relative intensities listed in Table XV are the numbers to use in any further studies on Es<sup>252</sup> decay.



MU-36396

Fig. 38. Partial decay scheme for Es<sup>252</sup>.

population as the second member (cf. Es<sup>254</sup> favored decay), and the ratio of alpha population to the second versus the first member of this lowest band in Bk<sup>248</sup> is thus some five times as great as would be expected for favored decay. Actually, the favored decay undoubtedly goes to the rotational band starting at 625 keV, but, since this band is not nearly so well defined as the lowest band, we will examine the characteristics of the latter extraordinarily carefully and use its assigned properties to work back and help us assign the properties of the favored band and of Es<sup>252</sup> itself.

There are two approaches to assigning the spins of the lowest band, and, at first glance, they give different results. First, examine the value of  $\hbar^2/2\mathcal{I}$  obtained from the spacing of the first two members of the band when different spins are assigned. This assumes only the simple rotational-energy equation,

$$E_I = E_0 + \frac{\hbar^2}{2\mathcal{I}}I(I + 1).$$

The values obtained with all base spins from 1 to 10 are tabulated in Table XVIII. Clearly, a high spin is indicated, but we cannot yet decide from among 5, 6, or 7, and possibly even 8 if we are dealing with a badly distorted band—remember that  $\hbar^2/2\mathcal{I}$  for the bands in Bk<sup>250</sup> varied from 5.83 to 4.26 keV. Second, examine the ratio of the spacings between the second and third member versus the first and second member,

$$R_{21} = \frac{E_{I+2} - E_{I+1}}{E_{I+1} - E_I} = \frac{(I + 2)(I + 3) - (I + 1)(I + 2)}{(I + 1)(I + 2) - I(I + 1)}.$$

The values of  $R_{21}$  are also listed in Table XVIII. for all base spins between 1 and 10; the experimental value is  $84/64 = 1.312$ , which would imply a base spin between 2 and 3, apparently a flat contradiction to the high base spin implied by the value of  $\hbar^2/2\mathcal{I}$  just obtained. However, remembering that this same type of contradiction, albeit to a somewhat lesser extent, occurred in connection with the  $K\pi = 7+$  and  $4+$  bands in Bk<sup>250</sup>, the contradiction itself tells us something about the

Table XVIII. Qualitative spin predictions for the lowest rotational band in  $Bk^{248}$ .

a) from  $\hbar^2/2\mathcal{I}$ , using the spacing between the first two members (see text)

<u>I = K</u>	<u>Experimental <math>\hbar^2/2\mathcal{I}</math> (keV)</u>	
1	32.0	
2	10.66	
3	8.00	
4	6.40	
5	5.33	} reasonable values for $\hbar^2/2\mathcal{I}$
6	4.57	
7	4.00	
8	3.56	
9	3.20	
10	2.91	

b) from  $R_{21}$ , using the spacings between the first and second and the second and third members (see text)

<u>I = K</u>	<u>Calculated <math>R_{21}</math></u>	
1	6/4 = 1.500	
→ 2	8/6 = 1.333	} experimental $R_{21}$ = 84/64 = 1.312
3	10/8 = 1.250	
4	12/10 = 1.200	
5	14/12 = 1.167	
6	16/14 = 1.143	
7	18/16 = 1.125	
8	20/18 = 1.111	
9	22/20 = 1.100	
10	24/22 = 1.091	

rotational band. The apparent spins, as obtained from values of  $R_{21}$ , for these bands in  $Bk^{250}$  were smaller than the actual spins because the Coriolis interaction had introduced a positive term in  $I^2(I+1)^2$  into the rotational-energy equation, and this, of course, increased the upper spacing more than the lower, making  $R_{21}$  too large. Also, these two bands in  $Bk^{250}$  had extraordinarily low values for  $\hbar^2/2\mathcal{I}$  for the same reason. This leads us to suspect that the band in  $Bk^{248}$  has a large base spin but is distorted by the Coriolis interaction. If the values of  $\hbar^2/2\mathcal{I}$  for the  $Bk^{250}$  distorted bands (4.40 and 4.26 keV) can be taken as a general indication of what to expect for  $\hbar^2/2\mathcal{I}$  for this band, then we would guess that its base spin is 6 or 7; since the contradiction between the predictions of spin from  $R_{21}$  and  $\hbar^2/2\mathcal{I}$  is a qualitative measure of the distortion of the band and the actual value of  $\hbar^2/2\mathcal{I}$  gets smaller as the distortion gets larger (see the qualitative discussion in Sec. II.C.6 or the more quantitative one in Sec. IV), the large contradiction for the  $Bk^{248}$  band probably indicates that this band is severely distorted and, consequently,  $\hbar^2/2\mathcal{I}$  is unduly small—this would shift our suspicion to slightly higher spins, say, from 6 or 7 to 7 or 8. Although the base spin has not been assigned definitely in this section, we have shown that it is large, that it is probably between 5 and 8, considering what are reasonable values of  $\hbar^2/2\mathcal{I}$ , and that, since the band is probably distorted, it can probably be narrowed down to 7 or 8.

Consider now the band starting at 388 keV, populated by the 6.257- and 6.227-MeV alpha groups. First, it should be pointed out that these alpha groups come from einsteinium and not from  $Cf^{248}$ , which may or may not be the granddaughter of  $Es^{252}$ . The principal alpha group of  $Cf^{248}$  has an energy of  $6.27 \pm 0.03$  MeV<sup>86</sup> and an abundance of 82%, while the second group has 45 keV less energy and an abundance of 18%. Although the energies are close to those populating the 388-keV band in  $Bk^{248}$ , the spacing is not quite right nor are the relative abundances. However, the conclusive evidence against these alpha groups coming from  $Cf^{248}$  was the chemical separation discussed in Sec. III.A.2, designed to remove the  $Cf^{252}$ . Alpha spectra taken before and after this chemical separation

showed a change in the relative intensity of the 6.093-MeV alpha group in the  $\text{Cf}^{252}$  vicinity, but the 6.257- and 6.227-MeV alpha groups remained constant with respect to the other einsteinium groups when the californium was removed.

Since only two members of this band are seen, we can make a prediction of its base spin only from the value of  $\hbar^2/2\mathcal{I}$  determined from the spacing between these two members, 31 keV. A reasonable value for  $\hbar^2/2\mathcal{I}$  is obtained for spin 2 or possibly spin 3 ( $\hbar^2/2\mathcal{I} = 5.16$  and 3.88 keV, respectively). However, as will be seen in the next section, we can explain neither of these spins in terms of single-particle states, so it may be necessary to conclude that the two states are not really members of a single rotational band.

As for the state at 556 keV, it would be dangerous and pointless to speculate on its spin at this time.

According to the calculated hindrance factors, the favored alpha decay populates the band starting at 625 keV. Again, it would be dangerous to assign the spin from the spacing between the two (?) members, since the upper one is questionable, but we can learn something about the spin with the aid of the alpha-decay properties of  $\text{Es}^{252}$ , namely that this band has a relatively high spin.  $\text{Es}^{252}$  is not thermodynamically stable toward beta decay<sup>87</sup> ( $Q_{\beta^-} = 0.24$  MeV;  $Q_{\text{EC}} = 1.23$  MeV), but neither electron capture nor  $\beta^-$  decay has been detected.<sup>78,84</sup> The best explanation for its relatively long half-life and its decay exclusively by alpha emission, then, is that it has a high enough spin to make beta decay (to states in even-even nuclei with low spins) very unfavorable. Considering that there is 1.23 MeV available for electron capture, this means that the  $\text{Es}^{252}$  and, consequently, the spin of the 625-keV band in  $\text{Bk}^{248}$  is probably 4 or higher.

Only a few gamma rays can be placed in the partial decay scheme; the others will have to wait until better and more complete data can be obtained. However, one can state immediately that the 398-keV gamma complex must originate from the 625-keV rotational band, simply because this rotational band is the only high-lying one that receives sufficient alpha

population to enable it to drop this gamma complex. Also, since  $228 \text{ keV} + 398 \text{ keV} = 626 \text{ keV}$ , the  $228\text{-keV } \gamma$  is probably also involved in de-exciting the  $625\text{-keV}$  band down to the ground state. In the next section, after the Nilsson states are discussed and assigned, it will be argued that the  $398\text{-keV } \gamma$  probably connects the  $625\text{-keV}$  level with a masked level at  $\approx 228 \text{ keV}$ , which then drops the  $228\text{-keV } \gamma$  down to the ground state. A component of the  $398\text{-keV}$  complex (at  $\approx 388 \text{ keV}$ ) may also depopulate the  $388\text{-keV}$  level down to the ground state, but this is by no means certain. Finally, the rather weak and poorly-defined gamma ray at  $\approx 565 \text{ keV}$  may depopulate the  $556\text{-keV}$  level down to the ground state. None of the other gamma transitions can be placed in the scheme with any certainty at all.

## 2. Nilsson-Level Assignments

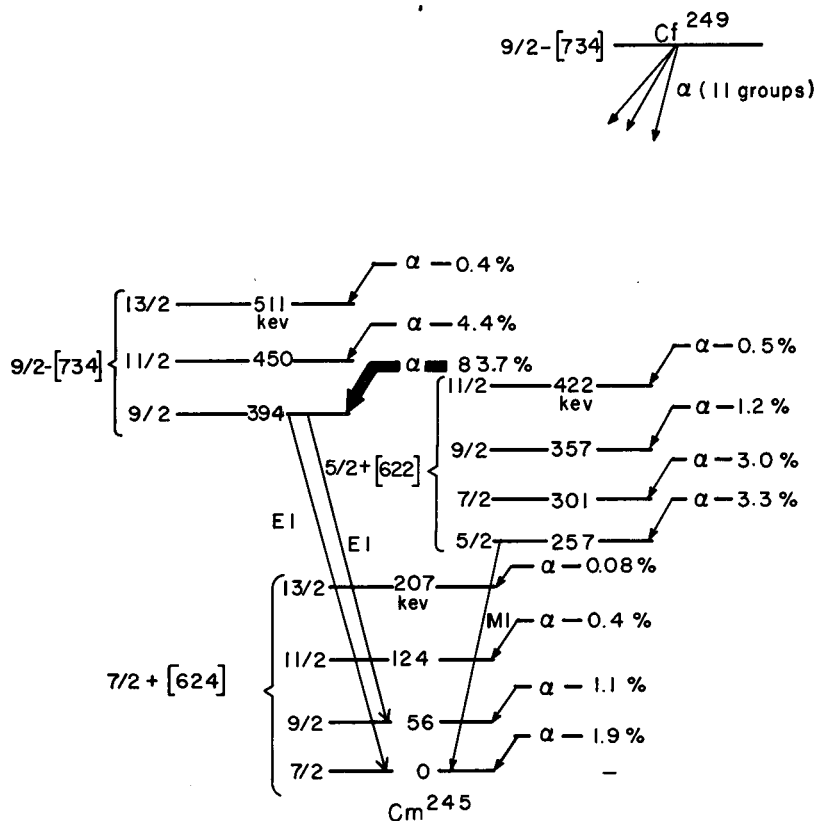
We shall consider the possible Nilsson single-particle states in much the same fashion as we did in Sec. II.C.2 for the  $\text{Bk}^{250}$  levels. We shall construct hypothetical bands in  $\text{Bk}^{248}$  out of the most probable single-particle states in the nearest odd-mass nuclei and then compare the properties of the observed bands with those of the hypothetical bands to see if any match. Since  $\text{Es}^{252}$  decays across the 152-neutron subshell, however, the procedure here cannot be so straightforward as it was for  $\text{Es}^{254}$  decay; the same single-proton states are involved as were involved there, but a number of neutron states are added from below the subshell, and not all of these are too well characterized. Also, we will have to be wary of confusing intrinsic and vibrational states; the neutron states coming from above the subshell and, consequently, the compound states formed from them will lie high enough in  $\text{Bk}^{248}$  to be in the same neighborhood with the vibrational states based on lower-lying compound states formed from neutrons below the subshell.

Before actually proceeding to the bands in  $\text{Bk}^{248}$ , we should examine the possibilities for the ground state of  $\text{Es}^{252}$ , where not so many potential states are involved.  $\text{Es}^{252}$  should have the same proton state as



$\text{Es}^{253}$  or  $\text{Es}^{251}$ , which means either the  $7/2+[633\uparrow]$  or the  $3/2-[521\uparrow]$  proton state. It should have the same neutron state as  $\text{Fm}^{253}$  or  $\text{Cf}^{251}$ . Since the ground state of  $\text{Fm}^{253}$  has not been assigned, we must decide on the neutron state from  $\text{Cf}^{251}$  alone. Either the  $1/2+[620\uparrow]$  neutron that forms the ground state (cf. Fig. 31) or the  $7/2+[613\uparrow]$  neutron at 106 keV is the most likely possibility. These four single-particle states, in all possible combinations, give rise to triplet couplings with  $K\pi = 4+, 7+, 2-,$  and  $5-$  and corresponding singlet couplings with  $K\pi = 3+, 0+, 1-,$  and  $2-$ . Remembering the arguments in the previous section that  $\text{Es}^{252}$  should have a spin of 4 or greater in order to explain its lack of beta decay, we can tentatively choose the  $4+, 7+,$  and  $5-$  triplet couplings as the most likely possibilities.

$\text{Bk}^{248}$  should contain the same proton states as  $\text{Bk}^{247}$  and  $\text{Bk}^{249}$ . Little is known about the states in  $\text{Bk}^{247}$ , except that its ground state is the  $3/2-[521\uparrow]$  proton state.<sup>88</sup> The proton states in  $\text{Bk}^{249}$  were used to construct the states in  $\text{Bk}^{250}$ , so we are already familiar with them (cf. Fig. 30).  $\text{Bk}^{248}$  should contain the same neutron states as  $\text{Cf}^{249}$  and  $\text{Cm}^{247}$ . Very little is known about  $\text{Cm}^{247}$ , and only the ground state of  $\text{Cf}^{249}$  is known (from its alpha decay to  $\text{Cm}^{245}$ ), which is the  $9/2-[734\uparrow]$  neutron state.<sup>89</sup> To get more information about the possible neutron states, one has to go to  $\text{Cm}^{245}$ , the levels of which are shown in Fig. 39, the decay scheme of  $\text{Cf}^{249}$  taken from Ref. 89. The neutron states there are the most likely possibilities for the low-lying neutron states in  $\text{Bk}^{248}$ , but the ordering in Fig. 39 is for neutron 149 rather than neutron 151. Thus, one can predict the  $9/2-[734\uparrow]$  neutron state to be involved in forming the ground state of  $\text{Bk}^{248}$ , but all one can predict about the states in  $\text{Bk}^{248}$  involving the  $7/2+[624\uparrow]$  or  $5/2+[622\uparrow]$  neutron states is that they will be "relatively low." And, of course, one must add the  $1/2+[620\uparrow]$  and  $7/2+[613\uparrow]$  neutron states to the available ones; states involving them, however, will lie rather high in  $\text{Bk}^{248}$  and will include in their energy predictions a term,  $\Delta$ , which is an energy gap caused by the neutron subshell. Thus, the predicted properties of



MU-21279

Fig. 39. The decay scheme of  $Cf^{249}$ , showing the levels in  $Cm^{245}$ , which probably are the "most available" single neutron states for constructing the lower-lying odd-odd states in  $Bk^{248}$ . From Ref. 89.

rotational bands based on states formed from the three proton states and five neutron states just discussed are listed in Table XIX. The predicted  $K$  and  $\pi$  are listed first for each state, with the higher-lying (and less likely to be seen) singlet coupling in parentheses. The energy for the triplet member is listed next; in most cases this can be only an estimate, for either the neutron state's position is not well known or it lies above the subshell and hence includes " $\Delta$ " in its energy prediction. Next comes a prediction for  $\hbar^2/2\mathcal{I}$ , which was obtained exactly as it was for Table VII, except that the even-even value of  $\hbar^2/2\mathcal{I}$  ( $=7.23$  keV) was taken from the more-appropriate  $\text{Cm}^{248}$ . The  $7/2+[633\uparrow]$  and  $5/2+[642\uparrow]$  proton states cause distortion of any band they form because of their Coriolis-coupling possibilities; thus, for these bands there is predicted a positive  $B$  term. However, we now find Coriolis coupling coming in from the neutron side as well—the  $9/2-[734\uparrow]$  neutron state, which originates from the  $j_{15/2}$  spherical level as an odd-parity state among many even-parity states, also will cause any band it forms a part of to suffer severe Coriolis-coupling distortion. Thus, these bands, too, will have positive  $B$  terms. Finally, a predicted alpha-decay hindrance factor is predicted. To predict this we had to jump ahead and realize that the alpha-emitting state in  $\text{Es}^{252}$  is probably the same as in  $\text{Es}^{254}$ , the  $7+$  made up from the  $7/2+[633\uparrow]$  proton and the  $7/2+[613\uparrow]$  neutron. Thus, the hindrance factors to states made from the  $7/2+[613\uparrow]$  or  $1/2+[620\uparrow]$  neutron states are predicted to be the same as for  $\text{Es}^{254}$  decay, if the state was seen there. Since states involving the  $5/2+[642\uparrow]$  proton state were not seen for sure in  $\text{Bk}^{250}$ , for their hindrance factors we take the predicted hindrance factors from Table VII. There are no known experimental hindrance factors for decay from the  $7/2+[613\uparrow]$  neutron state to the neutron states below the subshell, so we cannot make numerical predictions for hindrance factors to the states involving these neutrons. From alpha-decay systematics we would predict the hindrance factors to the  $9/2-[734\uparrow]$  and  $5/2+[622\uparrow]$  neutrons to be relatively small (small spin change, no change in  $\Sigma$ ), while that to the  $7/2+[624\uparrow]$  neutron should

Table XIX. Properties of rotational bands in  $Bk^{248}$ .

a) Predicted Properties

Proton states	7/2+[633↑]	3/2-[521↑]	5/2+[642↑]
Neutron states			
7/2+[613↑]	$K\pi = 7+ (0+)$ $E = \Delta + 106 \text{ keV}$ $\hbar^2/2\mathcal{I} = 4.32 \text{ keV}$ B, positive HF = 2.9	$K\pi = 5- (2-)$ $E = \Delta + 115 \text{ keV}$ $\hbar^2/2\mathcal{I} = 5.70 \text{ keV}$ B, negative HF = 136	$K\pi = 6+ (1+)$ $E = \Delta + 495 \text{ keV}$ $\hbar^2/2\mathcal{I} = 5.38 \text{ keV}$ B, positive HF = (34)
1/2+[620↑]	$K\pi = 4+ (3+)$ $E = \Delta \text{ keV}$ $\hbar^2/2\mathcal{I} = 4.20 \text{ keV}$ B, positive HF = 1270	$K\pi = 2- (1-)$ $E = \Delta + 9 \text{ keV}$ $\hbar^2/2\mathcal{I} = 5.49 \text{ keV}$ B, negative HF $\geq 1.3 \times 10^5$	$K\pi = 3+ (2+)$ $E = \Delta + 495 \text{ keV}$ $\hbar^2/2\mathcal{I} = 5.20 \text{ keV}$ B, positive HF, large
9/2-[734↑]	$K\pi = 8- (1-)$ $E = 0 \text{ keV}$ $\hbar^2/2\mathcal{I} = 3.56 \text{ keV}$ B, positive! HF, moderate	$K\pi = 6+ (3+)$ $K = 9 \text{ keV}$ $\hbar^2/2\mathcal{I} = 4.44 \text{ keV}$ B, positive HF, large	$K\pi = 7- (2-)$ $E = 389 \text{ keV}$ $\hbar^2/2\mathcal{I} = 4.25 \text{ keV}$ B, positive! HF, large
7/2+[624↓]	$K\pi = 0+ (7+)$ $E, \text{ low}$ $\hbar^2/2\mathcal{I} = 4.11 \text{ keV}$ B, positive HF, large	$K\pi = 2- (5-)$ $E, \text{ low}$ $\hbar^2/2\mathcal{I} = 5.35 \text{ keV}$ B, negative HF, large	$K\pi = 1+ (6+)$ $E, \text{ moderately high}$ $\hbar^2/2\mathcal{I} = 5.07 \text{ keV}$ B, positive HF, large
5/2+[622↑]	$K\pi = 6+ (1+)$ $E, \text{ low}$ $\hbar^2/2\mathcal{I} = 4.15 \text{ keV}$ B, positive HF, moderate	$K\pi = 4- (1-)$ $E, \text{ low}$ $\hbar^2/2\mathcal{I} = 5.40 \text{ keV}$ B, negative HF, large	$K\pi = 5+ (0+)$ $E, \text{ moderately high}$ $\hbar^2/2\mathcal{I} = 5.12 \text{ keV}$ B, positive HF, large

Table XIX (cont.).

b) Experimental Properties

		Proton states		
		7/2+[633↑]	3/2-[521↑]	5/2+[642↑]
Neutron states		$K\pi = 7+$ $E = 625 \text{ keV}$	probably not	not
	7/2+[613↑]	$\hbar^2/2\mathcal{I} = 5.0 \text{ keV ?}$ $B, ?$ $HF = 1.2$	observed	observed
	1/2+[620↑]	probably not observed	not observed	not observed
	...	...	...	...
	9/2-[734↑]	$K\pi = 8-$ $E = 0 \text{ keV}$ $\hbar^2/2\mathcal{I} = 3.56 \text{ keV}$ $B, \text{ positive}$ $HF = 16$	not observed	not observed
	7/2+[624↑]	not observed	not observed	not observed
	5/2+[622↑]	$K\pi = 6+$ $E \cong 228 \text{ keV}$ $\hbar^2/2\mathcal{I} = ?$ $B, ?$ $HF, \text{ masked}$	not observed	not observed

be large (change in  $\Sigma$ ). All that can be said about hindrance factors to states where both the proton and neutron states change is that they should be very large.

Now let us examine the experimental bands in  $Bk^{248}$ . The lowest band was found to have the following properties: spin = (6), 7, or 8;  $E = 0$  keV;  $\hbar^2/2\mathcal{I} = (4.57), 4.00, \text{ or } 3.56$  keV (for spins 6, 7, and 8, respectively); very severe band distortion, indicating an unusually large positive  $B$ ; and  $HF = 16$ . The choice of the  $K\pi = 8^-$  state made from the  $7/2+[633\uparrow]$  proton and the  $9/2-[734\uparrow]$  neutron seems definitely indicated. The only other contender would be the  $6^+$  state made from the same proton and the  $5/2+[622\uparrow]$  neutron, and this is a much less desirable choice because the energy prediction is poorer and because the  $6^+$  band would not be expected to have such severe Coriolis distortion as the  $8^-$  band. The predicted value of  $\hbar^2/2\mathcal{I} (=3.56$  keV) for the  $8^-$  band is in startling agreement with the experimental value.

Now consider the band at 625 keV, which receives the favored alpha decay. We have previously decided that this band and the ground state of  $Es^{252}$  were probably  $4^+, 7^+, \text{ or } 5^-$ . With the assignment of  $8^-$  for the  $Bk^{248}$  ground-state band, we can immediately eliminate the  $5^-$  assignment as a possibility. Since it is made up of the  $3/2-[521\uparrow]$  proton and the  $7/2+[613\uparrow]$  neutron, alpha decay to the  $8^-$  band would involve a change of both proton and neutron states, and the hindrance factor would be far greater than 16; in the similar situation in  $Es^{254}$  decay, the hindrance factor was  $\geq 1.3 \times 10^5$ . The choice between the  $4^+$  and  $7^+$  assignments is not so easy. In fact, at first glance one would favor the  $4^+$  assignment, for the 625-keV level decays by gamma-ray emission to an intermediate state instead of directly to the ground state, and one could ask, if the 625-keV level were  $7^+$ , why does it not decay down to the  $8^-$  ground state by a single 625-keV  $E1 \gamma$ . However, if one assigns the 625-keV band and the  $Es^{252}$  ground state  $4^+$ , august problems immediately arise. Not only is the hindrance factor for alpha decay to the ground-state band suspiciously low—after all, the  $L = 5^-$

alpha wave is the lowest allowed one, but also it turns out that it is completely impossible to fit the observed intensities to the three members of this band with allowed alpha waves, no matter what combination is tried. With the  $7+$  assignment, however, the observed intensity pattern can be fit quite easily, and the alpha-wave hindrance factors are quite reasonable. These facts will be aptly demonstrated in Sec. III.B.4. It is on this basis that the 625-keV rotational band in  $\text{Bk}^{248}$  and the ground state of  $\text{Es}^{252}$  are assigned  $7+$ , the same combination of  $7/2+[633\uparrow]$  proton and  $7/2+[613\uparrow]$  neutron that make up the ground state of  $\text{Es}^{254}$ . If the level at 706 keV is indeed the second member of the band, then  $\hbar^2/2\mathcal{I} \cong 5.0$  keV, higher than the predicted 4.32 keV. However, the 625-keV band in  $\text{Bk}^{248}$  is in exotic surroundings compared with the states in  $\text{Bk}^{249}$  and  $\text{Cf}^{251}$  from which the prediction was made; also, the 706-keV level is not well-enough defined to allow us to consider either the value of  $\hbar^2/2\mathcal{I}$  or the comparison as very meaningful. Of course, nothing can be said about the sign of  $B$ . The experimental hindrance factor ( $=1.2$ ) is lower than that predicted, but still reasonable.

We have seen and will see further that all the hindrance factors for  $\text{Es}^{252}$  decay are unusually small. This is probably partly due to some of the alpha decay being masked, thereby making the observed groups appear to be in greater intensity than they actually are, but it is probably also partly an indication that the Coriolis mixing, brought in both by protons and neutrons and strengthened by the proximity of vibrational and intrinsic states, is extremely severe in  $\text{Bk}^{248}$ , so the states are rather impure—everything contains a little of everything else!

With the 625-keV band assigned, we have the first estimate of  $\Delta$ , the distance between the  $9/2-[734\uparrow]$  and the  $1/2+[620\uparrow]$  neutron states, which is the energy gap or separation of the 152-neutron subshell. Using the energy prediction from Table XIX,  $\Delta$  is found to be  $625 - 106 = 519$  keV. This number can be refined somewhat by considering the (not observed)  $4+$  state to have an actual energy of  $\Delta$  keV, and then estimating the spacing between the  $4+$  and  $7+$  states. If the spacing between the  $4+$  and

7+ states is taken to be that found in  $Bk^{250}$  (50 keV), we find that  $\Delta$  is  $625 - 50 = 575$  keV. This is a rough value, really a lower limit, because the position of the Fermi surface will affect the value.

The band at 388 keV, or rather the states at 388 keV and 419 keV, cannot be explained. If the spacing of 31 keV between them is real, such a band cannot reasonably have a spin greater than 3, and 2 is actually a better prediction. Looking at the possible states in Table XIX, we find that there are no states with  $K = 2$  or 3 that lie in this region and would be expected to receive any appreciable amount of alpha decay. Two explanations are possible: either we did not take into account enough single-particle states, which means there might be a  $K = 2$  or 3 state formed from some more exotic combination, or the two members do not belong to the same band. The second explanation seems more plausible at this time, but there is no way, at this point, to determine what the characteristics of the states should be.

According to the alpha-decay behavior of  $Es^{254}$ , the only other high-lying intrinsic states in  $Bk^{248}$  that should receive any appreciable alpha population are the 4+ and 5- states. Even the 4+ can probably be eliminated, for, although the hindrance factors for  $Es^{252}$  decay are consistently smaller than those for  $Es^{254}$  decay, in  $Bk^{248}$  the hindrance factor for populating the 4+ band (=1270 in  $Bk^{250}$ ) would have to be lowered by a huge factor for us to have been able to detect any population in our solid-state alpha spectra. This leaves the 5- band. Considering its position in  $Bk^{250}$ , if it was seen at all in  $Bk^{248}$ , it is perhaps the questionable state at 659 keV; however, this is purely in the realm of speculation, and we cannot, without averting our eyes, state that it was seen and recognized.

Finally, the band or state at 556 keV. Its hindrance factor (=5.1) is so low that it must be very closely related to the present state. None of the intrinsic states are that closely related. Thus, it is likely a collective state of some kind. The choicest possibility is a 1-octupole vibration based on the 8- ground state, which could produce a  $K\pi = 7+$  state. Such a 7+ state, lying close to the intrinsic 7+ state



and having the proton in common, could be expected to contain an admixture of the intrinsic state. Thus, it should receive moderately strong alpha population. And, of course, it should decay directly to the ground state. This assignment is still just a possibility, albeit a strong one. It would also help to explain the rather low hindrance factors to the ground-state rotational band, for it could act as an intermediate to mix in some of the favored band with the ground-state band.

The most pressing remaining question is, why does the favored  $7+$  band not decay down to the  $8-$  ground state directly? Looking back again to Table XIX, we find that the most plausible choice for the intermediate state at  $\approx 228$  keV is the  $6+$  state made from the  $7/2+[633\uparrow]$  proton and the  $5/2+[622\uparrow]$  neutron. However, this would mean that the 625-keV level decays preferably by a  $\approx 398$ -keV M1 transition instead of a 625-keV E1. The single-particle estimates<sup>17</sup> for their half-lives are  $6 \times 10^{-13}$  sec for the M1 and  $10^{-15}$  sec for the E1, a factor of 600 in favor of the E1. However, often E1 transitions are retarded by factors of up to  $10^5$  in the heavy-element region. And, when we examine the particular states involved, it seems quite reasonable that the E1 would be greatly retarded. Both gamma transitions would involve a change in just the neutron state; the M1 would change the  $7/2+[613\uparrow]$  neutron into a  $5/2+[622\uparrow]$  neutron, while the E1 would change the  $7/2+[613\uparrow]$  neutron into a  $9/2-[734\uparrow]$  neutron. For the M1 transition the selection rules<sup>70</sup> of interest in the asymptotic quantum numbers are  $\Delta \Omega = \Delta \Lambda = \pm 1$ ;  $\Delta n_z = \frac{\pm 1}{\mp 1}$ ; and  $\Delta N = 0, \frac{\pm 2}{\mp 2}$ —thus, the  $\approx 398$ -keV M1 transition does not break any of these selection rules. For the E1 transition the selection rules of interest are  $\Delta \Omega = \Delta \Lambda = \pm 1$ ;  $\Delta n_z = 0$ ;  $\Delta N = \pm 1, \mp 1$ —the 625-keV E1 transition would have  $\Delta n_z = 2$ , so it would be highly retarded. Thus, it is to be expected that the  $\approx 398$ -keV M1 would be the transition to depopulate the 625-keV band, not the 625-keV E1, and we can thus assign the intermediate state  $6+$  even though its alpha population is masked.

The  $\approx 228$ -keV  $6+$  level apparently decays down to the ground state by the 228-keV  $\gamma$ , which then should be an M2. The single-particle estimate for the half-life of a 228-keV M2 transition<sup>17</sup> is about 80 nsec. The fact that such a half-life was not detected in the gamma-ray spectra presents no real difficulties, however, for, with the highly-admixed states that are expected in  $\text{Bk}^{248}$ , the transition could easily be enhanced over this single-particle estimate to the point it would not have been detected. The theoretical conversion coefficient<sup>55</sup> for a 228-keV M2 transition is about 8. Thus, even the intensity of the 228-keV  $\gamma$  ( $=0.23\%$ , i.e.,  $1/5$  the intensity of the  $\approx 398$ -keV  $\gamma$ ) is quite consistent with the assignment when one considers that the  $\approx 228$ -keV  $6+$  band should receive some alpha population on its own.

### 3. Relation between Bk<sup>248</sup> and Bk<sup>248m</sup>

Throughout the previous discussion there has been the tacit assumption that the 8-8 level is indeed the ground state of Bk<sup>248</sup>. It has not been, what you may call, absolutely proven, but there has been no evidence against it. The sole difficulty is that a Bk<sup>248</sup> has already been classified and its properties are not what one would expect from an 8-ground state. It has a half-life of  $16 \pm 3$  hr<sup>84</sup> and decays 70% by  $\beta^-$  emission ( $Q_{\beta^-} = 650$  keV)<sup>84,87</sup> to Cf<sup>248</sup> and 30% by electron capture ( $Q_{EC} = 690$  keV)<sup>87</sup> to Cm<sup>248</sup>. There is some uncertainty as to the spin, and both 1-<sup>83</sup> and 0-<sup>90</sup> have been suggested. The purpose of the present work is not to decide between these assignments, but it is obvious that neither of them agrees with the "ground state" that we have seen.

However, there is recent mass-spectrographic evidence<sup>91</sup> of a Bk<sup>248</sup> isomer with a half-life greater than 9 years, probably greater than 200 years. These investigators, favoring the 0- assignment for the "regular" Bk<sup>248</sup>, have picked the somewhat unlikely singlet coupling of the  $7/2+[633\uparrow]$  proton and the  $7/2-[743\uparrow](?!)$  neutron as the configuration for that Bk<sup>248</sup>. In turn, they have suggested that the long-lived Bk<sup>248</sup> could be the triplet coupling of the same states.

We already have some evidence that Es<sup>252</sup> does not propulate the 16-hr Bk<sup>248</sup>, for, as was discussed in the previous section, we probably did not see Cf<sup>248</sup>, which would have grown into the source from the 16-hr Bk<sup>248</sup>. To check this further, we collected recoils on several different occasions (onto a Pt plate 1/8-inch away from the source, standard pressure, 300-V across the gap) for three days at a time, and the recoils were then examined for gamma activity. In each case the 990-1032-keV  $\gamma$ 's from Bk<sup>250</sup> (daughter of the Es<sup>254</sup> in the source) were detected, and these appeared to decay with the expected 3-hr half-life, so the recoil-collection efficiency was reasonable. In each experiment, to look for the 16-hr Bk<sup>248</sup>, we looked for K x rays that decayed with a 16-hr half-life. In no case did we find them—in fact, no appreciable amount of K x rays at all was found. In such a negative experiment it is always possible that they were missed, and it must be admitted that we had a rather small source. However, this is unlikely, since we presumably knew what we were looking for.

We suggest, then, that  $\text{Es}^{252}$  does not populate the 16-hr  $\text{Bk}^{248}$  but a long-lived isomer, probably the one seen in the mass-spectrographic analysis. Also, we suggest that the ground-state of this isomer is  $K\pi = I\pi = 8^-$ . With the small  $Q$ 's both for  $\beta^-$  emission and for electron capture, such a high spin would preclude these modes of decay, and the isomer should decay eventually by alpha emission. The calculated  $Q_\alpha$  for  $\text{Bk}^{248}$  is 5.51 MeV.<sup>87</sup> Since  $\text{Bk}^{247}$ , with a  $Q_\alpha = 5.85$  MeV, has a half-life of  $1380 \pm 250$  y,<sup>91</sup> the long-lived  $\text{Bk}^{248}$  should have a half-life at least that long, and possibly as long as 2000 y.

With the long-lived  $\text{Bk}^{248}$  assigned  $8^-$ , we could speculate that the 16-hr  $\text{Bk}^{248}$  could easily be the singlet coupling of the same  $7/2+[633\uparrow]$  proton and  $9/2-[734\uparrow]$  neutron, which would make it  $\text{Bk}^{248m}$ . However, this is no proof, and there may be a situation here similar to that for the two  $\text{Es}^{254}$ 's, where completely different configurations are involved for the two isomers. Whatever the final assignment for 16-hr  $\text{Bk}^{248(m)}$ , it is highly unlikely that an isomeric transition between  $\text{Bk}^{248(m)}$  and  $\text{Bk}^{248}$  will ever be seen. If there are no intervening states, it would have to be an M7 or E8, and the half-life for either of these would be almost incredibly long.

#### 4. Alpha Transition Probabilities

The primary purpose of this section is simply to demonstrate that the experimental alpha populations to the ground-state band in  $\text{Bk}^{248}$  cannot be fit if  $\text{Es}^{252}$  is assigned a  $4+$  configuration. This result was already used in Sec. III.B.2 as an aid in assigning a  $7+$  configuration to the 625-keV band in  $\text{Bk}^{248}$  and the ground state of  $\text{Es}^{252}$ , for with the  $7+$  assignment, the alpha populations to the ground-state band in  $\text{Bk}^{248}$  can be fit quite well.

The calculation of alpha transition probabilities to the ground-state band in  $\text{Bk}^{248}$  is done just as it was for  $\text{Es}^{254}$  decay to the unfavored bands in  $\text{Bk}^{250}$ , Sec. II.C.3. The attempt to fit the alpha populations when  $\text{Es}^{252}$  is considered to have a  $4+$  configuration is shown in Table XXa. The 5- alpha wave is the lowest one that can go, and, to reach the third member of the band, the 8-10 level at 148-keV, the 7- alpha wave has to be

Table XX. Calculated alpha populations to the ground-state rotational band in  $Bk^{248}$ .

a) Using a $K\pi = 4+$ assignment for $Es^{252}$ :					
Excited-state energy (keV)	I	Relative alpha population			
		Calculated		Experimental	
<u>L = 5- alpha wave</u>					
0	8	100			100
64	9	63			15.3
<u>L = 7- alpha wave</u>					
0	8	100			100
64	9	273			15.3
148	10	192			2.8
$\approx 256$	11	31			masked
b) Using a $K\pi = 7+$ assignment for $Es^{252}$ :					
Excited-state energy (keV)	I	Relative alpha population			
		Calculated		Experimental	
<u>L = 1- and 3- alpha waves</u>					
		L = 1 (43%)	L = 3 (57%)	$\Sigma$ L	
0	8	58.2	41.8	100 (norm)	100
64	9	----	15.3	15.3 (norm)	15.3
148	10	----	1.3	1.3	2.8

Table XX. (Cont.)

Excited-state energy (keV)	I	Relative alpha population				Σ L	Experimental
		Calculated					
L = 1-, 3-, and 5- alpha waves							
		L = 1 (46%)	L = 3 (35%)	L = 5 (19%)			
0	8	67.9	27.4	4.7	100	100	
					(norm)		
64	9	----	10.0	5.3	15.3	15.3	
					(norm)		
148	10	----	0.87	1.92	2.8	2.8	
					(norm)		
≈256	11	----	----	0.24	0.24	masked	
≈393	12	----	----	0.006	0.006	not obs.	

used. It can be seen that even the 5- alpha wave gives the 8-9 level far too much alpha population relative to the 8-8 ground state, and the 7- alpha wave does even worse. As one progresses to higher alpha waves, he will find that the upper members of the band get hit more and more strongly, so it is impossible to find a combination of allowed alpha waves that will fit the experimental intensities.

On the other hand, there is no difficulty in fitting the experimental intensities when  $\text{Es}^{252}$  is assigned a 7+ configuration. The calculated alpha transition probabilities for this assignment are given in Table XXb. If one uses just the L = 1- and L = 3- alpha waves, the populations to the first two members can be fit, but then the predicted alpha population to the 8-10 member is less than half of what is found experimentally. Therefore, one must add the L = 5- alpha wave to the other two. A fit is obtained with 46% L = 1-, 35% L = 3-, and 19% L = 5- alpha waves, yielding respective alpha-wave hindrance factors of 21, 29, and 53. These are quite reasonable values.

Not enough is known with certainty about the relative alpha populations to the (two?) members of the favored, 625-keV band to make a calculated comparison very meaningful. The expected relative alpha populations to the members of this band actually should not vary much from what was found for the corresponding members of the favored band in  $\text{Bk}^{250}$ . Any further refinements would be mostly a waste of the reader's time at this stage of the game.

##### 5. Rotational Spacings

Only the ground-state band and the favored band in  $\text{Bk}^{248}$  are sufficiently well characterized to warrant discussing their rotational spacings. The procedure and rationale behind the predictions to be made are discussed thoroughly in Sec. II.C.6.

In Table XXI the rotational spacings are calculated for both the 625-keV and ground-state bands, using just the  $I(I+1)$  term in the rotational-energy equation, and for the ground-state band alone, using both the  $I(I+1)$  and  $I^2(I+1)^2$  terms. If and when the upper members of the 625-keV

Table XXI. Rotational-energy spacings in the bands of Bk<sup>248</sup>, calculated and experimental.

KπI	Energy of level (keV)		
	$E_I = E_0 + \frac{\hbar^2}{2\mathcal{I}} I(I+1)$	$E_I = E_0 + \frac{\hbar^2}{2\mathcal{I}} I(I+1) + BI^2(I+1)^2$	Experimental
for 8- band:	$E_0 = -256.3$ keV $\frac{\hbar^2}{2\mathcal{I}} = 3.56$ keV	$E_0 = -145.7$ keV $\frac{\hbar^2}{2\mathcal{I}} = 0.8$ keV $B = +0.017$ keV	
8-8	0 (norm)	0 (norm)	0
8-9	64 (norm)	64 (norm)	64
8-10	135	148 (norm)	148
8-11	214	256	masked
8-12	299	393	not obs.
for 7+ band:	$E_0 = 342$ keV $\frac{\hbar^2}{2\mathcal{I}} = 4.06$ keV	not evaluated	
7+7	625 (norm)		625
7+8	706 (norm)		(706)
7+9	797		not obs.
7+10	899		not obs.



band are seen, they will very likely be at somewhat higher energies than the predictions, since this band is expected to have a positive  $I^2(I+1)^2$  term in its rotational-energy equation, although we cannot yet evaluate its coefficient (cf. the 7+ band in Bk<sup>250</sup>).

The spacings of the ground-state band are startling, but expectedly so. Both the 7/2+[633↑] proton state and the 9/2-[734↑] neutron state have very large Coriolis matrix elements with the nucleon states originating in their respective spherical states, so one would predict that the band combining these two would be considerably more distorted than, say, any of the bands in Bk<sup>250</sup>. This is found to be the case. The  $\hbar^2/2\mathcal{S}$  value is the smallest yet known in the heavy elements, and the B coefficient is probably the largest. By comparing the two sets of predictions in Table XXI, one finds that even the third members is missed by some 13 keV if the  $I^2(I+1)^2$  term is not used, and, by the time the fifth member (8-12) is reached, the two predictions differ by 94 keV!

It is interesting to compare the moment of inertia of this band with the rigid value, which is given by the equation,

$$\mathcal{S}_{\text{rigid}} = \frac{2}{5} \text{MAR}_0^2 (1 + 0.31\beta + 0.44\beta^2 + \dots).$$

This is simply the classical equation for the moment of inertia of a sphere modified to take care of the elongation by a power series in  $\beta$ , a deformation parameter,<sup>92</sup>

$$\beta = \frac{4}{3} \left( \frac{\pi}{5} \right)^{1/2} \frac{\Delta R}{R}.$$

Using this equation, one finds that  $\mathcal{S}_{\text{rigid}}$  is  $1.67 \times 10^{-46}$  gm-cm<sup>2</sup>, or  $\hbar^2/2\mathcal{S}$  is 2.08 keV. Thus, although the moment of inertia for the 8- band has increased enormously over that of a typical even-even nucleus in this region ( $\hbar^2/2\mathcal{S} \cong 7$  keV), it still has some way to go before it reaches the value predicted for a classical rigid rotator.

Alternately, one can compare the moment of inertia of this band with the direct predictions from the cranking model. Using the theoretical values<sup>57,74</sup> calculated for the  $9/2-[734\uparrow]$  neutron ( $\mathcal{I} = \mathcal{I}_{e-e} + 0.23\mathcal{I}_{e-e}$  where  $\mathcal{I}_{e-e}$  is the rigid moment of inertia of the even-even core, i.e., nearest even-even nucleus, as calculated by the cranking model) and approximating that for the  $7/2+[633\uparrow]$  proton by the value calculated for the  $7/2+[633\uparrow]$  neutron in  $\text{Er}^{167}$  (calculated values are not available for the proton) ( $\mathcal{I} = \mathcal{I}_{e-e} + 0.29\mathcal{I}_{e-e}$ ), one finds an estimate of the cranking-model (rigid) moment of inertia to give  $\hbar^2/2\mathcal{I} = 3.37$  keV. Thus, according to this estimate, the moment of inertia for the 8- band is very close to the rigid value.

## 6. Conclusion

This concludes what we have to offer for  $\text{Es}^{252}$  decay. Although the decay scheme is not yet complete, what there is of it was well worth the difficulties of obtaining it. This nucleus is almost unique in the systematics of alpha decay, in that its decaying across the neutron subshell causes high-lying levels in the daughter nucleus to receive large amounts of alpha population. Also, because of the extreme Coriolis mixing of the levels in  $\text{Bk}^{248}$  and the fact that vibrational levels from the lower-lying intrinsic states are intermingled with the high-lying intrinsic states similar to the parent state, many levels in  $\text{Bk}^{248}$  will contain small admixtures of the parent state. Thus, many states that ordinarily would receive little or no alpha population and thus be experimentally lost, should, in this nucleus, receive some alpha population and be seen.

Unfortunately,  $\text{Es}^{252}$  will always be difficult to study, for to make it requires treacherous target materials and long, expensive bombardments. However, if a large amount of it, free from  $\text{Es}^{254}$ , can ever be obtained, a precision re-examination of its alpha decay would be most profitable. With a magnetic alpha spectrograph the extreme wealth of levels in  $\text{Bk}^{248}$  could be studied with precision. And a precise knowledge of these should produce information not only on the proton-neutron residual interaction

and the Coriolis interaction, but also on a great number of vibrational states, which apparently are more important in the study of nuclear states than has previously been expected.

#### IV. THE NUCLEAR CORIOLIS INTERACTION

##### A. Background and Development

What we speak of as the "nuclear Coriolis interaction" is a rotational perturbation in deformed nuclei that distorts and mixes the rotational bands. It originates as a cross-term, analogous to the classical Coriolis force, in the simple model of a particle (or particles) coupled to a rigid rotor. Its effect has been known for a considerable time, but it is often ignored because its most obvious result is a renormalization of the moments of inertia, and these can be adjusted empirically without explicitly considering the Coriolis term. However, in the nuclei we have been discussing, a combination of high spins and large matrix elements enhances the Coriolis interaction to such an extent that the distortions of some of the rotational bands, sometimes even their spins, cannot be explained without specifically invoking it.

We shall use the rotor model as the basis for our development. There are more general expositions of the coupling terms,<sup>93</sup> but the rotor model allows us to explain everything in the einsteinium decay schemes quite adequately, and it has the advantage of being the most physically vivid development of the interaction. The coupling schemes to be considered are shown in Fig. 40. We shall first consider a single nucleon coupled to a rotating core (rigid rotor) and then generalize the results to include two nucleons coupled to the same core.

The Hamiltonian for the case of a single particle coupled by a potential to a rigid rotor consists of the standard kinetic-energy and potential-energy terms plus a rotational-energy term,

$$H = \frac{p^2}{2m} + V(\vec{r}) + \sum_{k=1}^3 \frac{\hbar^2}{2\mathcal{I}_k} (R_k)^2, \quad (1)$$

where  $\vec{p}$  and  $\vec{r}$  are the linear momentum and position vector of the particle in the co-ordinate system based on the principal axes of the rotor,  $\vec{R}$  is the angular momentum of the rotor,  $\mathcal{I}_k$  are the principal



moments of inertia of the rotor,  $V(\vec{r})$  is the potential coupling the particle to the rotor, and  $m$  is the reduced mass of the system. In terms of  $\vec{j}$ , the angular momentum of the particle (in the rotating coordinate system), and  $\vec{I}$ , the total angular momentum of the system, this becomes

$$\mathcal{H} = \frac{p^2}{2m} + V(\vec{r}) + \sum_{k=1}^3 \frac{\hbar^2}{2\mathcal{I}_k} (I_k - j_k)^2. \quad (2)$$

We are interested primarily in the low-lying nuclear states that retain their axial symmetry, so we can consider the rotor and  $V(\vec{r})$  to have axial symmetry. Thus,

$$\mathcal{I}_1 = \mathcal{I}_2 \equiv \mathcal{I}. \quad (3)$$

We can then expand (2) and group the terms as follows:

$$\begin{aligned} \mathcal{H} = & \left[ \frac{p^2}{2m} + V(\vec{r}) + \frac{\hbar^2}{2\mathcal{I}} (j_1^2 + j_2^2 + j_3^2) \right] \\ & + \left[ \frac{\hbar^2}{2\mathcal{I}_3} (I_3^2 - 2I_3 j_3 + j_3^2) + \frac{\hbar^2}{2\mathcal{I}} (I_1^2 + I_2^2 + I_3^2 - I_3^2 - j_3^2) \right] \\ & + \left[ \frac{\hbar^2}{2\mathcal{I}} (-2I_1 j_1 - 2I_2 j_2) \right]. \end{aligned} \quad (4)$$

If we collect terms and remember that angular momenta components along the 1 and 2 axes can be written as shift operators,

$$I_{\pm} = I_1 \pm iI_2; \quad j_{\pm} = j_1 \pm ij_2, \quad (5)$$

the Hamiltonian becomes

$$\begin{aligned} \mathcal{H} = & \left[ \frac{p^2}{2m} + V(\vec{r}) + \frac{\hbar^2}{2\mathcal{I}} j^2 \right] + \left[ \frac{\hbar^2}{2\mathcal{I}_3} (I_3 - j_3)^2 + \frac{\hbar^2}{2\mathcal{I}} (I^2 - I_3^2 - j_3^2) \right] \\ & + \left[ -\frac{\hbar^2}{2\mathcal{I}} (I_+ j_- + I_- j_+) \right]. \end{aligned} \quad (6)$$

The  $j^2$  term in the first brackets does not affect the rotational energy except for adding a constant factor to the energy spectrum of each particle, regardless of what the rotor is doing, so it can be taken into  $\mathcal{H}_0$  with the first two terms. The shift-operator terms in the third brackets make up the Coriolis operator,  $\mathcal{H}_C$ . If we neglect them temporarily, we are left with the following Hamiltonian:

$$\mathcal{H} = \mathcal{H}_0 + \frac{\hbar^2}{2\mathcal{I}_3}(I_3 - j_3)^2 + \frac{\hbar^2}{2\mathcal{I}_3}(I^2 - I_3^2 - j_3^2). \quad (7)$$

It preserves the axial symmetry of the system, so  $I_3 \equiv K$  and  $j_3 \equiv \Omega$  will be good quantum numbers.  $\Omega$  becomes one of the quantum numbers for the solutions to  $\mathcal{H}_0$  because of the  $j^2$  term. The Nilsson wave functions<sup>4</sup> are the solutions of  $\mathcal{H}_0$  in most common use. Thus, the energy spectrum yielded by this Hamiltonian is

$$E = E_0(\Omega) + \frac{\hbar^2}{2\mathcal{I}_3}(K - \Omega)^2 + \frac{\hbar^2}{2\mathcal{I}_3}(I(I + 1) - K^2 - \Omega^2). \quad (8)$$

For the low-energy rotational bands we are concerned with,  $K = \Omega$ , so this leaves,

$$E = E_0(K) + \frac{\hbar^2}{2\mathcal{I}_3}(I(I + 1) - 2K^2), \quad (9)$$

or, incorporating  $-2K^2$  into the constant,

$$E = E_0 + \frac{\hbar^2}{2\mathcal{I}_3}I(I + 1), \quad (10)$$

which is the simple rotational-energy equation.

Now, what about the Coriolis terms that we neglected? First of all, it should be pointed out that  $\vec{I}$  and  $\vec{j}$  are not defined in the same co-ordinate system.  $\vec{j}$  is the angular momentum of the particle defined with respect to the rotor-centered co-ordinate system, i.e., a rotating co-ordinate system, whereas,  $\vec{I}$  is the total angular momentum of the

rotating system and hence defined with respect to the (non-rotating) laboratory system. In order to use the operator one must first transform either  $\vec{I}$  or  $\vec{j}$  into the co-ordinate system of the other. Since the wave functions on which they will be operating are defined with respect to the rotating co-ordinate system, it is better to transform  $\vec{I}$  into this system. When this is done, it can be shown<sup>94</sup> that the components of  $\vec{I}$  then follow so-called backward commutation relations,

$$\begin{aligned} [I_1, I_2] &= -i\hbar I_3, \\ [I_2, I_3] &= -i\hbar I_1, \end{aligned} \tag{11}$$

and

$$[I_3, I_1] = -i\hbar I_2,$$

with the result that, in the rotating co-ordinate system wherein  $\vec{j}$  is defined,  $I_+$  becomes the lowering operator and  $I_-$  becomes the raising operator. Thus, the matrix elements of  $I_{\pm}$  and  $j_{\pm}$  have the forms,

$$\langle IK | I_{\pm} | IK \pm 1 \rangle = [I(I+1) - K(K \pm 1)]^{1/2} \tag{12}$$

and

$$\langle j\Omega | j_{\pm} | j\Omega \mp 1 \rangle = [j(j+1) - \Omega(\Omega \mp 1)]^{1/2}. \tag{13}$$

These are sometimes written as  $[(I \mp K)(I \pm K + 1)]^{1/2}$  and  $[(j \pm \Omega)(j \mp \Omega + 1)]^{1/2}$ , but (12) and (13) are more convenient, since one can tell at a glance which states are being connected by the operators. The matrix elements of  $\mathcal{H}_C$ , the Coriolis operator, then become

$$\begin{aligned} \langle IKj\Omega | -\frac{\hbar^2}{2\mathcal{I}} I_{\pm} j_{\mp} | IK \pm 1 j\Omega \pm 1 \rangle = \\ -\frac{\hbar^2}{2\mathcal{I}} [I(I+1) - K(K \pm 1)]^{1/2} [j(j+1) - \Omega(\Omega \pm 1)]^{1/2}. \end{aligned} \tag{14}$$

Since the wave functions for deformed nuclei are linear combinations of different  $j$ 's, one has to take this into account when calculating the  $j_{\pm}$  matrix elements. However, the original  $j$  of the spherical state



from which the deformed state originated usually remains the predominant  $j$ , so this explains why those states that come from high- $j$  spherical states bring along a large Coriolis interaction—they have large  $j_{\mp}$  contributions to the Coriolis matrix elements.

Now let us consider how and why the Coriolis operator produces its specific distortions. Calling the limited Hamiltonian of (7)  $\mathcal{H}_K$ , the complete Hamiltonian for axial symmetry can be written,

$$\mathcal{H} = \mathcal{H}_K + \mathcal{H}_C. \quad (15)$$

Thus, for the Schrödinger equation, we have

$$\mathcal{H}_K \Psi + \mathcal{H}_C \Psi = E \Psi. \quad (16)$$

By expanding  $\Psi$  in a standard series in  $K$ ,

$$\Psi = \sum_K a_K \psi_K, \quad (17)$$

where

$$\sum_K a_K^* a_K = 1, \quad (18)$$

substituting this into (16), and multiplying through on the left by  $\Psi^*$  (expanded in a similar series), one obtains

$$a_K E_K + a_{K-1} \int \psi_{K-1}^* \mathcal{H}_C \psi_K + a_{K+1} \int \psi_{K+1}^* \mathcal{H}_C \psi_K = a_K E. \quad (19)$$

For the limited situation of a state  $K$  interacting with its closely related states  $K+1$  and  $K-1$  (to first order,  $\mathcal{H}_C$  can connect only states having the same  $I$  and differing in  $K$  by one unit) one obtains a set of three equations similar to (19); for a solution to exist the following secular equation must be satisfied:

$$\begin{vmatrix} E_K - E & H_{K,K-1} & H_{K,K+1} \\ H_{K-1,K} & E_{K-1} - E & 0 \\ H_{K+1,K} & 0 & E_{K+1} - E \end{vmatrix} = 0, \quad (20)$$

where  $H_{K,K\pm 1}$  is the Coriolis matrix element between  $\langle K|$  and  $|K\pm 1\rangle$  and, because of the symmetry of the operator, is numerically equal to  $H_{K\pm 1,K}$ . Expanding and partially solving for  $E$ , one obtains

$$E = E_K - \frac{(E_{K-1} - E)(H_{K,K+1})^2 + (E_{K+1} - E)(H_{K,K-1})^2}{(E_{K-1} - E)(E_{K+1} - E)}. \quad (21)$$

Now, in a real nucleus  $E$  is the experimental energy of the state  $K$ , as opposed to  $E_K$ , which is the energy obtained from  $\mathcal{H}_K$ . Since the Coriolis-interaction displacement is, hopefully, small compared with the normal spacing between related (i.e., originating from the same spherical state) states in the deformed nucleus,  $E$  should be much closer to  $E_K$  than to  $E_{K-1}$  or to  $E_{K+1}$ , and, as a first approximation, it could be replaced by  $E_K$  wherever it appears on the right side of (21). However, if this procedure is followed, the only contribution we find from  $\mathcal{H}_C$  to  $E$  is a negative term in  $I(I+1)$  lowering the empirical value of the rotation constant,  $\hbar^2/2\mathcal{I}$ , which can be considered as just a renormalization of the moment of inertia. A somewhat better approximation is to substitute the entire right side of (21) back into the equation for  $E$  each time  $E$  appears on the right side of the equation and only then to substitute  $E_K$  for  $E$  each time it appears on the right side of the resulting expression. Doing this, performing the necessary algebra, and substituting the notation  $H_+$  for  $H_{K,K+1}$ ,  $H_-$  for  $H_{K,K-1}$ ,  $W_+$  for  $E_{K+1} - E_K$ , and  $W_-$  for  $E_{K-1} - E_K$ , one obtains

$$E = E_K - \frac{H_+^2 W_- \left(1 + \frac{W_- H_+^2 + W_+ H_-^2}{W_-^2 W_+}\right) + H_-^2 W_+ \left(1 + \frac{W_- H_+^2 + W_+ H_-^2}{W_- W_+^2}\right)}{W_- W_+ \left(1 + \frac{W_- H_+^2 + W_+ H_-^2}{W_-^2 W_+}\right) \left(1 + \frac{W_- H_+^2 + W_+ H_-^2}{W_- W_+^2}\right)} \quad (22)$$

The two  $(1 + \dots)$  terms in the denominator can be expanded in a  $(1 - \dots)$  power series in the numerator. Doing this and then dropping all terms that involve the matrix elements to powers higher than the fourth (these terms would have denominators containing the energy difference to powers of five and greater, and hence should be very small), one obtains

$$E = E_K - \frac{H_+^2}{W_+} - \frac{H_-^2}{W_-} + \frac{H_+^4}{W_+^3} + \frac{H_+^2 H_-^2}{W_+^2 W_-} + \frac{H_+^2 H_-^2}{W_+ W_-^2} + \frac{H_-^4}{W_-^3} \quad (23)$$

Substituting from (10) for  $E_K$  and grouping terms:

$$E = E_0 + \left[ \frac{\hbar^2}{2S} I(I+1) - \left( \frac{H_+^2}{W_+} + \frac{H_-^2}{W_-} \right) + \left[ \frac{H_+^4}{W_+^3} + \frac{H_+^2 H_-^2}{W_+^2 W_-} + \frac{H_+^2 H_-^2}{W_+ W_-^2} + \frac{H_-^4}{W_-^3} \right] \right] \quad (24)$$

Since the matrix elements are proportional to  $[I(I+1)]^{1/2}$ , the first-order correction is to reduce the overall term in  $I(I+1)$ , thus effectively reducing the rotation constant and lowering the upper members of a rotational band with respect to the lower members. Thus, the entire band is said to become "compressed." The second-order correction adds a positive term in  $I^2(I+1)^2$ , which partially re-expands the band, but it does so much more drastically for the upper members than for the lower ones, so its overall effect is to make a high-spin band appear as if its spin were much lower. If one continued to make approximations in the spirit of that which produced (22), he would find that the higher-order terms would appear with alternating signs, i.e., a negative term in

$I^3(I+1)^3$ , a positive term in  $I^4(I+1)^4$ , etc. However, these terms rapidly become very small, and other effects, such as considering more states to be involved, become more important.

In this derivation we have considered only the first-order interaction of a state  $K$  with its related neighbors  $K+1$  and  $K-1$ . A more complete picture would be to consider, say, all the states originating from a particular spherical state. This was done, for example, for the  $i_{13/2}$ -based states in  $Bk^{250}$ , where a nine-by-nine matrix had to be evaluated. The discussion of procedure will be deferred until then (the next section) because the notation, although still unwieldy, becomes somewhat more tractable if it is given in terms of specific states.

The system considered thus far has had axial symmetry. What about vibration states when this axial symmetry is destroyed? When axial symmetry is relaxed, the following terms are added to the Hamiltonian<sup>76</sup> in (6):

$$\begin{aligned} \mathcal{H}_V = & \left( \frac{\hbar^2}{8\mathcal{S}_1} - \frac{\hbar^2}{8\mathcal{S}_2} \right) [-2(I_+j_+ + I_-j_-) \\ & + (j_+j_+ + j_-j_-) + (I_+I_+ + I_-I_-)]. \end{aligned} \quad (25)$$

One also has to account for any axial asymmetry introduced into the potential  $V(\vec{r})$ , which will change  $E_0(K)$  and thus also  $E_0$ . The term in  $j_{\pm}j_{\pm}$  would also get incorporated into  $\mathcal{H}_0$  very much as did the term in  $j^2$  (equation 6), and it, too, would change  $E_0(K)$  and  $E_0$ . The term in  $I_{\pm}j_{\pm}$  could connect only rather esoteric states, for it would involve  $\Omega$  getting shifted up while  $K$  was being shifted down or vice versa. The states affected would have to be something like, say, two 1- octupole vibrational states based on related states  $\Omega$  and  $\Omega+1$ , the vibrational states being  $K+1 = \Omega+1$  and  $K = (\Omega+1) - 1$ , respectively. However, the term in  $I_{\pm}I_{\pm}$  could connect many different types of states. It (and the  $I_{\pm}j_{\pm}$  term) could be expected to introduce terms proportional to  $I(I+1)$  and thus renormalize the moments of inertia. If one went through a procedure similar to that just completed for the Coriolis operator, he would

find that the  $I_{\pm}I_{\pm}$  operator introduced a positive term in  $I(I+1)$ , then a negative term in  $I^2(I+1)^2$ , etc. This is the source of the normally-found negative B-term in "well-behaved" rotational bands. This rotation-vibration operator and the Coriolis operator fight each other when the Coriolis operator is operative, and it is only in rather extreme cases, such as the states found in the Bk isotopes, when the Coriolis operator has sufficiently large matrix elements to overcome the rotation-vibration negative term in  $I^2(I+1)^2$ , producing an overall positive term.

One can usually get away with using the formalism just developed for odd-mass nuclei on odd-odd nuclear states as well, because the terms already discussed are usually the predominating ones. However, double terms and cross-terms can have effects, and it is well to examine them. If we use the coupling system typified in Fig. 40b, we find that the Hamiltonian (2) becomes

$$\mathcal{H} = \frac{p^2}{2m} + V(\vec{r}) + \sum_{k=1}^3 \frac{\hbar^2}{2\mathcal{I}_k} (I_k - j_{pk} - j_{nk})^2 + \tilde{V}(p \cdot n), \quad (26)$$

where  $\vec{j}_p$  is the angular momentum of the proton and  $\vec{j}_n$  is the angular momentum of the neutron, and  $\tilde{V}(p \cdot n)$  is the proton-neutron residual interaction potential. The axially-symmetric Hamiltonian (6) then becomes

$$\begin{aligned} \mathcal{H} = & \left[ \frac{p^2}{2m} + V(\vec{r}) + \tilde{V}(p \cdot n) + \frac{\hbar^2}{2\mathcal{I}} (j_p^2 + j_n^2) \right] \\ & + \left[ \frac{\hbar^2}{2\mathcal{I}_3} (I_3 - j_{p3} - j_{n3})^2 + \frac{\hbar^2}{2\mathcal{I}} (I^2 - I_3^2 - (j_{p3} + j_{n3})^2) \right] \\ & + \left[ - \frac{\hbar^2}{2\mathcal{I}} (I_+ j_{p-} + I_- j_{p+} + I_+ j_{n-} + I_- j_{n+}) \right] \\ & + \left[ \frac{\hbar^2}{2\mathcal{I}} (j_{p+} j_{n-} + j_{p-} j_{n+}) \right]. \end{aligned} \quad (27)$$

$\tilde{V}(p \cdot n)$  is grouped with the terms in the first brackets that are designated as  $\mathcal{H}_0$ , or, to distinguish it from the odd-mass operator, as  $\mathcal{H}_{00}$ . However, this term can include tensor forces, which can distort the rotational spacings, especially for odd-odd  $K=0$  bands.<sup>95</sup> Unfortunately, the residual interaction, which is also responsible for the splitting between the triplet and singlet couplings of a proton and a neutron, has not yet been satisfactorily treated, so it is included in  $\mathcal{H}_{00}$  partly just for this reason. The solutions of  $\mathcal{H}_{00}$  are no longer the simple Nilsson functions, but now they are Nilsson functions coupled as well as one can do, using a qualitative explanation of the residual interaction. The shift-operator terms in the third brackets again make up the Coriolis operator,  $\mathcal{H}_{CC}$ , while those in the fourth brackets are usually and wrongly called a "spin-spin" operator. Temporarily neglecting these two operators, we are left with the axially-symmetric Hamiltonian,

$$\begin{aligned} \mathcal{H} = & \mathcal{H}_{00} + \frac{\hbar^2}{2\mathcal{I}_3} (I_3 - j_{p3} - j_{n3})^2 \\ & + \frac{\hbar^2}{2\mathcal{I}_3} (I^2 - I_3^2 - (j_{p3} + j_{n3})^2). \end{aligned} \quad (28)$$

The energy spectrum that it yields is

$$\begin{aligned} E = & E_{00}(\Omega) + \frac{\hbar^2}{2\mathcal{I}_3} (K - \Omega_p - \Omega_n)^2 \\ & + \frac{\hbar^2}{2\mathcal{I}_3} [I(I+1) - K^2 - (\Omega_p + \Omega_n)^2]. \end{aligned} \quad (29)$$

Again, for the low-energy bands with which we are concerned, this reduces to

$$E = E_{00} + \frac{\hbar^2}{2\mathcal{I}_3} I(I+1). \quad (30)$$

Now let us examine the so-called spin-spin operator,

$$\mathcal{H}_{jj} = \frac{\hbar^2}{2\mathcal{I}}(j_{p\pm}j_{n\mp}). \quad (31)$$

It can connect proton and neutron states that have  $\Omega$ 's differing by two units. Thus, it can shift the odd and even members of a band with respect to each other, but it can do this only for  $K=0$  bands made up from an  $\Omega = \pm 1/2$  proton and an  $\Omega = \mp 1/2$  neutron. Thus, in  $\text{Tm}^{170}$ , for example,<sup>97</sup> it causes violent distortion of many bands, for it wrecks the  $K=0$  band, and this then gets mixed into the other bands by the Coriolis interaction. However, this operator may be ignored except in such special circumstances.

This leaves us the Coriolis operator,

$$\mathcal{H}_{CC} = -\frac{\hbar^2}{2\mathcal{I}}(I_{\pm}j_{p\mp} + I_{\pm}j_{n\mp}), \quad (32)$$

to examine. But—it contains no cross-terms, so, by following the same procedure as for  $\mathcal{H}_C$ , we would find that the proton and neutron parts of this operator can be applied separately. Each part produces exactly the same types of distortions as did the complete odd-mass operator, and these distortions are additive. When we examine the distortions in the  $\text{Bk}^{250}$  bands more quantitatively, we can, for all practical purposes, apply just the odd-mass operator, for in this nucleus only the proton states introduce any appreciable distortion. And, for the  $\text{Bk}^{248}$  bands, we could apply the odd-odd operator, or, equivalently, we could apply the odd-mass operator twice and add the results.

B. Application to Es<sup>254</sup> Decay (Bk<sup>250</sup>)

Our task is essentially completed. From the development in the previous section it is clear that the Coriolis interaction can and would be expected to cause distortions such as appear in the even-parity bands of Bk<sup>250</sup>. This means that we have justified our assignments for these bands and can have confidence in them even though they were far from obvious at first. Nevertheless, it would be well to examine the behavior of the Coriolis interaction in Bk<sup>250</sup> more quantitatively. This can be somewhat difficult, for there are many more unknowns and adjustable parameters than there are pieces of data to be fit. Many of these parameters, such as the placement of unknown states, etc., can be estimated within limits, however, so we shall do this and proceed to the calculations. It must be remembered that the calculated examples given below are not to be construed as fundamental truths—they are simply reasonably good fits to the experimental distortions that were made with a minimum amount of guesswork. It is always possible that one could get fits with other methods or other combinations of parameters—but, at this time, there is not enough precision knowledge about states in odd-odd nuclei to warrant more involved and sophisticated procedures. We could easily be fooling only ourselves if we tried them.

Since the 85-keV  $K\pi = 7+$  band in Bk<sup>250</sup> is known with the most precision, it will be taken as the specimen band in Bk<sup>250</sup>. We shall discuss the Coriolis-induced distortion on it in moderate detail, then leave the details concerning others bands to the future. We shall look at this band twice; first we shall consider it to interact only with its closest relatives, and then we shall look at its interaction with all available bands containing protons from the  $i_{13/2}$  spherical level, and then we shall compare the two approaches.

The  $7+$  band in Bk<sup>250</sup> is an especially favorable case for a specific Coriolis calculation, for the matrix elements involved are unusually large, the spins of the levels are large, and the individual states entering into the effect can be picked out rather easily. The



last is true because only the proton state,  $7/2+[633\uparrow]$ , is affected, and the only other even-parity proton states in this region are the closely related ones that originate, along with this one, from the  $1_{13/2}$  spherical level, which spin-orbit coupling has depressed so that it lies among the odd-parity levels of the fifth oscillator shell. Specifically, by far the largest effect is expected to result from the first-order interaction with the  $5/2+[642\uparrow]$  and  $9/2+[624\uparrow]$  proton states. In  $Bk^{249}$  the  $5/2+$  state appears at 393 keV above the  $7/2+$  state (cf. Fig. 30). In  $Bk^{250}$  its position is not too well-known, but the level at 434 keV may involve this state—this is a little bit closer to the  $7/2+$  state than it was in  $Bk^{249}$ , but, considering that the residual interaction with the  $7/2+[613\uparrow]$  neutron state to form the actual states in  $Bk^{250}$  has not been taken into account, the position is quite reasonable. The position of the  $9/2+[624\uparrow]$  proton state is not even this well defined. We know that the Fermi surface lies between the  $7/2+$  and  $5/2+$  proton states and is closer to the  $7/2+$  state than to the  $5/2+$ ; also, that the  $9/2+$  state lies on the same side of the Fermi surface as the  $7/2+$  state and on the side of the  $7/2+$  state away from the Fermi surface. However, quantitative predictions are difficult to make. The band of interest in  $Bk^{250}$  would be an  $8+$  band (again involving the  $7/2+[613\uparrow]$  neutron state), but this was not seen in our work. A calculation by Mang, using BCS methods, predicts that the single-proton state should lie 700-800 keV above the  $7/2+$  state in a "typical" berkelium nucleus, i.e., neglecting all neutron effects.<sup>98</sup> Other estimates have placed it at approximately 1 MeV above the  $7/2+$  state,<sup>99</sup> and there is some indication that it was seen at about this position in  $Bk^{249}$ , using gamma-alpha coincidence measurements.<sup>56</sup> Hence, we shall assume, albeit somewhat arbitrarily, that the  $8+$  band begins at 1 MeV in  $Bk^{250}$ , some 915 keV above the  $7+$  band.

The following matrix elements will be needed:

$$\langle \psi_K | H_C | \psi_{K\pm 1} \rangle = \frac{-\hbar^2}{28} \langle IK | I_{\pm} | I K \pm 1 \rangle \langle j\Omega | j_{\mp} | j \Omega \pm 1 \rangle. \quad (33)$$

The  $I_{\pm}$  portions can be evaluated directly from (12), but the  $j_{\mp}$  portions still require some comment besides their being calculated from (13) applied to states of mixed  $j$ 's. Nilsson has calculated values for the  $j_{\mp}$  matrix elements as a function of various deformations,<sup>100</sup> and he obtains 6.155 for  $\langle 7/2+ | j_{+} | 5/2+ \rangle$  and 5.647 for  $\langle 7/2+ | j_{-} | 9/2+ \rangle$  at a nuclear deformation  $\eta = 4$  ( $\delta \cong 0.2$ ). However, since the matrix element between the  $5/2+$  and  $7/2+$  states is across the Fermi surface, its value will not be so large as the calculated value. Actually, if a nucleus were to have a sharp Fermi surface, the matrix elements between hole states (like the  $5/2+$ ) and particle states (like the  $7/2+$ ) should be zero. The pairing force, which produces a diffuse Fermi surface and the quasi-particle states, allows matrix elements between quasi-particle and quasi-hole states, but these are diminished in magnitude over the values obtained from angular-momentum calculus. A reasonable fit was obtained for a similar calculation in  $Bk^{249}$  when this particular matrix element was cut by 40%.<sup>101</sup> We shall use this same value, which is 3.69, for  $\langle 7/2+ | j_{+} | 5/2+ \rangle$ .

Using equation (24), and adding the negative B-term from the rotation-vibration interaction, we find the levels of the  $7+7$  and  $7+8$  levels to be:

$$E_{7+7} = E_0 + \left[ \frac{\hbar^2}{2\mathcal{I}}(7)(8) - \left( \frac{H_{7+7,6+7}^2}{E_{6+7} - E_{7+7}} \right) \right] + \left[ (B)(7^2)(8^2) + \left( \frac{H_{7+7,6+7}^4}{(E_{6+7} - E_{7+7})^3} \right) \right] \quad (34)$$

and

$$\begin{aligned}
 E_{7+8} = E_0 + & \left[ \frac{\hbar^2}{2\mathcal{I}}(8)(9) - \left( \frac{H_{7+8,8+8}^2}{E_{8+8} - E_{7+8}} + \frac{H_{7+8,6+8}^2}{E_{6+8} - E_{7+8}} \right) \right] \\
 & + \left[ (B)(8^2)(9^2) + \left( \frac{H_{7+8,8+8}^4}{(E_{8+8} - E_{7+8})^3} + \frac{H_{7+8,8+8}^2 H_{7+8,6+8}^2}{(E_{8+8} - E_{7+8})^2 (E_{6+8} - E_{7+8})} \right. \right. \\
 & \left. \left. + \frac{H_{7+8,8+8}^2 H_{7+8,6+8}^2}{(E_{8+8} - E_{7+8})(E_{6+8} - E_{7+8})^2} + \frac{H_{7+8,6+8}^4}{(E_{6+8} - E_{7+8})^3} \right) \right]. \quad (35)
 \end{aligned}$$

Substituting 7.5 keV for  $\hbar^2/2\mathcal{I}$  (an undistorted even-even value for this nuclear region), -0.0046 keV for B (the value obtained for the 99-keV 5- band in  $\text{Bk}^{250}$ , which is presumed to be relatively free from Coriolis distortion), and the calculated values for the matrix elements, one obtains 58.7 keV for the difference in energy between the two levels, or a value of 3.67 keV for the empirical  $\hbar^2/2\mathcal{I}$ . Similarly, one obtains 63.4 keV for the spacing between the 7+8 and 7+9 levels, or a value of 3.52 keV for the empirical  $\hbar^2/2\mathcal{I}$ . In other words, the calculation has overcompensated for the effect. However, the real worth of this procedure is not to force a quantitative agreement or else, but it is simply to be able to explain the experimentally-found distortion of the rotational bands. And the calculation has done this acceptably. The rotational constant has been lowered drastically, and, if one examines the numerical coefficients of the terms in  $I^2(I+1)^2$  of (34) and (35), he finds they are positive. The actual numbers do not mean too much, for they depend on the value of B taken from the 99-keV 5- band really being a good value, which may be debatable. However, it is difficult to find an empirical value of B to put into the equations that is negative enough that the positive terms from the Coriolis calculation here do not overpower it, and, conversely, it is also difficult to explain the positive experimental B-term without the Coriolis interaction.

Next we shall take as quick a look as possible at the more complete calculation. We shall consider the 7+ band to interact by higher orders with all states made up from the  $7/2+[613\uparrow]$  neutron and various proton states originating from the  $1_{13/2}$  spherical state, if they lie anywhere in a reasonable vicinity. We have already seen that a 7+ and a 0+ state can be made using the  $7/2+[633\uparrow]$  proton itself. The  $5/2+[642\uparrow]$  proton forms a 6+ and a 1+; the  $3/2+[651\uparrow]$  proton, a 5+ and a 2+; and the  $1/2+[660\uparrow]$  proton, a 4+ and a 3+. Since the two halves of the wave function of the  $1/2+$  proton are themselves connected by the Coriolis operator, this proton state causes the 4+ triplet and the 3+ singlet states to be connected by the operator. This means that the set of singlet states, 3+, 2+, 1+, and 0+, are connected into the matrix with the triplet states. To this series of eight states, we add the 8+ state ( $9/2+[624\uparrow]$  proton) used in the previous calculation and hope that is enough. Naturally enough, very few of these states and the rotational bands based on them are known experimentally. It is necessary to place them arbitrarily, guided by whatever information or estimates we can find. The particular set of estimated positions that we used is listed in Table XXII.

The secular equation that have to be satisfied for this system is the following:

$$\begin{vmatrix}
 E_8-E & H_{78} & 0 & 0 & 0 & 0 & 0 & 0 & 0 \\
 H_{78} & E_7-E & H_{67} & 0 & 0 & 0 & 0 & 0 & 0 \\
 0 & H_{67} & E_6-E & H_{56} & 0 & 0 & 0 & 0 & 0 \\
 0 & 0 & H_{56} & E_5-E & H_{45} & 0 & 0 & 0 & 0 \\
 0 & 0 & 0 & H_{45} & E_4-E & H_{34} & 0 & 0 & 0 \\
 0 & 0 & 0 & 0 & H_{34} & E_3-E & H_{23} & 0 & 0 \\
 0 & 0 & 0 & 0 & 0 & H_{23} & E_2-E & H_{12} & 0 \\
 0 & 0 & 0 & 0 & 0 & 0 & H_{12} & E_1-E & H_{01} \\
 0 & 0 & 0 & 0 & 0 & 0 & 0 & H_{01} & E_0-E
 \end{vmatrix} = 0, \quad (36)$$

Table XXIII. The estimated positions of bands in  $Bk^{250}$  that were used for purposes of Coriolis calculations.

Proton state Neutron state	Triplet coupling		Singlet coupling	
	K $\pi$ I	Excited-state energy (keV)	K $\pi$ I	Excited-state energy (keV)
9/2+[624 $\uparrow$ ]	8+8	1000	not used in the calculation	
7/2+[613 $\uparrow$ ]	8+9	1082		
7/2+[633 $\uparrow$ ]	7+7	85.5	0+1 <sup>a</sup>	105
7/2+[613 $\uparrow$ ]	7+8	155.9	0+0	150
	7+9	240	0+3	154
			0+2	177
			0+5	235
			0+4	240
			0+6	339
			0+7	352
			0+8	474
			0+9	505
5/2+[642 $\uparrow$ ]	6+6	434	1+1	510
7/2+[613 $\uparrow$ ]	6+7	498	1+2	528
	6+8	572	1+3	555
	6+9	655	1+4	591
			1+5	636
			1+6	690
			1+7	753
			1+8	825
			1+9	906
3/2+[651 $\uparrow$ ]	5+5	930	2+2	1005
7/2+[613 $\uparrow$ ]	5+6	985	2+3	1032
	5+7	1047	2+4	1068
	5+8	1119	2+5	1113
	5+9	1200	2+6	1167
			2+7	1230
			2+8	1302
			2+9	1383

Table XXII. (cont.)

Proton state Neutron state	Triplet coupling		Singlet coupling	
	K $\pi$ I	Excited-state energy (keV)	K $\pi$ I	Excited-state energy (keV)
1/2+[660 $\uparrow$ ]	4+4	1400	3+3	1475
7/2+[613 $\uparrow$ ]	4+5	1445	3+4	1511
	4+6	1499	3+5	1556
	4+7	1562	3+6	1610
	4+8	1634	3+7	1673
	4+9	1718	3+8	1745
			3+9	1826

<sup>a</sup>For the peculiar spacings of K=0 bands, see ref. 95.

N.B. The energies given in this table are simply best estimates of the positions of mostly unknown states. They were prepared for the sole purpose of making demonstration calculations as discussed in the text and are not to be construed as predictions on our part as to where the states and levels in question are found experimentally.

where  $H_{ij}$  is the Coriolis matrix element between states of whatever I is being investigated in bands  $K=i$  and  $j$ , and  $E_i$  is the energy of whatever I is being investigated in band  $K=i$ . A somewhat different method of approximation will be used this time, since the series expansions and substitutions used for just three states become unwieldy here. We shall calculate the quantities  $E_7-E$ , i.e., the difference predicted between the experimental energies of the  $K=7$  levels ( $E$ ) and what would be calculated from  $N_0(E_7)$ .

We shall examine the 7+7 level first. This allows us to discard all the terms involving  $K=8$  after we have expanded the monstrosity (36). If we then factor out the quantity  $E_{7+7}-E$  from all terms that contain it, similarly factor out  $H_{67}^2/(E_{6+7}-E)$  from the terms (all the remaining ones) that contain it, and finally divide the entire equation

by  $\prod_{K=0}^8 (E_{K+7}-E)$ , which we designate simply as  $\Pi 012345678$ , the result is

$$\begin{aligned}
 (E_{7+7}-E) & \left[ 1 - \frac{H_{01}^2}{\Pi 01} - \frac{H_{12}^2}{\Pi 12} - \frac{H_{23}^2}{\Pi 23} - \frac{H_{34}^2}{\Pi 34} - \frac{H_{45}^2}{\Pi 45} - \frac{H_{56}^2}{\Pi 56} + \frac{H_{01}^2 H_{23}^2}{\Pi 0123} \right. \\
 & + \frac{H_{01}^2 H_{34}^2}{\Pi 0134} + \frac{H_{01}^2 H_{45}^2}{\Pi 0145} + \frac{H_{01}^2 H_{56}^2}{\Pi 0156} + \frac{H_{12}^2 H_{34}^2}{\Pi 1234} + \frac{H_{12}^2 H_{45}^2}{\Pi 1245} + \frac{H_{12}^2 H_{56}^2}{\Pi 1256} \\
 & + \frac{H_{23}^2 H_{45}^2}{\Pi 2345} + \frac{H_{23}^2 H_{56}^2}{\Pi 2356} + \frac{H_{34}^2 H_{56}^2}{\Pi 3456} - \frac{H_{01}^2 H_{23}^2 H_{45}^2}{\Pi 012345} - \frac{H_{01}^2 H_{23}^2 H_{56}^2}{\Pi 012356} \\
 & - \frac{H_{01}^2 H_{34}^2 H_{56}^2}{\Pi 013456} - \left. \frac{H_{12}^2 H_{34}^2 H_{56}^2}{\Pi 123456} \right] = \frac{H_{67}^2}{E_{6+7}-E} \left[ 1 - \frac{H_{01}^2}{\Pi 01} - \frac{H_{12}^2}{\Pi 12} \right. \\
 & - \frac{H_{23}^2}{\Pi 23} - \frac{H_{34}^2}{\Pi 34} - \frac{H_{45}^2}{\Pi 45} + \frac{H_{01}^2 H_{23}^2}{\Pi 0123} + \frac{H_{01}^2 H_{34}^2}{\Pi 0134} + \frac{H_{01}^2 H_{45}^2}{\Pi 0145} \\
 & \left. + \frac{H_{12}^2 H_{34}^2}{\Pi 1234} - \frac{H_{01}^2 H_{23}^2 H_{45}^2}{\Pi 012345} \right]. \tag{37}
 \end{aligned}$$

This equation demonstrates that the shift in energy of the 7+7 level is produced primarily by the  $H_{67}^2/(E_{6+7}-E)$  term, but that the original shift produced by this term alone is modified by the factor

consisting of the bracketed terms on the right side of the equations divided by the bracketed terms on the left side of the equation. Upon examining the equation, one can see that, in this instance, all the terms in the right brackets are also contained in the left brackets, but the left brackets include a few extra terms in addition. One would thus expect the modification factor to be in the vicinity of 1 unless one of these extra terms happened to be unusually large. For this particular level the factor is  $0.52/0.44 = 1.18$ . However, it is possible, although not probable, that such a term might blow up, if and when two distantly-related states happened to lie very close to each other, making an energy denominator small. This is perhaps more likely to happen in odd-odd nuclei, with their wealth of levels, than in odd-mass nuclei. In most cases, however, as in this one, the modification will be small. The actual matrix elements used for the 7+7, 7+8, and 7+9 levels are listed in Table XXIII. And  $E_{7+7} - E = (24.8)(1.18) = 29.2$  keV.

It is necessary to include one more ungainly equation, but that's all. The equation for the shift of the 7+8 level is somewhat more general than that for the 7+7 level because it contains the terms coming in through  $K = 8$  as well as those from  $K = 6$ :



Table XXIII. Coriolis matrix elements involved in calculating the distortion of the 7+ band in Bk<sup>250</sup>.

K,K+1	$\langle  j_-  \rangle^2$ <sup>a</sup>	$\langle \psi_K   H_C   \psi_{K\pm 1} \rangle^2$ (keV) <sup>2</sup>		
		I=7	I=8	I=9
01	(60% of 6.155) <sup>2</sup> <sup>b</sup>	37,370	48,070	60,070
12	(6.455) <sup>2</sup>	110,250	142,930	179,680
23	(6.595) <sup>2</sup>	106,580	140,630	179,000
34	(6.629) <sup>2</sup>	94,720	129,160	167,920
45	(6.595) <sup>2</sup>	76,730	110,790	149,160
56	(6.455) <sup>2</sup>	53,070	85,750	122,500
67	(60% of 6.155) <sup>2</sup> <sup>b</sup>	9,360	20,040	32,050
78	(5.647) <sup>2</sup>	---	24,990	53,120

<sup>a</sup>These were obtained from ref. 100 for  $\eta = 4$ .

<sup>b</sup>These matrix elements were diminished because they are between hole and particle states; see text.

$$\begin{aligned}
 (E_{7+8}-E) & \left[ 1 - \frac{H_{01}^2}{\Pi_{01}} - \frac{H_{12}^2}{\Pi_{12}} - \frac{H_{23}^2}{\Pi_{23}} - \frac{H_{34}^2}{\Pi_{34}} - \frac{H_{45}^2}{\Pi_{45}} - \frac{H_{56}^2}{\Pi_{56}} + \frac{H_{01}^2 H_{23}^2}{\Pi_{0123}} + \frac{H_{01}^2 H_{34}^2}{\Pi_{0134}} \right. \\
 & + \frac{H_{01}^2 H_{45}^2}{\Pi_{0145}} + \frac{H_{01}^2 H_{56}^2}{\Pi_{0156}} + \frac{H_{12}^2 H_{34}^2}{\Pi_{1234}} + \frac{H_{12}^2 H_{45}^2}{\Pi_{1245}} + \frac{H_{12}^2 H_{56}^2}{\Pi_{1256}} + \frac{H_{23}^2 H_{45}^2}{\Pi_{2345}} + \frac{H_{23}^2 H_{56}^2}{\Pi_{2356}} \\
 & + \left. \frac{H_{34}^2 H_{56}^2}{\Pi_{3456}} - \frac{H_{01}^2 H_{23}^2 H_{45}^2}{\Pi_{012345}} - \frac{H_{01}^2 H_{23}^2 H_{56}^2}{\Pi_{012356}} - \frac{H_{01}^2 H_{34}^2 H_{56}^2}{\Pi_{013456}} - \frac{H_{12}^2 H_{34}^2 H_{56}^2}{\Pi_{123456}} \right] = \frac{H_{67}^2}{E_{6+8}-E} \left[ 1 \right. \\
 & - \frac{H_{01}^2}{\Pi_{01}} - \frac{H_{12}^2}{\Pi_{12}} - \frac{H_{23}^2}{\Pi_{23}} - \frac{H_{34}^2}{\Pi_{34}} - \frac{H_{45}^2}{\Pi_{45}} + \frac{H_{01}^2 H_{23}^2}{\Pi_{0123}} - \frac{H_{01}^2 H_{34}^2}{\Pi_{0134}} - \frac{H_{01}^2 H_{45}^2}{\Pi_{0145}} \\
 & - \frac{H_{12}^2 H_{34}^2}{\Pi_{1234}} + \left. \frac{H_{01}^2 H_{23}^2 H_{45}^2}{\Pi_{012345}} \right] + \frac{H_{78}^2}{E_{8+8}-E} \left[ 1 - \frac{H_{01}^2}{\Pi_{01}} - \frac{H_{12}^2}{\Pi_{12}} - \frac{H_{23}^2}{\Pi_{23}} - \frac{H_{34}^2}{\Pi_{34}} - \frac{H_{45}^2}{\Pi_{45}} \right. \\
 & - \frac{H_{56}^2}{\Pi_{56}} + \frac{H_{01}^2 H_{23}^2}{\Pi_{0123}} + \frac{H_{01}^2 H_{34}^2}{\Pi_{0134}} + \frac{H_{01}^2 H_{45}^2}{\Pi_{0145}} + \frac{H_{01}^2 H_{56}^2}{\Pi_{0156}} + \frac{H_{12}^2 H_{34}^2}{\Pi_{1234}} + \frac{H_{12}^2 H_{45}^2}{\Pi_{1245}} \\
 & + \frac{H_{12}^2 H_{56}^2}{\Pi_{1256}} + \frac{H_{23}^2 H_{45}^2}{\Pi_{2345}} + \frac{H_{23}^2 H_{56}^2}{\Pi_{2356}} + \frac{H_{34}^2 H_{56}^2}{\Pi_{3456}} - \frac{H_{01}^2 H_{23}^2 H_{45}^2}{\Pi_{012345}} - \frac{H_{01}^2 H_{23}^2 H_{56}^2}{\Pi_{012356}} \\
 & - \left. \frac{H_{01}^2 H_{34}^2 H_{56}^2}{\Pi_{013456}} - \frac{H_{12}^2 H_{34}^2 H_{56}^2}{\Pi_{123456}} \right]. \tag{38}
 \end{aligned}$$

The energy shift of the 7+8 level is seen to be caused primarily by the first-order terms involving the 6+8 and 8+8 levels, and each of these is modified by a factor like the one before. However, the terms in the bracket multiplying the  $H_{78}^2/(E_{8+8}-E)$  term here is identical with the terms in the brackets on the left side of the equation, so no higher-order effects can make themselves felt through the 8+8 level. The modifying factor for the  $H_{67}^2/(E_{6+8}-E)$  term is similar to the factor in (37), here having the numerical value  $0.41/0.32 = 1.28$ , making  $E_{7+8}-E = 98.7$  keV.

A similar calculation was made for the 7+9 level. Again it was found that small, but present higher-order effects entered through the  $K = 6$  band.  $E_{7+9}-E$  was found to be 176.5 keV.

In order to turn these energy shifts into meaningful quantities one has to evaluate the predicted energies produced by  $\mathcal{H}_K$ . This can be done with moderate accuracy by assigning the even-even value of  $\hbar^2/2\mathcal{I}$  in the rotational-energy equation and evaluating  $E_0$  with the experimental energy of the first level, i.e., 7+7 at 85.5 keV. When this is done, one can use the energy shifts to obtain the spacings of the band. The difference between the 7+7 and 7+8 levels yields a value for  $\hbar^2/2\mathcal{I}$  of 2.66 keV, while that between the 7+8 and 7+9 levels yields a value of 2.67 keV. Thus, the complete treatment overcompensates even more strongly than did just considering three interacting states. Even if one uses just the first-order terms (neglecting the modifying factors), one finds that the procedure of evaluating energy shifts overcompensates just slightly more than did the three-state procedure; the difference comes mostly from difficulties in evaluating the values produced by  $\mathcal{H}_K$ . The results from all the calculations are listed in Table XXIV for comparison.

The most probable reason for the overcompensation is that  $H_{67}$  is still too large. As we mentioned before, the only reason that this matrix element is not zero is because the pairing force produces a diffuse Fermi surface and quasi-particle states that can be connected across the Fermi surface. This pairing force is reduced, however, with each orbital near the Fermi surface that is "blocked," i.e., occupied by a single particle and thereby made unavailable for the pairs of particles to be scattered into. The effective number of orbitals,  $\Gamma$ , that contribute to the pairing force is only eight or ten,<sup>2</sup> so each blocked orbital not only reduces the pairing force but does so significantly. In odd-odd nuclei there are at least two orbitals blocked as opposed to at least one in odd-mass nuclei, so one could reasonably expect that the pairing force would be less in odd-odd nuclei than it would be in odd-mass nuclei. If the pairing force is less, the matrix elements across the Fermi surface should also be diminished; and we can validly hope that the matrix element between the  $5/2+[642\uparrow]$  and  $7/2+[633\uparrow]$  proton states could be diminished even further in  $Bk^{250}$  than it is in  $Bk^{249}$ . With

Table XXIV. Comparison table of Coriolis calculations.

	3-state calcula- tion	Complete calculation				Experi- mental
		$H_{67}$ cut 40%		$H_{67}$ cut 54%		
		1st order	complete	1st order	complete	
$E_{7+7}-E$		24.8 keV	29.2 keV			
$E_{7+8}-E$		83.5 keV	98.7 keV			
7+8 posi- tion		138.8 keV	128.0 keV		155.9 keV (norm)	155.9 keV
Spacing between 7+7 and 7+8	58.7 keV	53.3 keV	42.5 keV		70.4 keV (norm)	70.4 keV
$n^2/2s$	3.67 keV	3.33 keV	2.66 keV		4.40 keV (norm)	4.40 keV
$E_{7+9}-E$		146.9 keV	176.5 keV	112.9 keV	130.0 keV	
7+9 posi- tion		201.4 keV	176.2 keV		222.7 keV	240 keV
Spacing between 7+8 and 7+9	63.4 keV	62.6 keV	48.2 keV		66.8 keV	85 keV
$n^2/2s$	3.52 keV	3.48 keV	2.67 keV		3.71 keV	4.72 keV

this in mind, we performed the same calculations as before, only this time we left  $H_{67}$  as an adjustable parameter and forced the calculation to yield the experimental spacing between the 7+7 and 7+8 levels. This could be done successfully if  $H_{67}$  was cut not 40% but 54% from the straightforwardly calculated value. Using this value of  $H_{67}$ , we then calculated the spacing between the 7+8 and 7+9 levels and  $\hbar^2/2\mathcal{S}$  from this spacing.  $\hbar^2/2\mathcal{S}$  was still too low, so this technique did not cure all the ills, but  $\hbar^2/2\mathcal{S}$  was much closer to the experimental value. These numbers are also included in Table XXIV.

Considering the number of approximations that could not be avoided, the calculations have been amazingly successful. You will notice that we have not attempted to evaluate the  $a_K$ 's of (17) and (18), i.e., determine the actual amount of mixing of the various bands. These coefficients are remarkably sensitive to slight shifts in energy, so, until the quality of the data are such that the energies can be predicted with precision, it would be fairly useless to make such evaluations.

The procedure for the 4+ band and perhaps for the 416-keV 5-band are essentially the same as we have just gone through for the 7+ band. In each case one would calculate the interaction of the  $7/2+[633^1]$  proton with some or all of the related proton states from the  $i_{13/2}$  spherical state; the actual odd-odd states involved would all contain the same neutron, which would go along for the ride. And in each case the calculations would exhibit the same tendency to overcompensate. However, they would at least, even with our insufficient data and many approximations, fully justify our spin assignments.

C. Application to Es<sup>252</sup> Decay (Bk<sup>248</sup>)

The tearing down of barriers and consequent mixing of states in Bk<sup>248</sup> is expected to be far more complex than in Bk<sup>250</sup>; yet we have fewer pieces of driftwood on which to hand our calculations or explanations. The basic situation is this: In Bk<sup>248</sup>, especially in the ground-state rotational band, the neutron states as well as the proton states can have large Coriolis matrix elements, and the spins are even higher, so a huge distortion is to be expected. Also, not only would there be super-enhanced Coriolis mixing, there would be duper-enhanced rotation-vibration interactions because of the juxtaposition of intrinsic states and vibration states based on related intrinsic states.

Consider the ground-state 8- rotational band, which is a triplet coupling of the same  $7/2+[633\uparrow]$  proton state that has just led us through such a lab-(rynth) and the  $9/2-[734\uparrow]$  neutron state from the  $j_{15/2}$  spherical level, which should have perhaps even larger Coriolis matrix elements with its cohort states. From equation (32) and the discussion thereabout it is evident that we can perform the proton and neutron calculations separately and then add them, and a qualitative estimate would lead us to expect up to twice as much distortion in this band as was found in the 7+ band in Bk<sup>250</sup>. This is indeed seen to be the case—not only does  $n^2/2\mathfrak{S}$  have the lowest value yet catalogued and is probably kept from going lower only because it is approaching the (cranking-model) rigid-rotor value, but also the B-term in  $I^2(I+1)^2$  is the largest positive one yet trapped. Add to all this mixing and distortion the rotation-vibration distortion and mixing, and it is easy to see why the alpha-decay hindrance factors are low for every band and state seen. Literally, in this nucleus everything contains a little of everything else!

Seriously, if and when more complete information can be obtained about this nucleus, it should definitely become one of the most rewarding in the entire chart of nuclides for interesting and worthwhile calculations and deductions. It only remains for some enterprising young scientist to coerce Cf<sup>252</sup> into temporarily becoming beta active until enough Es<sup>252</sup> can be accumulated to study its decay scheme with great precision.

## V. CONCLUSION

Perhaps the most startling fact to come out of this study of odd-odd nuclei is that so much can be explained so successfully simply by considering the neutron and proton effects separately. That this can be done should lend new impetus to the study of other alpha-emitting odd-odd nuclei, for their wealth of levels can probably be untangled in a similar fashion. Such a worked-out odd-odd system, together with its odd-mass neighbors, can be a very powerful tool for studying the proton-neutron residual interaction and the nuclear force in general—and it should be simpler than the multi-particle levels in the spherical regions that have been used for the same purposes.

Much has been explained about the einsteinium decay schemes, but, as usual in work of this sort, much remains to be explained. Perhaps this work can be a starting point for continued study of these nuclei in the near future. I hope that all speculation in this thesis has been clearly labelled as such and that most of the remainder will stand up to further scrutiny. If not, I only plead: "For now we see through a glass, darkly; but then face to face: now I know in part; but then shall I know even as also I am known." And perhaps there will be some charity for human failings.

#### ACKNOWLEDGMENTS

By its very nature the work described in this thesis represents a joint effort and the co-operation and support of a number of people. In particular, I wish to express my thanks to the following:

Professor Isadore Perlman, under whose direction and motivation the work was undertaken;

Dr. Frank Asaro and Dr. Frank Stephens, under whose direct supervision the work was conducted, and who provided a great deal of day-to-day assistance;

Mrs. Helen Michel, who has devoted much time and effort in chemical and other technical assistance;

Mr. Al Ghiorso and Mr. Robert Latimer, for carrying out the Es<sup>252</sup> target production, bombardments, and initial chemical separations; also, for initial chemical separations on the Es<sup>254</sup>;

the Chemistry Technical Support Group, for keeping the electronics in working order and assisting in some experiments—in particular, Mr. Duane Mosier, Mr. Milton Firth, and Mr. Ed Arnold;

Mr. Mitch Nakamura and his group, for designing and maintaining the versatile time-to-height converter;

a number of other members of the Staff of the Lawrence Radiation Laboratory, for useful discussions and clarifications of difficult mathematical and physical points—in particular, Professor John Rasmussen, Dr. Richard Diamond, and Dr. Earl Hyde;

my wife, Rilla, for her assistance and fortitude while working on a Ph.D. in physics at the same time;

my parents, for their continued interest and support and early direction.

I also wish to express my appreciation to the National Science Foundation for a pre-doctoral fellowship during the early stages of this work.

This work was done under the auspices of the U.S. Atomic Energy Commission.



REFERENCES AND NOTES

1. The term "subshell" has reference to an accidentally large energy gap in the spacing between adjacent neutron levels in deformed nuclei that occurs at neutron number 152. Its existence was first noted experimentally by an interruption in the smooth variation of alpha-decay energies in the series of californium isotopes. Cf. Fig. 33, the Nilsson diagram for neutrons. From this it can be seen that this gap occurs only at large deformations and is strictly a result of the deformed potential.
2. O. Nathan and S. G. Nilsson, in K. Siegbahn, Alpha, Beta, and Gamma-Ray Spectroscopy (North-Holland Pub. Co., 1965), p. 601.
3. A. Bohr and B. Mottelson, Dan. Mat.-Fys. Medd. 27, No. 16 (1953).
4. S. G. Nilsson, Dan. Mat.-Fys. Medd. 29, No. 16 (1955).
5. P. R. Fields, M. H. Studier, J. F. Mech, H. Diamond, A. M. Friedman, L. B. Magnusson, and J. R. Huizenga, Phys. Rev. 93, 1428 (1954), and 94, 209 (1954).
6. S. G. Thompson, A. Ghiorso, B. G. Harvey, and G. R. Choppin, Phys. Rev. 94, 1080 (1954).
7. J. Unik, P. Day, and S. Vandenbosch, Nucl. Phys. 36, 284 (1962).
8. B. G. Harvey and co-workers, unpublished results (1955), reported by E. Hyde, I. Perlman, and G. T. Seaborg, The Nuclear Properties of the Heavy Elements (Prentice-Hall, Englewood Cliffs, N.J., 1964), p. 960. This number (270 d) also agrees with indirect evidence reported in ref. 7, p. 290.
9. R. P. Schuman, T. A. Eastwood, H. G. Jackson, and J. P. Butler, J. Inorg. Nucl. Chem. 6, 1 (1958), give the half-life as  $480 \pm 70$  d.
10. F. S. Stephens, Jr., Ph. D. Thesis, Lawrence Radiation Laboratory Report UCRL-2970 (1955).
11. F. S. Stephens, Jr., F. Asaro, and I. Perlman, unpublished results (1957, 1960). Some of these can be found in Hyde, Perlman, and Seaborg, op. cit., p. 957.
12. F. Asaro, S. Bjørnholm, and I. Perlman, Phys. Rev. 133, B291 (1964).

13. S. Vandenbosch, H. Diamond, R. K. Sjoblom, and P. R. Fields, *Phys. Rev.* 115, 115 (1959).
14. H. Rytz, *Helv. Phys. Acta* 34, 210 (1961); H. Rytz, H. H. Staub, and H. Winkler, *Helv. Phys. Acta* 34, 960 (1961); A. H. Wapstra, *Nucl. Phys.* 57, 48 (1964).
15. F. Asaro and I. Perlman, unpublished results (1960), reported in Hyde, Perlman, and Seaborg, *op. cit.*, p. 958.
16. J. M. Hollander, C. L. Nordling, and K. Siegbahn, *Ark. Fys.* 23, No. 2, 35 (1962).
17. A. H. Wapstra, G. J. Nijgh, and R. van Lieshout, Nuclear Spectroscopy Tables (North-Holland Pub. Co., 1959), p. 73.
18. F. Asaro, M. C. Michel, S. G. Thompson, and I. Perlman, Comptes Rendus du Congrès International de Physique Nucleaire, Paris, 1964 (Editions du Centre National de la Recherche Scientifique, Paris), p. 564.
19. See, e.g., Hyde, Perlman, and Seaborg, *op. cit.*, and the references therein, pp. 769, 859, and 871.
20. F. Asaro, F. S. Stephens, S. G. Thompson, and I. Perlman, *Phys. Rev.* 98, 19 (1955).
21. S. Vandenbosch and P. Day, *Nucl. Phys.* 30, 177 (1962).
22. Nathan and Nilsson, *op. cit.*, p. 673; also, S. G. Nilsson and O. Prior, *Dan. Mat.-Fys. Medd.* 32, No. 16 (1961).
23. This procedure was carried out by and under the direction of Dr. S. Fried, Lawrence Radiation Laboratory.
24. S. Fried and H. Schumacher, Lawrence Radiation Laboratory Report UCRL-10023 (1962).
25. G. R. Choppin, B. G. Harvey, and S. G. Thompson, *J. Inorg. Nucl. Chem.* 2, 66 (1956).
26. L. Phillips and R. Gatti, unpublished results, referred to in G. A. Higgins, *Natl. Acad. Sci., Nuclear Science Series NAS-NS 3031* (1960), p. 13.
27. K. Street, unpublished results (1950), reported by S. G. Thompson, B. G. Harvey, G. R. Choppin, and G. T. Seaborg, *J. Am. Chem. Soc.* 76, 6229 (1954).

28. M. Jones, R. P. Schuman, J. P. Butler, G. Cowper, T. A. Eastwood, and H. H. Jackson, Phys. Rev. 102, 203 (1956).
29. A. Ghiorso, M. H. Studier, C. I. Browne, et. al., Phys. Rev. 99, 1048 (1955); 102, 180 (1956); 119, 2000 (1960).
30. G. R. Choppin, S. G. Thompson, A. Ghiorso, and B. G. Harvey, Phys. Rev. 94, 1080 (1954).
31. F. S. Stephens, F. Asaro, S. G. Thompson, and I. Perlman, Bull. Am. Phys. Soc. Ser. II 2, 394 (1957).
32. T. A. Eastwood, J. P. Butler, M. J. Cabell, H. G. Jackson, R. P. Schuman, F. M. Rourke, and T. L. Collins, Phys. Rev. 107, 1635 (1957).
33. F. Asaro, F. S. Stephens, B. G. Harvey, and I. Perlman, Phys. Rev. 100, 137 (1955).
34. F. Asaro, S. G. Thompson, F. S. Stephens, and I. Perlman, Lawrence Radiation Laboratory Report UCRL-9382 (1960); presented in somewhat different form by I. Perlman, in Proceedings of the International Conference on Nuclear Structure, Kingston, Canada, 1960 (University of Toronto Press), p. 553; also reported in Hyde, Perlman, and Seaborg, op. cit., p. 951.
35. L. Phillips, R. Gatti, R. Brandt, and S. G. Thompson, J. Inorg. Nucl. Chem. 25, 1085 (1963).
36. D. L. Judd and S. A. Bludman, Nucl. Inst. 1, 46 (1957).
37. R. C. Pilger, Ph. D. Thesis, Lawrence Radiation Laboratory Report UCRL-3877 (1957).
38. C. P. Ruiz, Ph. D. Thesis, Lawrence Radiation Laboratory Report UCRL-9511 (1961).
39. This energy was originally measured relative to the  $\text{Es}^{253}$  6.640-MeV alpha group by F. Asaro and I. Perlman, unpublished results (1958).
40. G. N. Flerov, S. M. Polikanov, V. L. Mikheev, V. P. Perelygin, and A. A. Pleve, Proceedings of the Third Conference on Reactions between Complex Nuclei (University of California Press, 1963), p. 219; G. N. Flerov, et. al., Phys. Letters 13, 73 (1964); also, A. Ghiorso, A. Larsh, and I. Perlman, unpublished results (1964).

41. A. Ghiorso, unpublished results, in E. K. Hyde, The nuclear Properties of the Heavy Elements, Vol. III: Fission (Prentice-Hall, 1964), p. 77.
42. W. G. Smith and J. M. Hollander, Phys. Rev. 101, 746 (1956).
43. M. Holtz and J. M. Hollander, unpublished results (1964).
44. See the tables assembled in L. B. Magnusson, Phys. Rev. 107, 161 (1957).
45. F. W. Breivogel and M. D. Holtz, Lawrence Radiation Laboratory Report UCRL-10494 (1962).
46. J. M. Hollander, M. D. Holtz, T. Novakov, and R. L. Graham, Ark. Fys. 28, 375 (1965).
47. See, e.g., M. E. Rose, Internal Conversion Coefficients (North-Holland Pub. Co., 1958), or L. A. Sliv and I. M. Band, Coefficients of Internal Conversion of Radiation, Part II: The L Shell (Trans. from the Akad. Nauk report and published by University of Illinois, NP-tr-217, 1958).
48. J. O. Newton, B. Rose, and J. Milsted, Phil Mag. 1, 981 (1956); F. Asaro and I. Perlman, unpublished results (1962).
49. This system was designed and built by F. Goulding and co-workers, Berkeley.
50. See, e.g., J. H. Elliot, Lawrence Radiation Laboratory Report UCRL-9538 (1961); or various brochures accompanying commercial detectors.
51. P. Alexander, F. Boehm, and E. Kankeleit, Phys. Rev. 133, B284 (1964).
52. B. L. Robinson and R. W. Fink, Rev. Mod. Phys. 27, 424 (1955); 32, 117 (1960).
53. J. K. Beling, J. O. Newton, and B. Rose, Phys. Rev. 86, 797 (1952); 87, 670 (1952).
54. This instrument was designed and built by M. Nakamura, Lawrence Radiation Laboratory, Berkeley.
55. From Sliv and Band, op. cit. (ref. 47).
56. The actual experimental setup is described in C. M. Lederer, Ph. D. Thesis, Lawrence Radiation Laboratory Report UCRL-11028 (1963).
57. B. R. Mottelson and S. G. Nilsson, Dan Mat.-Fys. Skr. 1, No. 8 (1959).

58. C. J. Gallagher and S. A. Moszkowski, Phys. Rev. 113, 212 (1959); also, C. J. Gallagher, Nucl. Phys. 16, 215 (1960).
59. Ref. 33; by comparing, e.g., the values for the various even-even nuclei in this neighborhood (Hyde, Perlman, and Seaborg, op. cit.) one can see that this value does not change drastically with different isotopes.
60. G. L. Struble and J. O. Rasmussen, Lawrence Radiation Laboratory Report UCRL-16102 (1965).
61. M. A. Preston, Phys. Rev. 71, 865 (1947).
62. A table of hindrance factors calculated in a similar manner is given in H. Michel, Lawrence Radiation Laboratory Report UCRL-9229 (1960); we use her values for the nuclear radii and her computer program for some of the calculations.
63. A. Bohr, P. O. Froman, and B. R. Mottelson, Dan. Mat.-Fys. Medd. 29, No. 10 (1955); P. O. Froman, Dan. Mat.-Fys. Skr. 1, No. 3 (1957).
64. H. J. Mang and J. O. Rasmussen, Dan. Mat.-Fys. Skr. 2, No. 3 (1962); H. J. Mang and H. D. Zeh, Nucl. Phys. 29, 529 (1962).
65. M. Lederer, F. Asaro, and I. Perlman, unpublished results (1963).
66. R. R. Chasman and J. O. Rasmussen, Phys. Rev. 115, 1260 (1959).
67. G. Alaga, K. Alder, A. Bohr, and B. T. Mottelson, Dan. Mat.-Fys. Med. 29, No. 9 (1955).
68. F. Asaro and I. Perlman, unpublished results (1965).
69. F. Asaro, F. S. Stephens, J. M. Hollander, and I. Perlman, Phys. Rev. 117, 492 (1960).
70. G. Alaga, Nucl. Phys. 4, 625 (1957).
71. Hyde, Perlman, and Seaborg, op. cit., p. 857.
72. V. Subrahmanyam, Ph. D. Thesis, Lawrence Radiation Laboratory Report UCRL-11082 (1963).
73. G. Alaga, K. Alder, A. Bohr, and B. T. Mottelson, Dan. Mat.-Fys. Medd. 29, No. 9 (1955).
74. S. G. Nilsson and O. Prior, Dan. Mat.-Fys. Medd. 32, No. 16 (1961); also, D. R. Ingles, Phys. Rev. 96, 1059 (1954); 97, 701 (1955); ref. 2.
75. For example, F. Asaro and I. Perlman with Am<sup>242m</sup> and F. S. Stephens with Es<sup>253</sup>, unpublished results (1964).

76. A. K. Kerman, Dan. Mat.-Fys. Medd. 30, No. 15 (1956).
77. O. Prior, Ark. Fys. 16, 15 (1959); also, ref. 64.
78. B. G. Harvey, A. Chetham-Strode, A. Ghiorso, G. R. Choppin, and S. G. Thompson, Phys. Rev. 104, 1315 (1956).
79. The atomic masses were obtained from A. G. W. Cameron, Chalk River Report, CRP-690 (1957).
80. The target preparation and bombardment were carried out by and under the direction of A. Ghiorso and R. Latimer of the Lawrence Radiation Laboratory.
81. D. Metta, et. al., J. Inorg. Nucl. Chem. 27, 33 (1965).
82. The digital gain stabilizer was designed and built by M. Nakamura and R. LaPierre of the Lawrence Radiation Laboratory.
83. A. Chetham-Strode, F. Asaro, and I. Perlman, unpublished results (1955).
84. A. Chetham-Strode, Ph. D. Thesis, Lawrence Radiation Laboratory Report UCRL-3322 (1956).
85. Nathan and Nilsson, op. cit., p. 668.
86. E. K. Hulet, unpublished results (1956-57), cited by Hyde, op. cit., p. 931.
87. B. M. Foreman, Jr., and G. T. Seaborg, J. Inorg. Nucl. Chem. 7, 305 (1958).
88. F. S. Stephens, F. Asaro, and I. Perlman, Phys. Rev. 113, 212 (1959).
89. F. S. Stephens, F. Asaro, S. G. Thompson, and I. Perlman, Bull. Am. Phys. Soc., Ser. II. 2, 394 (1957); also cited in Hyde, op. cit., p. 933.
90. H. C. Griffin, K. F. Flynn, A. M. Friedman, L. F. Glendenin, and J. Milsted, to be published, cited in ref. 91.
91. J. Milsted, A. M. Friedman, and C. M. Stevens, preprint; also cited in Hyde, op. cit., p. 919.
92. See, e.g., Hyde, op. cit., p. 108.
93. See, e.g., Nathan and Nilsson, op. cit., p. 647; the development of the first part of this section will use that of Kerman, ref. 76, as a point of departure.

94. See, e.g., M. A. Preston, Physics of the Nucleus (Addison-Wesley Pub. Co., 1962), Appendix A.
95. N. D. Newby, Jr., Lawrence Radiation Laboratory Report UCRL-9764 (1961).
96. F. S. Stephens, F. Asaro, S. Fried, and I. Perlman, Lawrence Radiation Laboratory Report UCRL-16192 (July 1965).
97. Z. L. Szymanski, et. al., unpublished results (1965), communicated at a seminar in Berkeley.
98. H. J. Mang, unpublished results (1960).
99. F. S. Stephens, unpublished results (1961); also, Lawrence Radiation Laboratory Report UCRL-9566 (1961).
100. S. G. Nilsson, unpublished results (1960).
101. F. S. Stephens, unpublished results (1964); also, J. M. Hollander, M. D. Holtz, T. Novakov, and R. L. Graham, in Lawrence Radiation Laboratory Report UCRL-11213 (1964), p. 4.
102. H. J. Mang, in Annual Review of Nuclear Science (Annual Reviews, Inc., 1964), Vol. 14, p. 1; also, H. J. Mang, J. K. Poggenburg, and J. O. Rasmussen, Nucl. Phys. 64, 353 (1965).

LIST OF FIGURES

1.	Closed cycle placing $\text{Es}^{254}$ and $\text{Es}^{254m}$	4
2.	$\text{Es}^{254m}$ decay scheme	5
3.	Path of build-up for producing einsteinium through neutron capture on lower actinides	9
4.	$\text{Es}^{254}$ wide-range alpha spectrum, solid-state detector	11
5.	$\text{Es}^{254}$ narrow-range alpha spectrum, solid-state detector	14
6.	$\text{Es}^{254}$ alpha spectrum taken with magnetic spectrograph, favored alpha groups centered	18
7.	$\text{Es}^{254}$ alpha spectrum taken with magnetic spectrograph, low-energy alpha groups centered	19
8.	$\text{Es}^{254}$ conversion-electron plates, permanent-magnet spectrograph	24
9.	$\text{Es}^{254}$ conversion-electron spectrum, solid-state detector	29
10.	$\text{Es}^{254}$ gamma-ray spectrum (fast coinc. with $\alpha$ 's), NaI scintillator	31
11.	$\text{Es}^{254}$ gamma-ray spectrum (fast coinc. with $\alpha$ 's), Ge gamma detector	32
12.	Block diagram of fast-slow coincidence circuit	33
13.	Singles comparison between $\text{Es}^{254}$ (63-keV) and $\text{Am}^{241}$ (60-keV) $\gamma$ 's	37
14.	Coincidence comparison between $\text{Es}^{254}$ (63-keV) and $\text{Am}^{241}$ (60-keV) $\gamma$ 's	38
15.	Comparison between $\text{Es}^{254}$ and $\text{Es}^{253}$ L x rays	39, 40
16.	Time-to-height coincidence curve determining half-life of $\text{Es}^{254}$ 63-keV $\gamma$	43
17.	Block diagram of time-to-height converter and its associated equipment	45
18.	Time-to-height coincidence curve determining half-life of long delay in $\text{Es}^{254}$ L x rays	47
19.	Time-to-height coincidence curve showing "dip" following prompt pulses	48
20.	Predicted composite delay curves for no equilibrium and for transient equilibrium	49
21.	Time-to-height coincidence curve determining half-life of shorter delay in $\text{Es}^{254}$ L x rays	51



22.	Time-to-height coincidence curve showing that only the shorter L-x-ray follows $\text{Es}^{254}$ 63-keV $\gamma$	53
23.	Block diagram of apparatus used to obtain three-component delay curve	56
24.	Three-component time-to-height coincidence curve that shows the $\text{Es}^{254}$ cascade graphically	57
25.	Block diagram of apparatus used to obtaine delayed gamma-ray spectra	60
26.	$\text{Es}^{254}$ delayed gamma-ray spectrum	61
27.	$\text{Es}^{254}$ trial decay scheme	63
28.	$\text{Es}^{254}$ $\alpha$ 's in fast coincidence with 63-keV $\gamma$	66
29.	$\text{Es}^{254}$ decay scheme	67
30.	$\text{Es}^{253}$ decay scheme	69
31.	$\text{Fm}^{255}$ decay scheme	70
32.	Nilsson proton diagram	71
33.	Nilsson neutron diagram	72
34.	$\text{Es}^{254}$ $\alpha$ 's in fast coincidence with $>275$ -keV $\gamma$ 's	93
35.	$\text{Es}^{252}$ alpha spectra, grid chamber, taken in June 1964 and Feb. 1965	110
36.	$\text{Es}^{252}$ alpha spectrum, low-geometry solid-state detector and stabilizer	111
37.	$\text{Es}^{252}$ gamma-ray spectra in fast coincidence with all $\alpha$ 's, 110- and 20-nsec resolving times	116, 117
38.	$\text{Es}^{252}$ partial decay scheme	123
39.	$\text{Cf}^{249}$ decay scheme	130
40.	Coupling schemes for particles and a rigid rotor	149

LIST OF TABLES

I.	Activities present in $\text{Es}^{254}$ source	13
II.	$\text{Es}^{254}$ (complex) alpha groups, solid-state spectrum	15
III.	$\text{Es}^{254}$ alpha groups, magnetic-spectrograph spectra	20
IV.	$\text{Es}^{254}$ conversion-electron lines	25-27
V.	$\text{Es}^{254}$ K-conversion electrons, solid-state spectrum	30
VI.	$\text{Es}^{254}$ gamma rays	35
VII.	Properties of rotational bands in $\text{Bk}^{250}$	75
VIII.	$\text{Es}^{254}$ alpha-decay hindrance factors	80
IX.	$\text{Es}^{254}$ calculated alpha populations, favored decay	83, 84
X.	$\text{Es}^{254}$ calculated alpha populations, unfavored decay	85
XI.	$\text{Bk}^{250}$ delayed gamma transitions	88
XII.	$\text{Bk}^{250}$ K-conversion coefficients for higher-energy gamma rays	95
XIII.	$\text{Es}^{254}$ calculated alpha populations, to the 416-keV band in $\text{Bk}^{250}$	98
XIV.	Rotational spacings of bands in $\text{Bk}^{250}$	105, 106
XV.	$\text{Es}^{252}$ alpha groups	113
XVI.	$\text{Es}^{252}$ gamma rays	115
XVII.	$\text{Es}^{252}$ alpha-decay hindrance factors	122
XVIII.	Qualitative spin predictions for lowest band in $\text{Bk}^{250}$	125
XIX.	Properties of rotational bands in $\text{Bk}^{248}$	132, 133
XX.	$\text{Es}^{252}$ calculated alpha populations	141, 142
XXI.	Rotational spacings of bands in $\text{Bk}^{248}$	144
XXII.	Estimated positions of bands in $\text{Bk}^{250}$ used for Coriolis calculations	165, 166
XXIII.	Coriolis matrix elements for $\text{Bk}^{250}$ 7+ band	169
XXIV.	Comparison table of Coriolis calculations	172

This report was prepared as an account of Government sponsored work. Neither the United States, nor the Commission, nor any person acting on behalf of the Commission:

- A. Makes any warranty or representation, expressed or implied, with respect to the accuracy, completeness, or usefulness of the information contained in this report, or that the use of any information, apparatus, method, or process disclosed in this report may not infringe privately owned rights; or
- B. Assumes any liabilities with respect to the use of, or for damages resulting from the use of any information, apparatus, method, or process disclosed in this report.

As used in the above, "person acting on behalf of the Commission" includes any employee or contractor of the Commission, or employee of such contractor, to the extent that such employee or contractor of the Commission, or employee of such contractor prepares, disseminates, or provides access to, any information pursuant to his employment or contract with the Commission, or his employment with such contractor.

